

Quantum effects in charge control of semiconductor surfaces as elucidated by *ab initio* calculations – a review

by Stanisław Krukowski, Paweł Kempisty and Paweł Strak

Institute of High Pressure Physics, Polish Academy of Sciences, Sokołowska 29/37,
01-142 Warsaw, Poland

Abstract

Recent progress in the investigations of the charge role in semiconductor surfaces is reviewed. That include elucidation of Coulomb interaction of the separated subsystems, such as slab copies or far distant adsorbate and the slab. The progress was partially related to the new methods used in *ab initio* simulations of the slabs representing the surfaces. These new methods include application of Laplace correction method in *ab initio* calculations and averaging of potential profiles get smoothed long-range variation, the real space variation of band profiles, use of projected density of states (PDOS) and Crystal Orbital Hamilton Population (COHP) in determination of the surface states. These methods were supported by the elucidation of the relation between the charge distribution in the space and the long-range potential variation in the slab systems. Thus these data have direct connection to the band profile in real space used to gain more insight into the bonding close to the surfaces. They are supplemented by the application of quantum statistical methods to bonding of atoms in the bulk and at the surface including concept of the fractional occupation of the resonant states that allowed to resolve existing inconsistencies between the bonding and the lattice symmetry. The quantum nature of the bonding leads to emergence of the external surface dipole, which was well recognized prior to these investigations. The role of the external dipole layer in the thermalization of the adsorbate is proposed and formulated. It is demonstrated that the kinetic energy loss occurs via tunneling of electrons in the strong electric field at the boundary of the crystal which leads to deceleration of the positively charged adsorbate and its smooth attachment at the surface. At the same time tunneling electrons transport the excess energy deep into the solid interior where is its dissipated by emission of phonons. Prior to these investigation the internal dipole charge is also well known to exist at the surface. The new finding include the simulation of these dipole fields within slab model, pinning the Fermi level at the surface and the role of bulk and surface

charge. These findings were used in the simulation of the properties of the surfaces of several semiconductors that led to identification of the surface states Stark effect. This was connected to charge balance at the surface, especially important in the course of adsorption processes. It was shown that the charge balance is affected by the adsorption processes by the increase of the number of the electrons transported by the adsorbate and the creation of new quantum states. These numbers could be different which leads to redistribution of the electrons among the surface states, changes of these states occupation, which in some cases could lead to the change of the pinning of Fermi level at the surface and considerable change of the adsorption energy at some critical coverages. At this coverage the Fermi level becomes free, the surface dipole could disappear and the bands are flat. This is translated into the change of the equilibrium vapor pressures by several orders of magnitude, which is likely to occur during growth of crystals as the used pressure frequently are within this pressure interval. The modification of the adsorbate by quantum effect may include the change of stability points as its bonding may include resonant bonding and fractional occupation of the bonding states. This could also occur at the activated complex point where the energy of these states could be increased into the vicinity of Fermi level or even higher so that this affects the energy barrier for diffusion. Therefore the explicit incorporation of quantum effects in the charge role in the semiconductor surfaces changes their properties considerably as described in this review.

I. Introduction

Crystalline semiconductors are important class of the solid state systems that were in the focus of the intensive research for the recent 80 years [1,2]. They are indispensable for the development of modern civilization. This stems from their unique properties that were investigated in fundamental research first and subsequently applied in the technology. These applications are always related to the investigations, control and manipulation of the electric charge.

Therefore the charge is the most essential factor in the semiconductor physics and chemistry. The charge manipulation is indispensable for the computer logic, control of the electric current flow, detection of the changes in environment, absorption and emission of electromagnetic radiation, generation and measurements of vibration including the sound, measurements of time, frequency etc. These functions are possible due to different functionalities of specially designed semiconductor structures, built in the depth of the semiconductors and also close to and on the surface. Therefore the surface charge state is important factor affecting functioning of semiconductor devices [3].

Emergence of the locally unbalanced charge at semiconductor surfaces creates electric fields in the surrounding [3-5]. That induces the changes in the semiconductor bulk by emergence of the screening charge that limits the field penetration into the semiconductor bulk. This is a long-range effect of the charge balance related to creation of surface electric dipole on the internal side of the surface. The properties of the dipole, such as charge separation, dipole density, etc. depend on the mobile charge in the semiconductor interior. In general the dipole may have different orientation depending on the charge accumulated, located on the surface donors or acceptors. In addition to this effect, on the other side of the surface an additional, second dipole is present. The latter charge effect is related exclusively to quantum-mechanical properties of the solid state bonding. Accordingly, it is typical for all solids, with the most dramatic consequences for semiconductors. Wavefunctions of the valence band states extend behind the outermost layers of atoms, or more precisely behind the outermost layer of atomic nuclei thus creating external layer of negative charge. In conjunction with the positive charge of these atomic nuclei that creates electric dipole layer, preventing electron escape, i.e. constituting electron work function [3,7,8]. The external dipole layer was recognized fairly early by Lang and Kohn [7,8]. This phenomenon is different from the previous one as it is high magnitude, narrow thickness electric dipole field. The field is strongly localized in the direction perpendicular to the surface. At the same time it is slowly varying, long-range in the direction

parallel to the surface [7, 8]. In contrast to the internal dipole, the outside dipole is always directed in the same direction, so that the electron energy is lower in the solid interior.

These two effects are purely physical in nature, i.e. they are basically identical for all surfaces. They could have chemical counterpart in relative secondary sense, i.e. their amplitude can be modified. In addition, the semiconductor surfaces have also the properties that are different in nature. They are related to the bonding between atoms, i.e. they are chemical in nature. These are the bonds or rather quantum states associated with the bonding between atoms, i.e. valence band (VB) states. In standard semiconductors these bonds are interpreted in terms of the overlap between sp^3 hybridized orbitals of metal and nonmetal, such as Ga and As. This picture is not universal, as shown by soft x-ray emission spectroscopy of nitrides: AlN [9] and GaN[10]. From *ab initio* simulations it was found that valence band consist of the two separate subbands: the upper created by metal sp^3 hybridized orbitals and nitrogen p orbitals [9-11]. The lower has s orbitals and possible contribution of d orbitals of gallium [10,11]. In case of AlN this contribution is missing. Therefore the bonding of nitrogen in tetrahedral coordination is created via four resonant states [12]. This has drastic consequences both in the bonding of the bulk and also at the surfaces.

Surface atoms have their bonds broken, i.e. with no overlap as the neighbors are missing [3]. Therefore these states have their energies higher than VB states, usually they are located in the bandgap. These states may be occupied, fully, partially or they may be empty. They are be modified by relocation of atoms that will lead to the emergence of their overlaps with the other atoms that change of their energies and occupation. That changes the surface symmetry, i.e. new reconstructions emerge [3]. In addition, adsorption of additional species could bring similar effects. These adsorption processes may also involve charge transfer between different surface states. Therefore the interplay between charge distribution, reconstruction and possible adsorption of the species is extremely complex. These phenomena are predominantly quantum in nature therefore the elucidation of these phenomena by *ab initio* calculations and their relation to other approaches and final verification by the experiment is the subject of the present review.

The subject will be presented in the following order: first the main features of the calculation models, based on *ab initio* methods addressed to surfaces, are presented. The methodological part will be followed by the precise and concise presentation of the recent development of the field divided into: surface charge screening layer, work function, complemented by: the charge role in the reconstruction, adsorption and diffusion. These results will be finally summarized.

II. The *ab initio* calculation models of semiconductor surfaces

The calculation models used for simulation of the properties of the surfaces stem from the difficult compromise between the limited computing resources available for calculations and the long distance coupling existing in these systems. In addition, the requirement of numerical efficiency enforces application of the mathematical methods based on Fourier transform which imposes severe limitations on the construction of the possible models. This entails periodic boundary conditions in all three directions. In the plane parallel to the surface this is natural choice, subject to the system size only. Essentially, that reduces effective simulations to the flat surface only. These systems are therefore also denoted as supercells as they contain large number of single unit cells of the crystalline lattice. In the direction perpendicular to the surface the simulations have to overcome the long range coupling which acts against the periodicity of the potential and the wavefunctions. The solution is to use a slab of atoms, i.e. several layers of atoms in the lattice of the solid surrounded by empty space, i.e. having two surfaces. The basic one is natural, i.e. the real one that is simulated, the second is artificial as it replaces the crystal bulk. In this unnatural way the basic periodicity in the dimension perpendicular to the surface is recovered. The boundaries of the simulated volume in the perpendicular direction may be selected in any way, the preferable choices are: inside the atomic layers or in the vacuum space. Note that this entails an infinite periodic chain of slabs in the direction perpendicular to the surface.

The slab as a whole has to be electrically neutral which is necessary condition for the stability of the infinite chain of the slabs. Nevertheless the three different factors can contribute to the charge separation in the slab creating electric dipole and subsequently the potential difference across the slab: a spontaneous polarization, the polarity of the surfaces and localization of the charge on the surface states. All these factors contribute to the potential difference across the slab. In the result this potential difference has to be compensated by the artificially designed opposite term. The first remedy was proposed by Neugebauer and Scheffler, who introduced compensating dipole layer in the vacuum space [13]. The next solution was proposed by Bengtsson who also proposed dipole correction [14]. Finally, Krukowski et al. proposed Laplace correction method to compensate the field in the vacuum space [15]. In the latter case, in absence of any special measures, the potential difference is compensated by the additional uniform electric field in the vacuum space [15].

In fact, the Neugebauer and Scheffler solution compensates slab dipole by the additional compensating dipole which is inserted in the vacuum space at the short distance from the slab.

This compensation could be affected by the error related to imprecise representation of the charge density by finite grid and miscalculation of the slab dipole [16]. In addition presence of the dipole affects the wavefunctions of the slab, despite the fact that they are at some distance. Thus this solution could potentially deteriorate the convergence in self-consistent field (SCF) solution loop of nonlinear equations [15]. Bengtsson method is based on the periodic solution of Poisson equation with the potential jump added to Hartree potential. Therefore Bengtsson method is essentially an introduction of direct potential jump at the boundary of simulated volume obtained from the dipole calculated for the simulated volume [14]. This version again suffers from imprecise representation of the charge density field [16]. The finite size dipole is replaced by potential jump. Finally, in the paper by Krukowski et al. Laplace correction is used as a field compensation method [15]. The method adds solution of Laplace equation, i.e. uniform electric field, opposite to the field in the vacuum space. Therefore the field is compensated, within the precision of the determination of the field in the empty space. Naturally this is with the finite precision only which creates a possible source of errors in the application of this method. In summary, in any situation the electric potential has the difference between both sides of the slab which is exactly in the case of the surface finite layer of atoms at the real semiconductor surfaces. Therefore no additional energy term has to be added to Laplace correction method [15].

As mentioned, the surface dipole in the slab calculations may be related to several factors. First is the spontaneous polarization of the crystals having the symmetry allowing emergence of the vectorial quantity. In wurtzite semiconductors the spontaneous polarization is allowed while in cubic zinc blende lattice it is not [17,18]. Thus among all semiconductors the wurtzite nitrides have nonzero spontaneous polarization [19]: $\text{BN} - P_3(\text{BN}) = 0.061 \text{ C/m}^2$, $\text{AlN} - P_3(\text{AlN}) = 0.059 \text{ C/m}^2$, $\text{GaN} - P_3(\text{GaN}) = 0.011 \text{ C/m}^2$, $P_3(\text{InN}) = 0.014 \text{ C/m}^2$. These values can vary depending on the model calculations, e.g. for AlN the reported values are: $P_3(\text{AlN}) = 0.081 \text{ C/m}^2$ [19,20], $P_3(\text{AlN}) = 0.090 \text{ C/m}^2$ [21] or even $P_3(\text{AlN}) = 1.351 \text{ C/m}^2$ [22]. These value has to be recalculated for single surface site using wurtzite lattice data. The lattice parameters of the bulk wurtzite boron nitride, obtained from typical recent *ab initio* calculations are: $a_{\text{BN}}^{\text{DFT}} = 2.5417 \text{ \AA}$ and $c_{\text{BN}}^{\text{DFT}} = 4.2019 \text{ \AA}$, while x-rays give: $a_{\text{BN}}^{\text{exp}} = 2.550 \text{ \AA}$ and $c_{\text{BN}}^{\text{exp}} = 4.227 \text{ \AA}$ [23]. DFT lattice data calculated for wurtzite AlN are: $a_{\text{AlN}}^{\text{DFT}} = 3.1126 \text{ \AA}$ and $c_{\text{AlN}}^{\text{DFT}} = 4.9815 \text{ \AA}$, in agreement with x-ray data from bulk aluminum nitride wurtzite crystal: $a_{\text{AlN}}^{\text{exp}} = 3.111 \text{ \AA}$ and $c_{\text{AlN}}^{\text{exp}} = 4.981 \text{ \AA}$ [24]. The calculated values for wurtzite GaN are: $a_{\text{GaN}}^{\text{DFT}} = 3.1955 \text{ \AA}$ and $c_{\text{GaN}}^{\text{DFT}} = 5.2040 \text{ \AA}$, in good agreement with x-ray data:

$a_{GaN}^{exp} = 3.1890 \text{ \AA}$ and $c_{GaN}^{exp} = 5.1864 \text{ \AA}$ [25]. For InN these data are: $a_{InN}^{DFT} = 3.5705 \text{ \AA}$ and $c_{InN}^{DFT} = 5.7418 \text{ \AA}$. They are in good accordance with the experimental data for wurtzite InN: $a_{InN}^{exp} = 3.5705 \text{ \AA}$ and $c_{InN}^{exp} = 5.703 \text{ \AA}$ [26]. The following area for single site $S_{wz} = a^2\sqrt{3}/2$ was used for experimental lattice parameters to obtain these values: $S_{wz}(BN) = 5.595 \text{ \AA}^2 = 5.595 \times 10^{-20} \text{ m}^2$, $S_{wz}(AlN) = 8.390 \text{ \AA}^2 = 8.390 \times 10^{-20} \text{ m}^2$, $S_{wz}(GaN) = 8.843 \text{ \AA}^2 = 8.843 \times 10^{-20} \text{ m}^2$, and $S_{wz}(InN) = 10.104 \text{ \AA}^2 = 1.0104 \times 10^{-19} \text{ m}^2$. These values could be used for determination of the polarization charge for the single site $q_{sp-pol} = P_3/S_{wz}$ to get: $q_{sp-pol}(BN) = 3.81 \times 10^{-3}e$, $q_{sp-pol}(AlN) = 3.68 \times 10^{-3}e$, $q_{sp-pol}(GaN) = 6.87 \times 10^{-4}e$ and $q_{sp-pol}(InN) = 8.74 \times 10^{-4}e$. These values are relatively low, especially for GaN and InN, indicating that the fields associated with the spontaneous polarization are relatively small. This was confirmed by the work by Kempisty et al. for GaN(0001) surface where the compensation of the leftover polarization field was achieved using fractional charge hydrogen pseudoatoms of the charge $\Delta Z \approx 0.01$ [27].

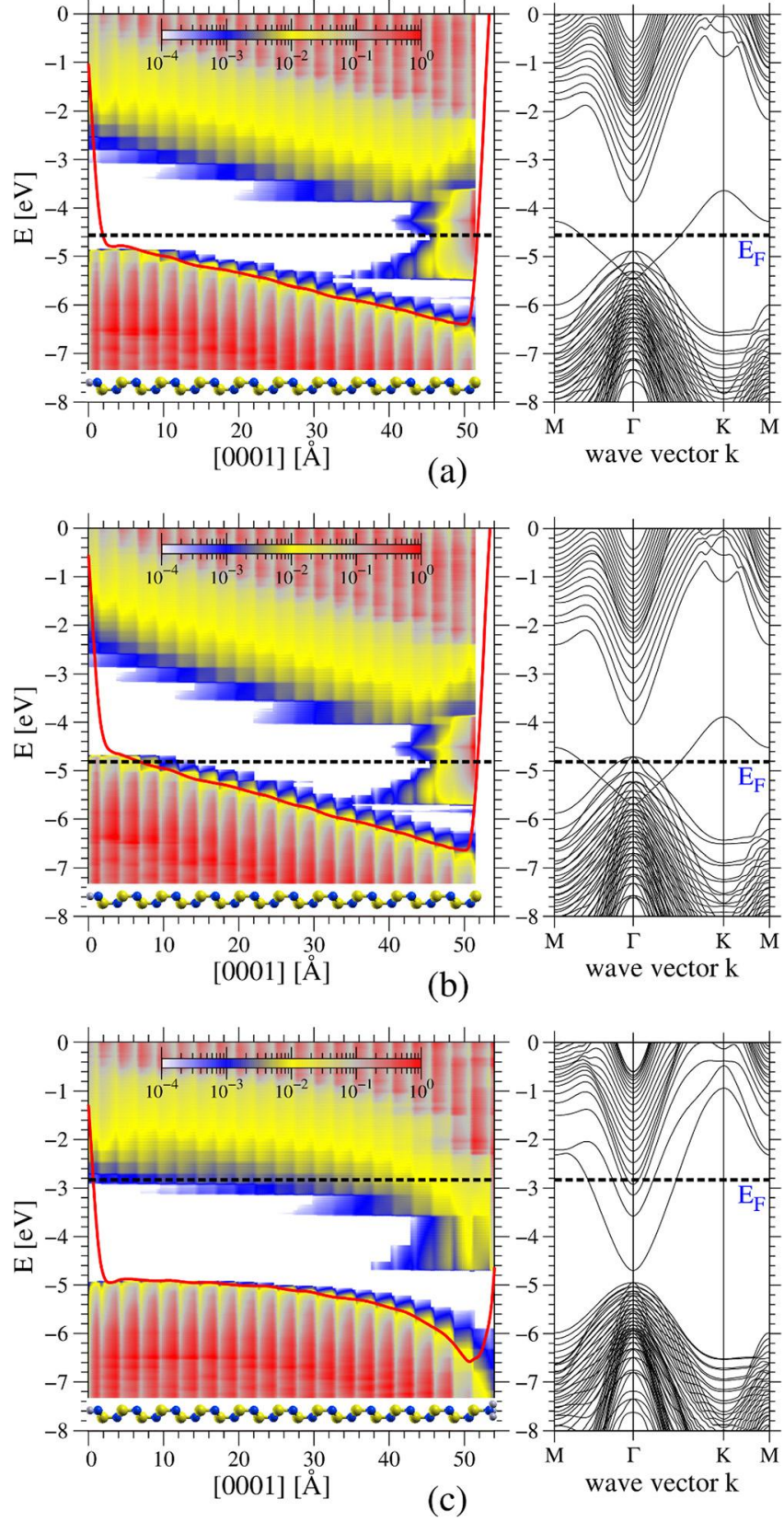


Fig. 1. Left diagram—the electric potential distribution, averaged in the plane perpendicular to c -axis, shown as electron energy (red line), and the density of states projected on the atom

quantum states (P-DOS), showing the spatial variation of the valence and conduction bands in the slabs having 20 DALs used for a simulation of a surface donor. The shades are (in arbitrary units): red—above 0.5, grey—0.1 yellow—0.01, blue— 0.001, white below 0.0001. Right diagram—the band diagram of the slab (VASP). The diagrams represent: (a) clean GaN(0001) surface with termination by $Z = 0.715$ hydrogen pseudoatoms (SIESTA); (b) clean GaN(0001) surface with termination by $Z = 0.635$ hydrogen pseudoatoms (SIESTA); (c) GaN(0001) surface covered by 1 ML of ammonia with $Z = 0.735$ hydrogen termination pseudoatoms (SIESTA). The schemes of the GaN slabs are presented beneath the spatial band variation diagrams. Reproduced Fig. 9 from Ref. 30 [30].

The use of hydrogen pseudoatoms at the opposite, termination surface was proposed to reduce the effect of broken bonds states both in quantum mechanical and electric potential aspects [28,29]. This is related to the presence of the charge located on the surface states, and ensuing emergence of the electric field at the surface [4, 5, 27]. The simulations recover such fields in finite thickness layer, therefore the obtained energies of the states within the slab are affected in function of their position. The effect is illustrated in Fig. 1 copied from Ref 26. where this effect was discussed.

Similar results were obtained by Yoo et al. in simulations of ZnO slab supercell calculations [31]. Natural consequence of the field presence is the skewed band diagram in which the projection of the states, necessary to create the typical band diagram in momentum space, leads to apparent reduction of the bandgap as shown in Fig. 1. This effect was not considered in the early publications dealing with semiconductor surfaces. The composed volume-surface band structure of ideal and relaxed nonpolar GaN surfaces calculated in local density approximation (LDA) was presented first by Northrup and Neugebauer [32]. In their diagram the band states are presented as shaded area while the surface states are presented as line in energy- momentum (parallel) coordinate system. This approach, necessary to avoid overshadowing of the surface states, was employed in number of later publications [33-37]. These diagrams are not incorrect, nevertheless they do not capture the complexity of the semiconductor surfaces.

In fact, the surface states are a part of the total band structure of the surface slab that is composed of the bulk states and the surface states. The examples of such diagram are presented in Fig. 2 where the band diagrams of the slab presenting clean polar AlN (0001) and AlN(000 $\bar{1}$) surfaces are presented [38]. The calculated slabs contained 24 double atomic layers (DAL) of Al-N slabs, without any coverage on both sides. The image presents band diagrams

in momentum and real space and also partial density of states (PDOS). As it is shown, the surface states exist on both surfaces. The states associated with Al-terminated surface, located close to conduction band minimum (CBM), have large dispersion, about 2 eV wide. This is related to the overlap of Al states between neighboring top Al atoms. The states associated with N-terminated surface have reduced dispersion, of order of 0.3 eV and they are located close to valence band maximum (VBM). Their dispersion is small, related to small size of nitrogen wavefunctions and much smaller overlap between neighbors. These three diagrams represent p-type, n-type and semi-insulating (SI) AlN bulk, which is reflected by the position of the Fermi level inside the slab, close to conduction band, valence band, and in the gap center, respectively. The latter diagram is specific which is associated with the absence of the bulk charge, leading to linear dependence of the electric potential. The two other diagrams have strongly nonlinear potential profiles, confirming the presence of the charge in the bulk [38]. In addition, the field is present at both edges of the slab, leading to the energy shift of the surface and the band states which was identified as surface states Stark effect [27,39,40]. The identification is correct as the surface states energies are affected by the electric field present in the slab.

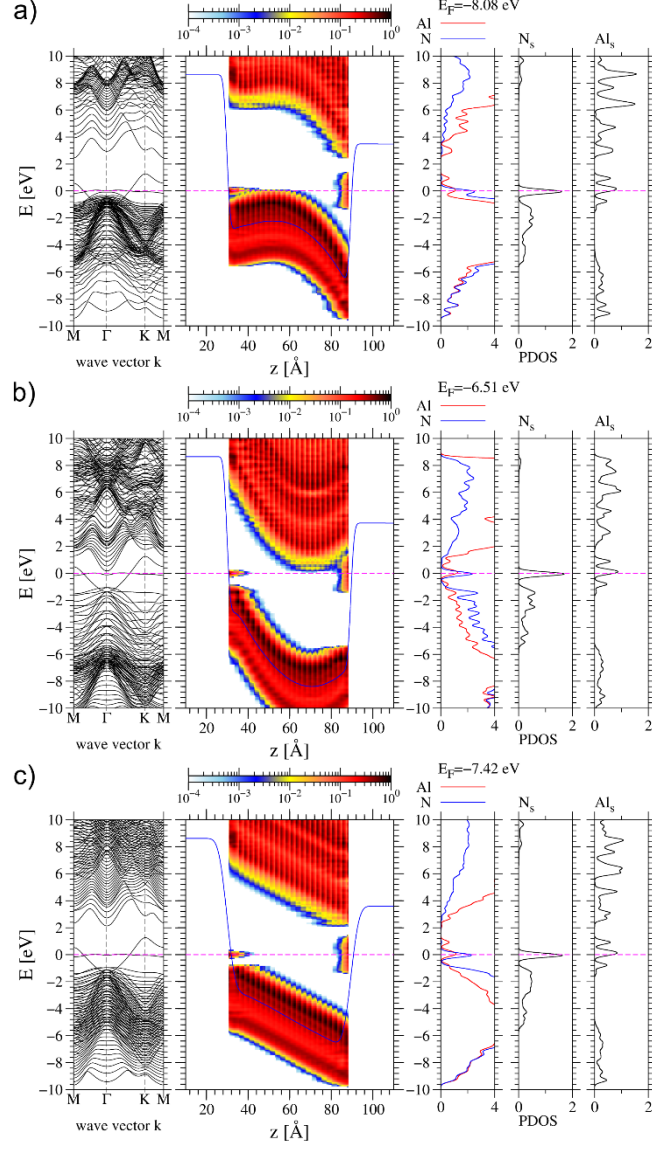


Fig. 2. Band diagram in momentum (left) and position space (middle) of the WZ 24 DALs AlN slabs and the density of states (DOS) of surface Al atoms (right): (a) p-type, (b) n-type, (c) SI. The blue line superimposed on the position space diagram is electric potential, derived as above, plotted in units of electron energy. The colors in the central panel represent electron density according to the scale at the top. Reproduced Fig. 4 from Ref. 38 [38].

The presence of the field inside the slab is closely related to the partial occupation of the surface states. In fact these surface states are broken bond states, i.e. states without overlap with the states of the neighboring atoms as they are missing. In essence they originated from the valence band, their higher energy is due to absence of the overlap. Thus their energies are

located typically in the bandgap. The example of such states are the surface states of AlN(0001) polar slabs, presented in Fig. 2. These states are partially filled thus the Fermi energy is there so that they are pinning the Fermi level.

In general, the presence of Fermi level pinned at both slab sides stabilize potential difference with respect to the external field applied. Such result, plotted in Fig. 3, was obtained by Krukowski et al. in Ref. 15 [15].

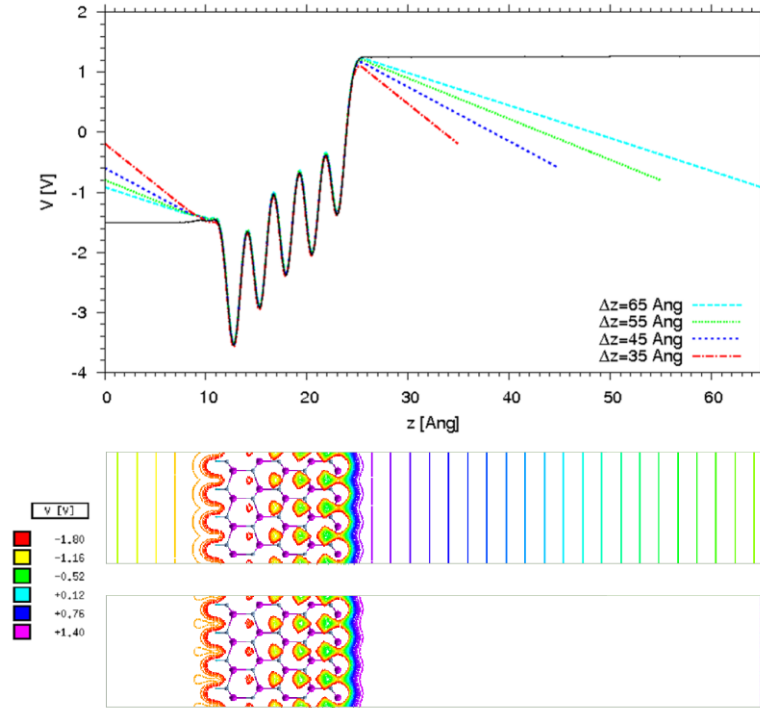


Fig. 3. Electric potential distribution (SIESTA) for different thickness of the spacer, obtained with and without Laplace correction. Top diagram presents the potential profiles along the channeling path. The black line correspond to the solution with, the color lines - without Laplace correction. Bottom diagrams the sections across the slab with (upper) and without (lower) gradient correction, drawn for the largest width of the spacer. Reproduced Fig. 4 from Ref. 15 [15].

The potential difference may be manipulated by the change of the electron charge in the termination hydrogen pseudoatoms, or by the distance between these atoms and the bottommost slab atoms. That will lead to the difference in the field within the slab as it is shown in Fig. 4.

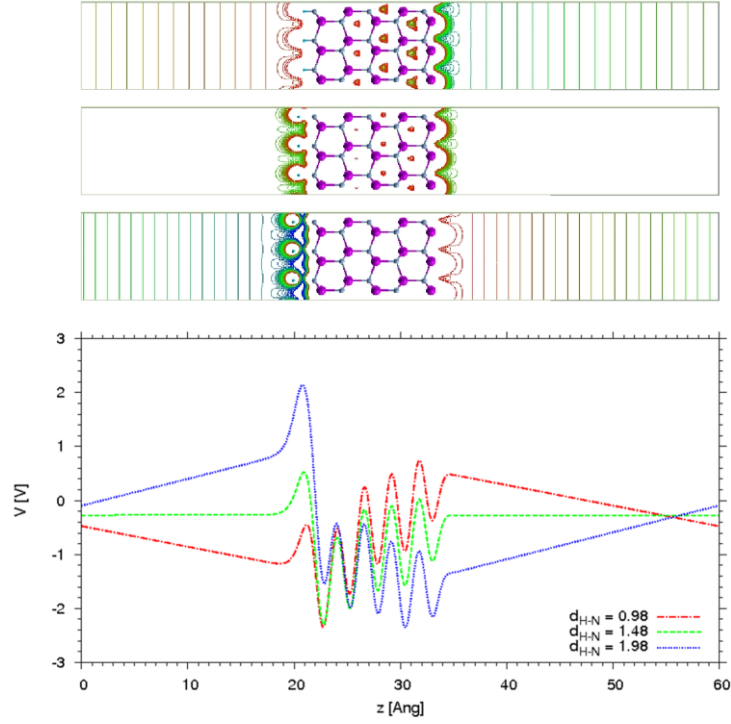


Fig. 4. Electric potential distribution in 3x3 Ga-N slab, fulfilling PBC, obtained for three different distances between N bottom atoms and H saturation atoms in SIESTA: a) 0.98 Å, b) 1.48 Å and c) 1.98 Å. Top- the sections across the slab, bottom - the potential profiles along the channeling path. Reproduced Fig. 2 from Ref. 15 [15].

The potential profiles, presented in Figs. 3 and 4, are affected by the presence of atomic cores, giving rise to high amplitude fluctuations. These fluctuations were removed by the averaging methods described in Ref. 41 [41]. The method allows one to obtain long range variation of the electric potential which, presented as electron energy in Fig. 2, proves that the bands variation in the real space follows strictly the change of the electric potential, confirming identification of the surface states Stark effect.

At both slab edges, the diagram show steep change of electric potential, of order of several volts. This is evidence of the external surface dipole contributing to the work function of the semiconductor, identified first by Lang and Kohn [7,8]. This dipole may be affected by the adsorption of the species at the surface, which is sometimes related to the charge transfer and creation of additional dipoles. Both dipoles contribute to overall dipole of the slab as shown in Fig. 2.

It has to be added, that in the investigations of the adsorption processes, additional spurious effects may arise which can affect adversely the precision of the obtained results. In

fact, the separation of the quantum system into two isolated subsystems may lead to different positions of Fermi levels in both parts. This is pure quantum effect, in fact it is a combination of quantum effects and the Fermi-Dirac statistics. Formally, the overlap always exist as the wavefunction asymptotic behavior at the far distance is always exponential. Thus formally the subsystems have coherent single wavefunction at any distance. This weak mathematical link is destroyed by thermal fluctuation, as the systems are in partial equilibrium. Therefore the remote subsystems are essentially independent, having possibly different Fermi energies.

The standard DFT procedures use single common position of the Fermi level for the entire system. That may entail artificial redistribution of the charge between subsystems, such as the slab and the separate adsorbate. This effect is not due to the tunneling of the electrons, in fact this is mere reshuffling of the electrons. Nevertheless this may create significant physical effect, such as an electric interaction between the charged species and the slab. This is illustrated in the case of Ga atom close to GaN slab presented in Fig. 5.

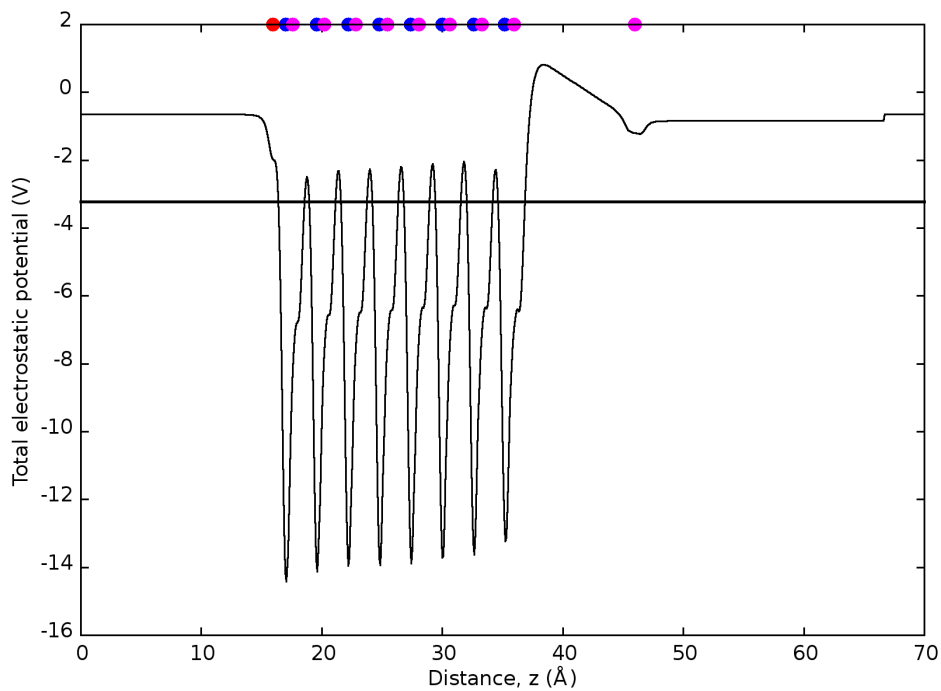


Fig. 5. Electric potential profile averaged in a plane perpendicular to the c-axis, plotted across the slab representing a bare GaN(0001) surface and d Ga atom at a distance of 10 Å from the surface, z – distance along c-axis. Positions of atoms are denoted by circles (blue – Ga, magenta – N, red – H) on top of the diagram. Reproduced Fig. 4. from Ref 42 [42].

The effect may be used for simulations of interaction of the plasma charged species: atoms and molecules. In fact this charge redistribution may affect the calculations of the adsorption energy using standard procedure of translation of the species away from the surface

and determination of the total system energy in function of the distance. It is assumed that above critical distance, at which the overlap of the wavefunctions of the slab and the adsorbate is negligible, the energy attains the constant asymptotic value. In the case of the charged species this is not observed as the Coulomb interaction is long ranged. This is proven in Fig. 6, where the energy of the GaN(0001) surface – Ga system is plotted [42]. The total energy has considerable variation at far distances, so that precise determination of the adsorption using this procedure is not possible. The other procedure based on separate calculation of the species and the slab is evidently superior.

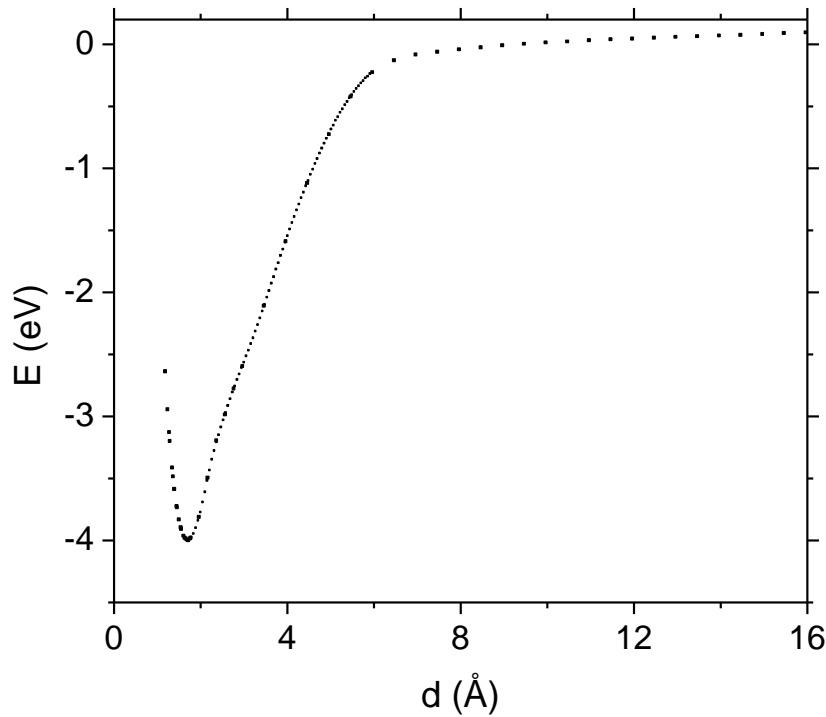


Fig. 6. Energy E of the system as a function of the distance d between a Ga adatom and a bare GaN(0001) surface. Zero energy level is set for a large distance from the surface. The distance is measured as a difference between the position of the Ga adatom and a position of the topmost layer of Ga surface atoms. Reproduced Fig. 3 from Ref 42 [42].

In the critical discussion of the slab representation of the semiconductor surfaces it is necessary to repeat that the separation of the two quantum subsystem could not be complete. Therefore the residual overlap is always present. This is visible in the overlap of the wavefunctions of the real and termination (opposite) surface atoms of the slab, shown in Fig. 7. From these data it follows that the far distance decay of wavefunction is exponential, always universal as it is the solution of the linear equation. Therefore the overlap between two surfaces does not vanish, it is reduced in exponential asymptotic way. Therefore the statements claiming

that the interaction between these two surfaces is not observed are not precise. These influence is reduced in the exponential manner with no critical width of the slab present. Therefore this indicates that the requirement for the number of the atomic layers in the slab simulations are severe, requiring large number of the atomic layers. This increases the considered system to the one having several hundreds of atoms. This is particularly unfortunate as high precision calculated employing Heyd-Scuseria-Ernzerhof (HSE) are not possible for such large number of atoms [43]. The other approximations like PBE or PBESol are much less precise in the determination of the energy of quantum states, leading to the bandgap error or order of 30% [44,45]. On the other hand, they recover mechanical properties well, so they are useful in determination of the surface structures, e.g. surface reconstruction. The other possible choice is to use the band correction scheme of Ferreira et al. known as GGA-1/2 approximation that gives the proper band gap energies, effective masses, and band structures [46,47]. This approach provides incorrect mechanical properties, so these calculation may be used only in the final determination of the energy of quantum states, without any relaxation.

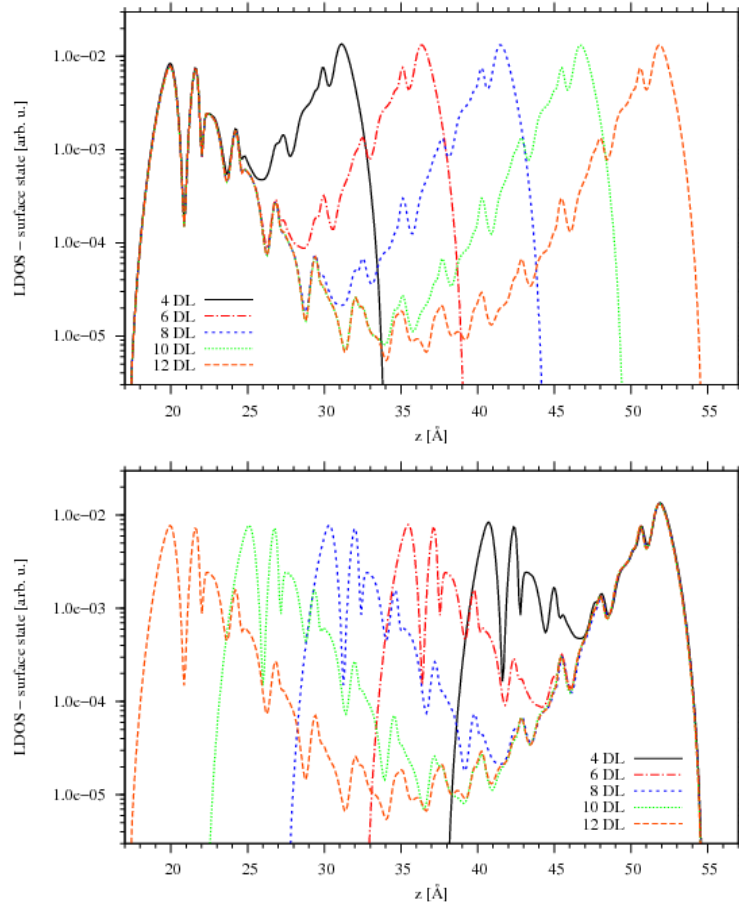


Fig. 7. Electron density profiles of the sum of the surface states related to real and artificial surfaces. The colors denote (1 x 1) GaN (0001) slabs, having four (black), six (red), eight

(blue), ten (green) and twelve (yellow) double atomic layers, all terminated by H atoms. The plots correspond to left and right-adjusted diagrams. Reproduced Fig. 4 from Ref. 39 [39].

From the above plotted diagram it follows that the wavefunction overlap of the real and termination surfaces is considerable for the slab thickness of 4 and 6 DALs. In case of 8 10 and DALs this is much lower. The extension from 8 to 10 DALs brings relatively smaller reduction, while the shift to 12 DALs brings only minor improvement. Thus the slab for high precision calculation should have at least 8 DALs while 10 or 12 DALs can be used for verification purposes.

These considerations prove that the *ab initio* simulations of the properties of semiconductor surfaces still face considerable obstacles in the route towards full precise determination of their properties. The goal is to simulate relatively thick slab of the size in plane large enough to capture basic symmetry properties of the surfaces. As it will be shown, the size of the simulated slab may severely distort the symmetry of obtained results. The same condition applies to the slab thickness. Here, the quantum independence should be correlated with the proper electric potential and charge modelling that again increases the size of the simulated systems. The precise requirement depends on the properties of the simulated system as they differ from one case to the other considerably. Nevertheless, the standard requirement for simulations of the semiconductor surface properties is several hundreds of atoms. This effectively precludes application of highly precise calculations such as in HSE approximation. Thus less precise versions of *ab initio* calculations, such as PBE and related approximation is the proper choice. On the other hand, the insight into the properties and processes on semiconductor surfaces is evidently incomplete. Therefore the optimal approach is to direct research towards understanding of the basic processes and phenomena , even at the cost of high precision. In the following Sections we will describe the state of knowledge in several aspect showing that the basic understanding of the physics and chemistry of the semiconductor surfaces need basic research and formulation of the basic ideas in the first instance.

III. Bonding in semiconductors – charge in the bulk and at the surface

It is widely accepted that tremendous majority of semiconductor crystal, both elemental such as diamond, silicon or germanium and compound such as GaAs, InSb, AlP or CdSe, HgTe are characterized by cubic symmetry of the lattice (i.e. zinc blende or diamond) and tetrahedral coordination. This is intimately related to the hybridized sp^3 bonding both elemental and compound [48, 49] . In the latter, the covalent bonding is supplemented by partial ionic

contribution. Due to symmetry of zinc blende lattice, the ionic contribution is neutralized in the bulk, so that charge separation effect does not manifest itself in the form of spontaneous polarization [17,18].

In fact ionic contribution is directly proportional to the energy difference of the hybridized sp^3 states [48]. It is absent in case of elemental semiconductors. It is also relatively small in case of the II-VI and most of III-V compounds. This is directly related to cubic lattice structure of the crystals. In case of the group III metal nitrides: BN, AlN, GaN and InN it is considerably larger. In the result, the lattice structure is changed to hexagonal, tetrahedrally coordinated wurtzite. In this structure spontaneous polarization is allowed and is observed in the compounds and also in the mixed crystals [12-17]. These effects are accompanied by the different bonding in these semiconductors. Despite tetrahedral structure, the GaN bonding include hybridized sp^3 orbitals of gallium and separated s and p orbitals of nitrogen. In addition d orbitals of gallium are involved. Therefore bonding overlap include separate overlaps of gallium d and nitrogen s orbitals. The second bonding involve hybridized sp^3 orbitals of gallium and p orbitals of nitrogen. That creates two separate sub-bands of valence band (VB) which was measured experimentally by soft x-ray spectroscopic measurements by Magnuson et al. [10]. By *ab initio* calculations the existence of two subbands was confirmed and the nature of the bonding was identified [10,11]. In case of AlN the subband separation was also identified, with the lower subband due to nitrogen s orbitals only [9].

The subband identification does not solve problems, in fact it creates more. The nitrogen atom is in tetrahedral surrounding, connected to four Ga neighbors. But the bonding in upper subband is created from 3 nitrogen p states. The lower $d-s$ subband is not compatible with the tetrahedral coordination at all. Therefore four bonds are necessary. This is in fact possible due to existence of resonant bonds proposed long ago by German chemist F. A. Kekule [50]. The concept of delocalization of electrons within sp^2 bonds was formulated in terms of probability of occupation of the nonorthogonal states, fully compatible with the quantum field theory. In addition π bonds in the direction perpendicular to the ring were incorporated [51]. Slightly different formulation was proposed by P. W. Anderson that involved the different feature of quantum mechanics, namely wave theory. This described the bonding as the resonant bonds, i.e. the wave states in full resonance, i.e. having the same frequency, i.e. the energy [52]. This formulation was subsequently applied to the description of high temperature superconductivity of the copper oxide structures [52]. Subsequently the concept was extended to other systems [53].

GaN case was considered only recently during study of N adatom at GaN(0001) surface [12]. Accordingly, the quantum states of N atom in GaN bulk were obtained and are presented in Fig. 6a. As it is shown in PDOS diagram in the case of N atom in the bulk the two basic states are present at approximately -5 eV and at -9 eV. As shown in COHP data these states are created by hybridized sp^3 orbitals of gallium and p orbitals of nitrogen and gallium d and nitrogen s orbitals, respectively.

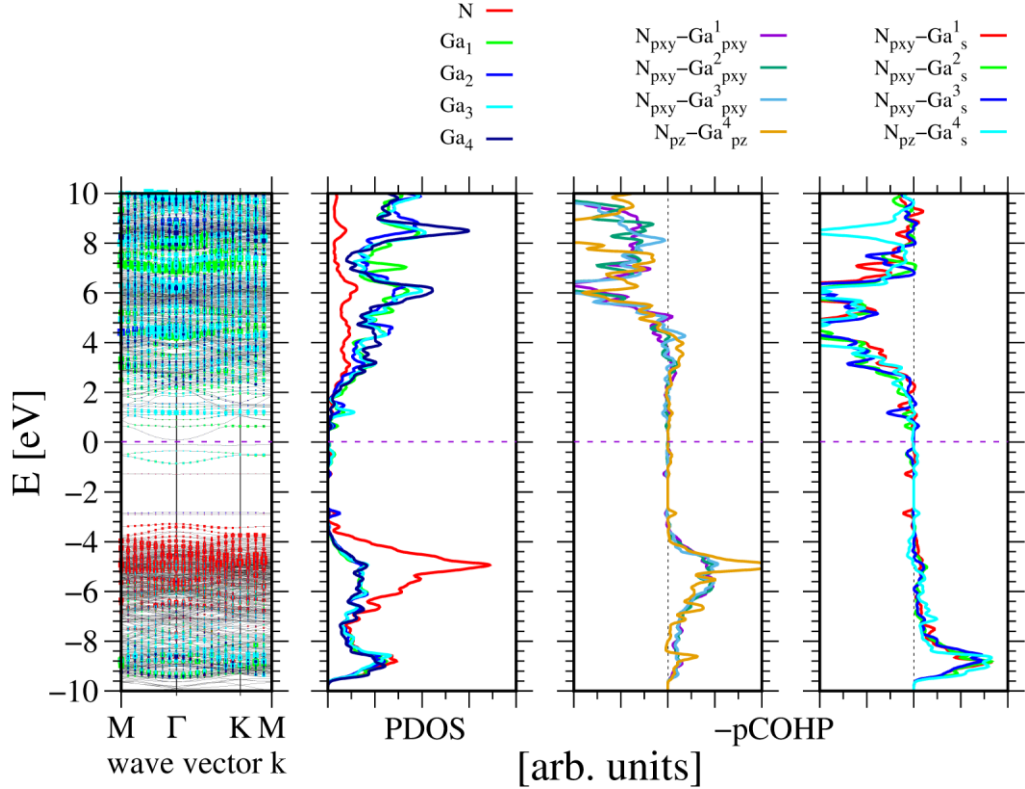


Fig 6a. Energies of the quantum states of nitrogen and gallium states located in the GaN bulk of $(2\sqrt{3} \times 2\sqrt{3})$ slab representing clean GaN(0001) surface with single N adatom located in H3 site. The panels represents, from the left: energy of the quantum states in the momentum space, projected density of states (PDOS) of the N and Ga atoms distinguished in Fig 2 (a), and the right two panel - Crystal Orbital Hamilton Population (COHP) [54,55]. The COHP data correspond to N adatom and the closest topmost Ga atoms. The Fermi energy is set to zero. COHP positive values correspond to the bonding overlap.

The COHP data indicate that upper state is due to four states created by overlap of $|N_{2p}\rangle$ states and $|Ga_{4sp^3}\rangle$ of four atoms. Thus this number is four states while they are created from three $|N_{2p}\rangle$ states. Thus this number is extended to four because these states are resonant

states, as in the case of benzene [50-31]. Naturally these states have to be nonorthogonal, they are occupied with the probability $P = 3/4$. Naturally, these states of the same energy are four, i.e. sufficient to create tetrahedral bonding pattern in the wurtzite lattice symmetry. This is confirmed by the angles created by these bonds which are in the plane: $\varphi = 110.14^\circ$ or $\varphi = 109.73^\circ$, i.e. close to the ideal tetrahedron. The c-axis angles are slightly different, $\varphi = 106.92^\circ$ or $\varphi = 109.32^\circ$. It is worth to underline that these states are located deep below Fermi energy, their occupation probability stems from electron distribution among large number of states. The number of the electron on these resonant states is 6 thus occupation probability $P = 3/4$. These states have important consequence for the charge analysis of the surface states.

IV. Work function

Wide applications of electron vacuum devices require creation of the cold cathodes that are effective sources of electrons. For some advanced applications the necessary condition is to emit the electrons efficiently of approximately kinetic energy. Thus cold emission is needed as it is the optimal way to attain this result. Therefore the electron affinity (EA), i.e. energy difference between conduction band minimum and the vacuum should be possibly low, or even negative.

The two other, EA related quantities, i.e. work function (WF) and the ionization energy (IE), are defined using the energy of the Fermi level and of the valence band maximum, respectively [3,5,42]. Naturally the common reference energy for all these three quantities is the vacuum level, i.e. far distance energy value. The measurement of these quantities is complex as these values are affected by the surface states, adsorbate etc. [56,57]. Thus the absolute value of any of these quantities is derived from the emission experiments which may be affected by number of factors [56]. Their absolute values, were finally determined to be $EA[AlN(0001)] = 1.9 \text{ eV}$ [41] and $3.2 \text{ eV} \leq EA[GaN(0001)] \leq 3.4 \text{ eV}$ [6]. The *ab initio* calculations gave for GaN $EA^{DFT}[GaN(0001)] \cong 3.73 \text{ eV}$ [3d]. More extensive *ab initio* calculation give smaller value for different surface coverage $EA^{DFT}[GaN(0001)] \cong 2.93 \text{ eV}$ [39].

It has to be noted that the potential profiles, plotted in Fig. 5 cannot be used directly for determination of these three surface characteristics (EA, WF and IE). These potentials were calculated in the case of periodic potential along c-axis, therefore far distance value is absent. The potential is corrected by the additional compensation gradient in the vacuum space [13,14] or the Laplace correction field [15]. Therefore the potential level is different on both sides of

the slab presented in Fig. 2. The workfunction is obtained using scaled value for Al in Ref. 34 [38].

The obtained potential profile is still very useful in different aspect. Adsorption of additional species may affect surface characteristics (EA, WF and IE) by additional surface dipole, in case when the adsorbed species are charged. This was studied in case of nitride surface covered by cesium adsorbed layer [38]. It is well known that the Cs 6s state has low binding energy, locating this level high in the absolute energy scale. In fact Cs atom attached to *GaN*(0001) surface is stripped of the electron and attached by electrostatic force only [38]. That creates additional electric dipole opposite to the fundamental dipole of the solid. Therefore the electric potential barrier is reduced from 9V to 5 V i.e. by about 4 V . Nevertheless the charge is compensated by the opposite charge at the surface thus not changing the potential profile within the slab as presented.

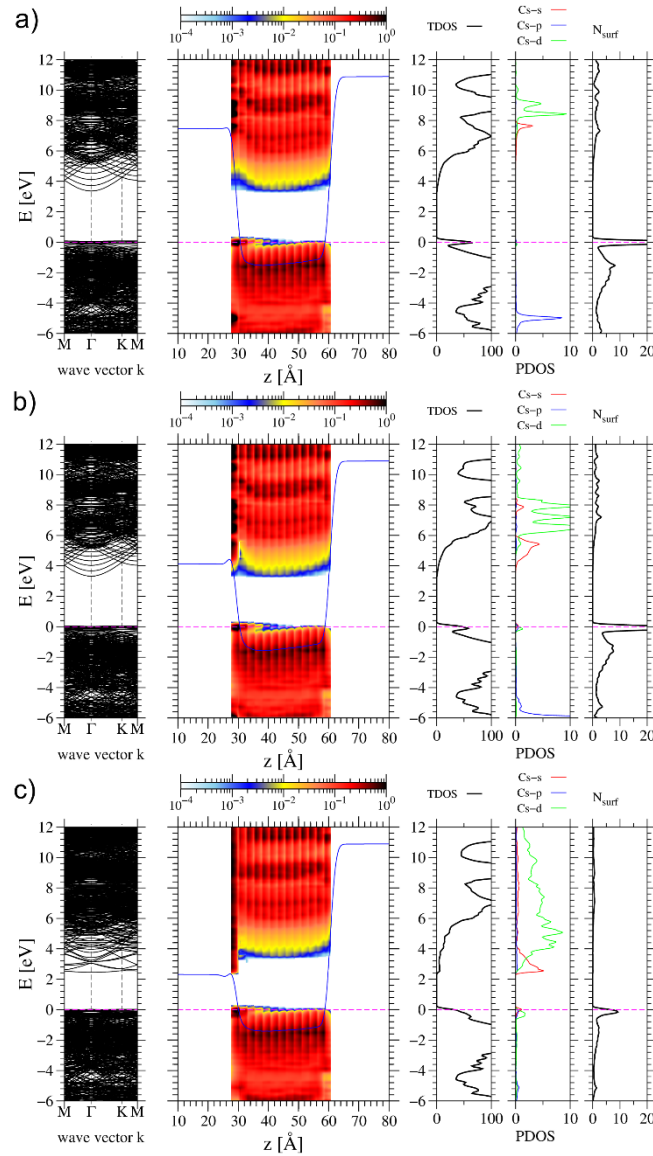


Fig. 7. Band diagram in momentum (left panel) and position space (middle panel) of the following number of Cs atoms: (a) single, (b) four, (c) eight atoms, attached to 4 x 4 slab representing wurtzite N-side GaN(0001) surface (i.e. 0.0625, 0.25 and 0.5 ML coverage). The panels on the right present density of states (DOS): total, Cs adatom and N surface atoms. The blue line superimposed on the position space diagram is electric potential, derived as above, plotted in units of electron energy. The colors in the central panel represent electron density according to the scale at the top. Reproduced Fig. 8 from Ref 38 [38].

The surface dipole layer and associated potential jump may be important for the course of adsorption processes at solid surfaces. Solid surfaces in contact with the vapor undergoes constant bombardment by vapor species. In the result, a fraction of these is attached, the others are repelled. The attachment at the surface requires energy loss during scattering, i.e. in relatively short time. Then the adsorbate could be immobilized in the potential well at the surface attaining the vibrational energy in accordance with the temperature of the solid, i.e. the adsorbate is thermalized [58]. The kinetic energy of the adsorbate at the temperature $T = 1000\text{ K}$ is of order of $kT = 86.17\text{ meV}$. The benchmark energy of the adsorbate attachment is $\Delta E = 1\text{ eV}$, i.e. at least one order of magnitude higher. Thus the parallel motion of the adsorbate is relatively slow, the adsorbate moves almost perpendicular to the surface. Therefore the other proposed scenario of the creation of the “hot” atoms [59 - 63], i.e. the adsorbate sliding along the surface over large distance to dissipate the kinetic energy does not capture the essence of the kinetic energy loss. The duration of the scattering event may be estimated assuming that the extension of the potential well is $d = 0.5\text{ nm}$ and the velocity is $v_{th} = \sqrt{\frac{\Delta E}{2M}} \approx 450\text{ m/s}$ the collision time is $\tau_{coll} \approx 10^{-12}\text{ s}$ [58]. Therefore the duration of the entire collision process is no longer than the typical frequency of the Brillouin zone boundary phonons in GaN which is of order of 15 - 20 THz [65,66]. Thus the collision time is of order of single phonon frequency. The emission of phonon bunches was proposed as thermalization channel [65]. The thermalization require emission large number of phonons in this period, thus nonlinear effects would result in creation of surface defects. The bombardment is intense, nevertheless creation of surface defects is not observed therefore other, faster more effective mechanism should be responsible for the effect. This channel should involve electronic degrees of freedom as these processes are fast to be effective in so short time scale. Therefore the electron tunneling

mechanism was proposed [58]. The existence of strong electric field induced by dipole layer causes electron jump from the approaching atoms into the solid interior. The estimated time of the jump is $\tau_{jump} \leq 10^{-14}$ s, therefore fast enough to be completed within collision time. Afterwards the high electron remains in the solid interior, that can dissipated the excess kinetic energy. This process may last longer but the essential for the course of the collision process is the retardation of the positively charged adsorbate. This is due to the interaction with the dipole layer electric field which act repulsively due to the opposite, positive charge of the adsorbate. The scheme of electric potential is presented in Fig. 8.

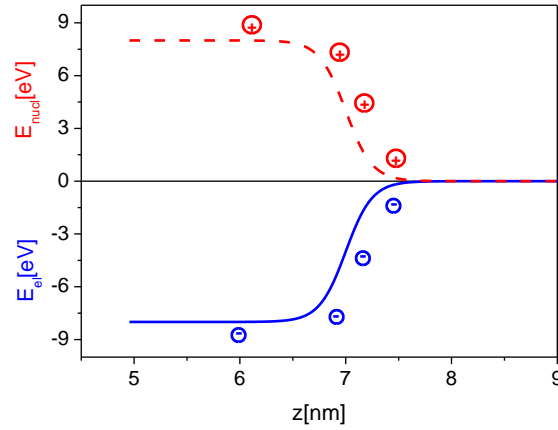


Fig. 8. The potential energy of the electron (blue solid line) and the positive ion (red dashed line) derived from AlN slab by *ab initio* method modeling. Reproduced Fig. 5 from Ref 58 [58].

It has to be added that these are preliminary investigations. The proposed scenario assumes that Born-Oppenheimer approximation, customarily used for description of the adsorption processes should be abandoned. In this approximation, the kinetic energy of the atomic motion is neglected, the energy is calculated with the immobile atoms. This is equivalent to the incorporation of additional, imaginary external force which stops adsorbate at each point along the adsorption path. In reality this is not the case, the adsorbate attains the kinetic energy. The dissipation by the proposed electrostatic repulsion involves the potential collectively so that the force is exerted on large number of the surface atoms directly and also via indirectly via interaction with electron charge. This new scenario needs to be further investigated as it could be helpful in the understanding of number of properties. This involves inevitably the surface dipole layer and associated electric potential.

V. Surface-internal charged dipole layer formation

In striking contrast to the external dipole layer influence discussed above, the internal surface dipole layer effects are well described for a long time [3 - 5]. The layer is in fact a consequence of pinning of Fermi level by fractionally occupied surface states. The band bending, necessary to attain uniformity of Fermi level over the entire conductive solid is related to accumulation of the mobile charge, i.e. screening. That leads to creation of internal surface dipole. In contrast to the earlier described external dipole of Lang and Kohn, the internal dipole is partially classical effect. The effect is described by screening length determined from Lindhard theory of charged gas screening [66]. In long distance limit this result is compatible with Thomas-Fermi screening length λ_{TF} for degenerate electron gas [3]:

$$\lambda_{TF} = \sqrt{\frac{2\varepsilon\varepsilon_0 E_F}{3ne^2}} \quad (1a)$$

and in the case of nondegenerate electron gas this is the Debye-Huckel screening length λ_{DH} [3]:

$$\lambda_{DH} = \sqrt{\frac{\varepsilon\varepsilon_0 kT}{ne^2}} \quad (1b)$$

where ε is the dielectric constant which for the case of GaN is: $\varepsilon = 10.28$. Other quantities are: k – Boltzmann constant, ε_0 – permittivity of vacuum, e - elementary charge, n – charge density and T – temperature in kelvins. The screening length depends on the temperature and the charge density. This value may be evaluated for typical conditions: for $T = 300\text{ K}$ and typical electron density for n-type GaN, i.e. $n = 10^{18}\text{ cm}^{-3}$ and $n = 10^{19}\text{ cm}^{-3}$ these lengths are: $\lambda_{DH} = 3.83\text{ nm}$ and $\lambda_{DH} = 1.21\text{ nm}$, respectively. Thus these conditions could be recovered in *ab initio* simulations. Therefore such simulations were made for GaN(0001) surface by Kempisty and Krukowski [67]. In these simulations two different cases of GaN(0001) surface was considered: bare and under full H – coverage. Both p – type and n-type doping was considered. The doping was made by the addition of the uniform charge background over the part of the volume occupied by the cores of the functional basis set in SIESTA, such that the total charge added is equivalent to a single electron. Thus for positive charge background additional electron has to be added for the occupation numbers which is equivalent to n-type doping. In the case of negative charge the number of the electrons occupying quantum states is smaller by one so that this corresponds to p-type doping. The doping level may be therefore estimated assuming single charge for 20 elementary cells, where the cell volume for GaN is $V_{GaN} = 46.0\text{ \AA}^3$. The calculations were made for the 20 GaN DAL slab therefore the doping level was $n = p \cong 10^{21}\text{ cm}^{-3}$. In order to achieve the convergence, the electron temperature was set to $T =$

1000 K. From the estimate it was that $\lambda_{DH}(10^{21} \text{ cm}^{-3}, 1000 \text{ K}) = 2.2 \text{ \AA}^3$. The simulation results for clean GaN(0001) surface are presented in Fig. 9.

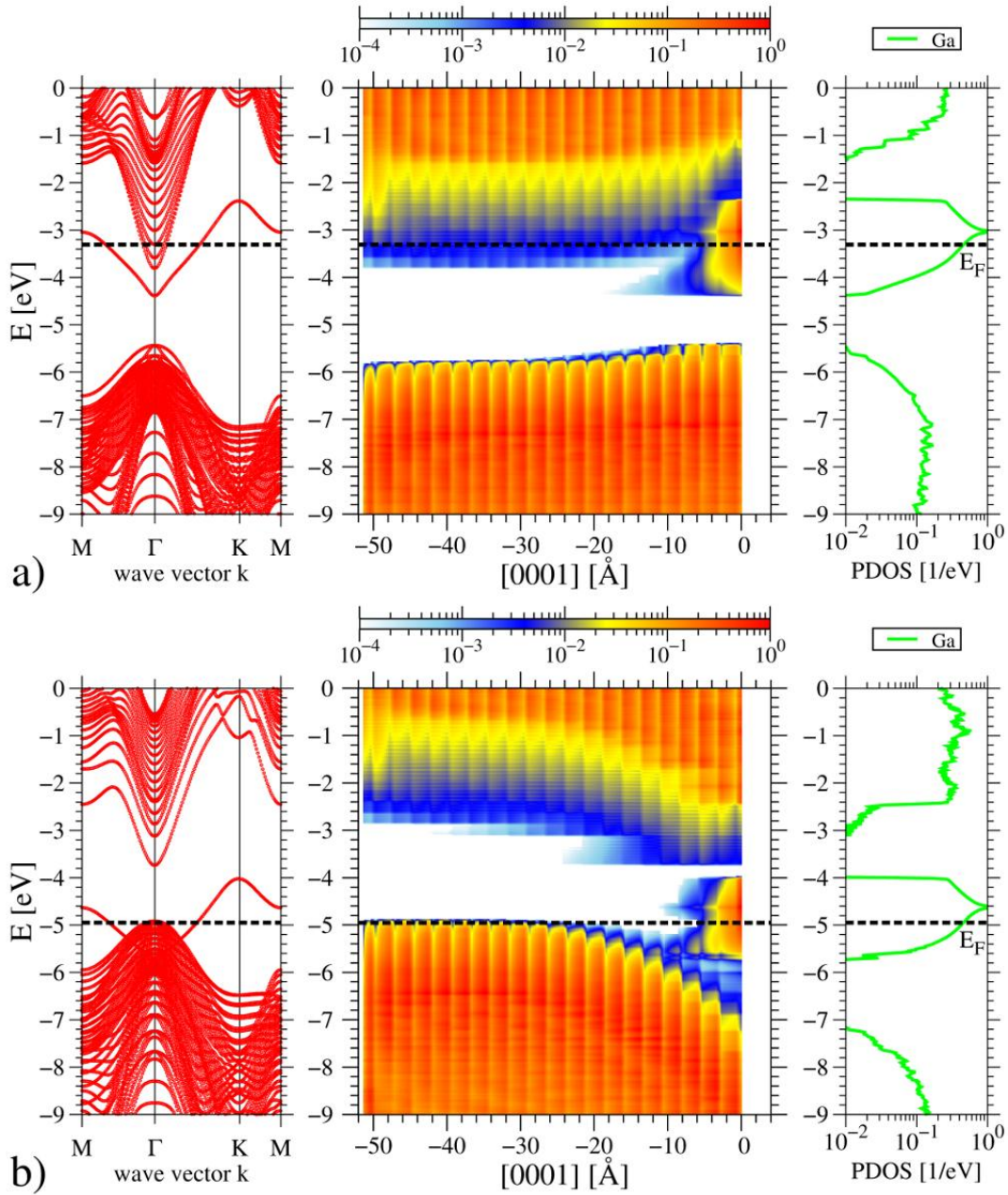


Fig. 9. Dispersion relations (left), space alignment of the bands derived from atom projected density of states (P-DOS) (middle) and DOS projected on surface gallium atoms (right) for clean GaN(0001) surface: a) n-type; b) p-type, obtained from 1 x 1 slab. The electronic temperature was 1000K. Reproduced Fig. 1 from Ref 67 [67].

It is well known that clean GaN(0001) surface, terminated by Ga-broken bond atoms has the surface with its energy located close to CBM. The state has wide dispersion about 2 eV wide and is partially filled. In case of n-type doping the Fermi level is pinned close to the CBM so that there is no band bending or nonlinear potential profile as the opposite side is not pinned. Drastic difference is observed for p-type doping. Here again the Fermi level is pinned by Ga-broken bond state, close to CBM. Thus the amplitude of the band bending is about the bandgap, i.e. $E_g \sim 3.47 \text{ eV}$. This is high difference so that the linear theory is not precise. The estimated screening length is $\lambda_{DH}(10^{21} \text{ cm}^{-3}, 1000 \text{ K}) = 2.2 \text{ \AA}$. In the simulation this length is close to $\lambda_{DH} \sim 10 \text{ \AA}$. Naturally, the doping level was estimated only, so that this could also contribute to the observed results.

Similar data are obtained for the case of Fermi level close to VBM, presented in Fig. 10.

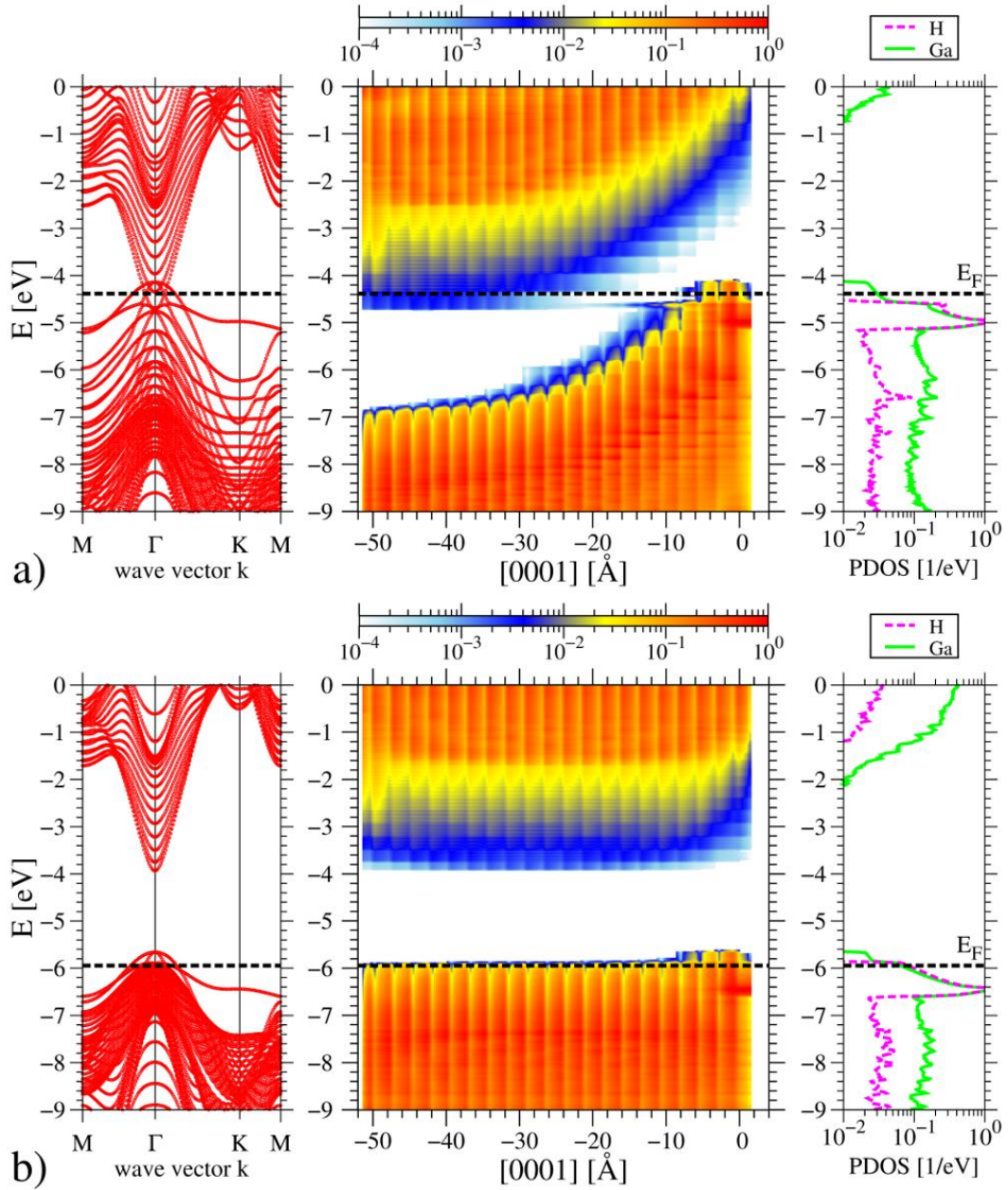


Fig. 10. Dispersion relations (left), space alignment of the bands derived from atom projected density of states (P-DOS) (middle) and DOS projected on surface gallium and hydrogen atoms (right), for fully hydrogen-covered GaN(0001) surface: a) n-type; b) p-type, obtained from 1×1 slab. The electronic temperature was 1000K. Reproduced Fig. 2 from Ref. 67 [67].

The results presented in Fig. 10 were obtained for GaN(0001) surface fully covered by H atoms in the on top positions [67]. This creates Ga-H bonding state of the energy close, but below VBM. The state has $n_e = 1 \frac{3}{4}$ electrons, one from H and $3/4$ from Ga broken bond, i.e. it is not fully occupied. Therefore the state is pinning Fermi level at the surface. In the case of p-type the pinning is close to Fermi level in the bulk so that no band bending occurs. In the case of n-

type band bending is again close to bandgap, i.e. $E_g \sim 3.47 \text{ eV}$. Again band bending extends much wider than the estimate. This may be attributed to several factors, such as charge carrier density lower than estimated, or nonlinear effects.

In general, the majority of the simulations use undoped slabs, thus the screening is much less effective. Therefore in the most cases, the potential profiles are linear which is related to the absence of the bulk charge and the difference in the energy of the states pinning Fermi level at both surfaces [15]. Such situation is typical, and is observed in Fig. 1 (a) and (b) and also in Fig 2 (c). In other cases, such as Fig. 1 (c) and Fig 2 (a) and (b), the profile is nonlinear which is related to the penetration of Fermi level in the bands and existence of the band charge. In case of Fig. 1(c) the Fermi level is in the conduction band in more than half of the slab thickness that leads to downward band bending close to Ga(0001) surface. In case of Fig. 2(a) Fermi level penetrates into valence band so that the holes are present close to $GaN(000\bar{1})$ surface. The band bending indicates presence of positive charge in the bulk. In case of Fig. 2 (b) this is the opposite, the negative charge is present in the bulk. Generally, these cases correspond to the presence of mobile charge and the screening of the charge occupying surface states.

Summarizing this part it is worth to stress out that the *ab initio* calculations are capable to catch the characteristic features of the doping in the bulk of the solids and its consequences to the surface internal dipole layer. It is possible to simulate the mobile charge at the surface and the screening of the surface charge in the interior. This is due to the presence of the mobile charge so that the Fermi level penetrates the bands close to the surface. Precise account of screening is possible in case of very heavy doping, of order of $n = p \cong 10^{20} \div 10^{21} \text{ cm}^{-3}$. For lower doping the other effective mass approaches could be used [4,5].

VI. Charge role in surface reconstruction

Reconstruction of semiconductor surface is one of the most prominent feature of the semiconductor surfaces that differs them from the surfaces of the other substances. In the case of the surfaces of other type substances, the phenomenon of reduction of translational symmetry is reduced and relatively rarely observed. Nevertheless in such cases a small displacement is sufficient to remove symmetry, therefore the small amplitude reconstructions are observed for surfaces of other crystals. The reconstructions that could drastically change the properties of the surfaces, and are large in magnitude are mainly observed in the case of semiconductor surfaces. Therefore, the main efforts of investigation of the reconstructions were directed towards investigation of reconstructions of semiconductor surfaces. They are intensively

investigated for many years so that large number of the various patterns was identified [3, 68, 69].

In these investigations several principal rules, governing the reconstruction selection, were identified. These rules in general indicate the transformation to semiconducting (insulator) surface by:

- (i) atomic relaxation that leads to lower total energy of the system by separation of the empty and occupied states,
- (ii) creation of new bonds,
- (iii) relaxation according to the electron counting rule (ECR).

Generally, these arguments are well based, as the transformations (i-iii) lead to the modification of the overlap of the quantum states by the atomic motion so that the occupied states have their energies lowered and the empty increased. As the occupied states are the only ones that contribute to the total energy of the system, the total energy value is decreased, i.e. more stable structure is attained.

ECR was proposed first by Chadi for the tight-binding analysis of As-rich reconstruction of GaAs surfaces [70] and then applied by Pashley in the interpretation of Transmission Electron Microscopic (TEM) images of GaAs(0001) – (2 x 4) surface [71]. The rule is essentially a simple calculation of electron occupation of the surface states, assuming the fractional charge contribution from broken bond state derived from chemical valence concept [70-72]. Thus, the fractional charge contribution from Ga broken bond is $q_{Ga} = 3/4$. Similarly, the fractional charge contributions from N and Si broken bonds are $q_N = 5/4$ and $q_{Si} = 1$, respectively. The contribution from the other elements from the same row in Periodic Table is identical. ECR calculation is proceeded as follows: assume that the total number of valence electron is: $Q = \sum_i q_i$ and the number of the quantum states below the supposed Fermi energy is: $N = \sum_j n_j$. Then the occupation of all states is $f = Q/N$. The following results can be obtained

- i) $f = 2$. The Fermi level is located above the higher energy of all included states, and below the energy of the first higher energy quantum state not included. Naturally each state is double spin degenerated. In case spin degeneration is removed, the f value should be changed to 1.
- ii) $f > 2$. The number of the states is not sufficient. The additional states should be added to until the condition $f \leq 2$ is attained. In the case the condition is attained assume that the lower energy states have occupation $f = 2$, subtract the

charge and the value. The ratio of the residue of the charge and the number of states gives the fractional charge of the highest energy state.

- iii) $f < 2$. The highest energy state or states are fractionally occupied. Then the highest states should be removed and the calculation repeated, to obtain the fractional occupation according to (ii).

In fact ECR procedure is equivalent to the well-known treatment of HOMO and LUMO orbitals in quantum chemistry [73]. Additionally the ECR calculation is a very simple version of the determination of the occupation of the one-electron states in DFT procedure. In the latter it is assumed that the occupation of the one-electron states is determined by Fermi-Dirac (F-D) statistics, i.e. the occupation fraction is real number obtained from F-D distribution at the selected temperature. ECR mimics this calculation in a drastically simplified way. In fact the surface states are taken into account only, those degenerated with valence band (VB) and conduction band (CB), are assumed to be occupied or empty, respectively. The important addendum is the assumption that these in the bandgap (i.e. broken bond states) are fractionally occupied. The latter is correct in the case when these surface states are located far away from the band states in energy scale. Thus ECR could be applied in case of bandgap surface states that are located deep in the bandgap. Nevertheless, in the difference to the Fermi-Dirac occupation numbers, ECR has the advantage to be informative, intuitively appealing when addressed to small number of states. Therefore it was applied and in large number of *ab initio* simulations [33-40]. Afterwards it was extended to use in the adsorption at semiconductor surfaces [67].

ECR provides basically correct guidance to the treatment of the structures of semiconductor surfaces. The minimal energy criterion is generally applicable to any systems in equilibrium. The deviation stems from the fact that such simple formulation does not take into account all contribution to the energy [74]. This formulation is not sufficiently elaborate to describe such different phenomena as those existing in semiconductor surfaces [3]. Even those that are limited to pure elemental semiconductor are not within the scope of the application of ECR.

Stoichiometric gallium nitride Ga-terminated GaN(0001) surface originally was identified as reconstruction-free [35]. This finding was confirmed by a number of other reports [36-39]. In addition, the Fermi level was determined to be pinned at the surface Ga broken bond, about 0.5 eV below conduction band minimum (CBM) [35-39]. As a rule these calculations employed small (2×2) slabs. Later investigation discovered (2×1) row

structure [75,76]. It was discovered that the difference between these two structures were very small and that the unreconstructed surface was due to persistent metastability.

Recently more detailed investigations of the stoichiometric GaN(0001) surface were undertaken using larger different size slabs, including (4×4) , (6×4) and (8×4) [77]. It was shown that reconstruction of GaN(0001) leads to division of the top Ga atom surface later into sp^3 and sp^2 coordinated Ga atoms. That leads to the division of the Ga-broken bond band into two separate subbands as shown in Fig. 12.

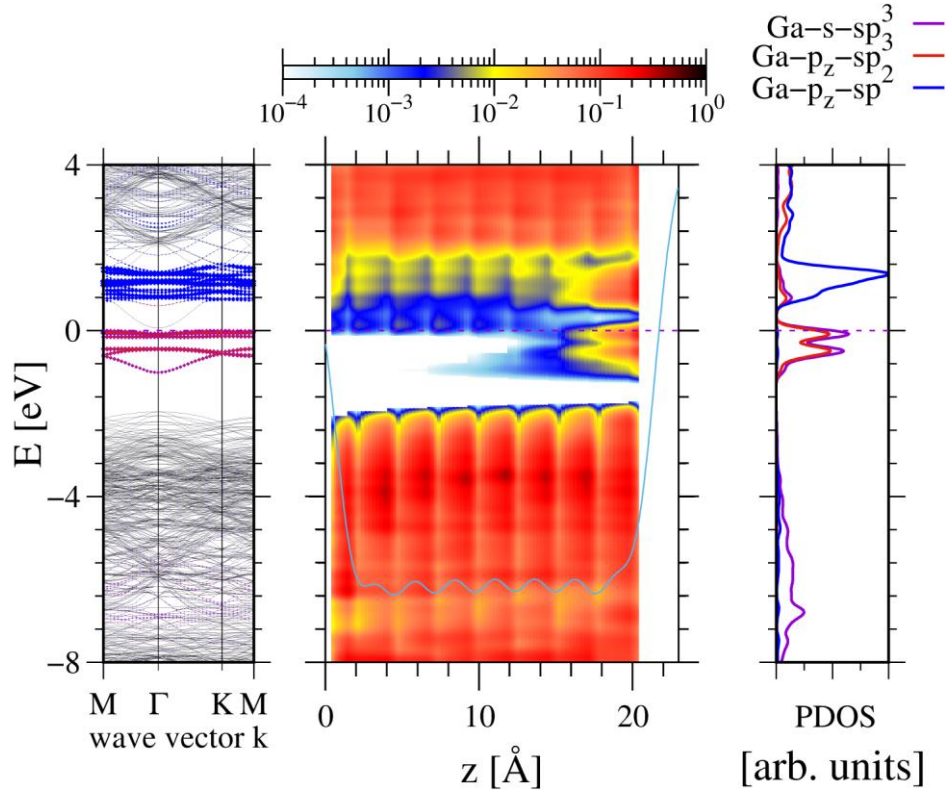


Fig. 11. Electronic properties of (4×4) 8 double Ga-N atomic layers (DALs) thick slab, representing stoichiometric Ga-terminated GaN(0001) surface: left – band diagram in momentum space, center - energy bands in real space, plotted along c-axis, right - partial density of states (PDOS) plotted for the top layer Ga atoms. The blue and magenta color represent surface layer Ga atoms: $Ga4sp^3$ hybridized and $Ga4p_z$ orbital states -in conjunction to $Ga4sp^2$ hybridized states, respectively. Reproduced from Fig. 1 Ref. 77 [77].

The first is created by the gallium sp^2 hybridized orbitals, the second with p_s states of sp^2 hybridized topmost Ga atoms. The existence of such separation is confirmed by the plots of GaN slabs in Fig. 12.

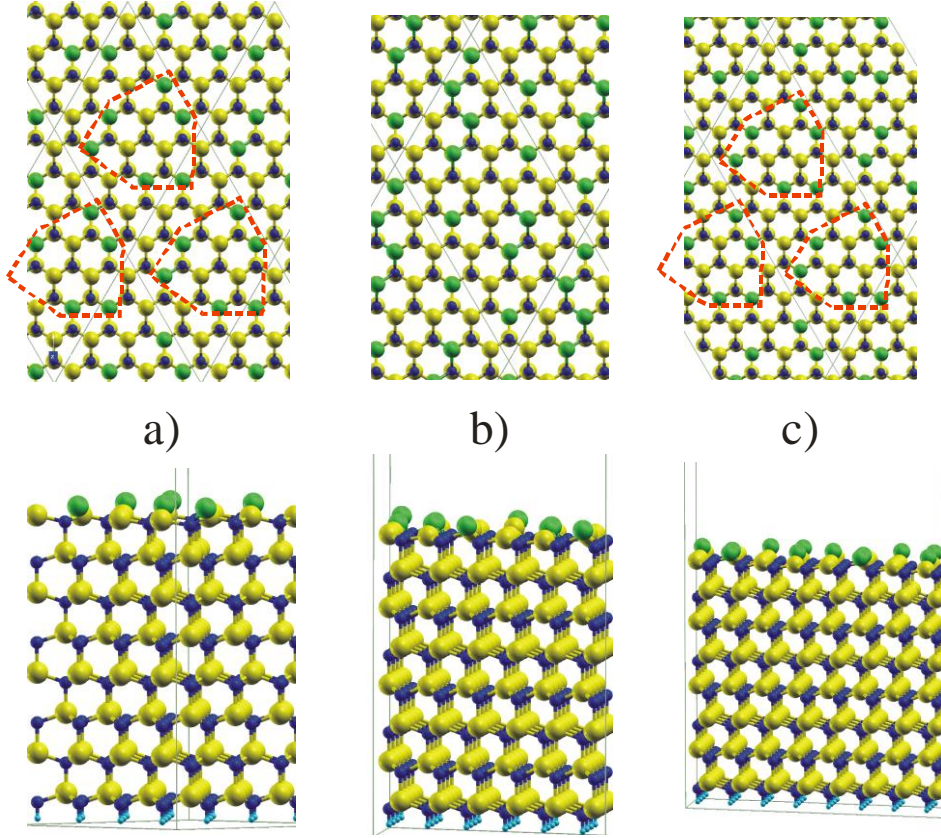


Fig. 12. Gallium nitride 8 Ga-N double atomic layer (DALs) thick slabs representing Ga-terminated GaN(0001) surface: a) (4×4) slab, b) (6×4) slab, c) (8×4) slab. The upper and lower rows present the top and side view, respectively. The balls represent the following atoms: blue – nitrogen, yellow – gallium, green – surface layer gallium (sp^3) hybridized, cyan – hydrogen termination pseudoatoms. The red color broken lines mark the basic units of (4×4) reconstruction pattern. Reproduced from Fig. 2 of Ref 77 [77].

As it is shown a fraction of topmost atoms are located in the plane of nitrogen layer atoms below, clearly indicating sp^2 reconstruction. In this figures the (4×4) reconstruction unit was identified. In fact this size was determined by ECR charge balance as follows. All Ga-N bonds are occupied therefore the excess charge for surface Ga top layer atom broken bond (i.e. vertical) is $(3/4)$ electron (elementary charge) for single Ga topmost atom. The ECR based electron charge balance thus assumes occupation by 2 electrons the vertical bond state in sp^3 configuration, i.e. a fraction of $(1-x)$ sites, and 0 electrons in p_z orbital in sp^2 hybridized atom, i.e. a fraction of x sites:

$$(1 - x) \times 2 + 0 \times x = \frac{3}{4} \quad (2)$$

From this relation it follows that the fraction of sp^2 hybridized Ga atoms is: $x = \frac{5}{8}$. The remaining fraction $1 - x = \frac{3}{8}$ Ga atoms is sp^3 hybridized. In fact, in (4×4) slab 10 Ga atoms should be located in the N atom plane while the remaining 6 Ga atoms are predicted to be located in the higher, lattice compatible positions. The distribution of Ga atoms in the topmost plane remains in a perfect agreement with this prediction. Similarly, in the case of (6×4) slab 15 and 9 Ga atoms are in the predicted position in a full agreement with the ECR argument. And finally, in the case of (8×4) slab, 20 and 12 Ga atoms are in sp^2 and sp^3 hybridization, respectively. In summary, the *ab initio* results fully confirms prediction based on ECR analysis, therefore the atoms are hybridized due to the electron redistribution. In the case of (4×4) and (8×4) slabs, the emerging (4×4) reconstruction is compatible with the slab periodicity. In case of (6×4) it is not, therefore this reconstruction is not observed. Thus successful simulations of the surface reconstruction requires proper choice of the simulation slab. Therefore for large size surface (4×4) reconstruction based on electron redistribution is energetically stable configuration of GaN(0001) stoichiometric surface. This identification was confirmed by the simulations of Mg and Si doped slabs where the fraction of the sp^3 and sp^2 hybridized Ga topmost atoms was changed.

The driving force of the above reconstruction is the difference of the energy of $Ga - s$ and $Ga - p$ orbitals. Therefore this reconstruction can occur for surfaces of typical III-V semiconductors such as GaAs(111). In case of the nitrides, Ga terminated surfaces can undergo this reconstruction such as investigated GaN(0001). On the contrary, nitrogen terminated surfaces will not undergo this reconstruction at N-terminated $GaN(000\bar{1})$ surface [12,34, 36]. Due to large difference in the energies of nitrogen s and p orbitals, the bonding of the solid does not involve sp^3 hybridization of nitrogen, therefore such reconstruction is not observed.

In conclusion it is claimed that these results prove the charge balance control of the energy optimization of semiconductor surfaces via reconstruction. This mechanism was proved in case of simple sp^3 to sp^2 bonding transition. More elaborate bonding, such as bridge formation, etc. need elucidation by the investigation of the charge contribution to the energy optimization in the future.

VII. Charge role in adsorption

1. Basic description

During adsorption of any species, the positively charged nucleus and negatively charged electrons are attached to the surface. In most cases when no charged species are present, e.g. in

exclusion of plasma processes, the attached adsorbate is electrically neutral. Thus, the existence of the external and internal dipole layers does not affect the adsorbate as the interactions between the field and the charge cancel out. Nevertheless, there is other charge related contribution that is not balanced perfectly [78, 79].

Adsorption at semiconductor surfaces generally leads to creation of the new covalent bonds between adsorbate and the surface. Thus, the quantum states are modified, so that their energy is lower. Additionally some of the states in the adsorbate, are added. In the process the number of the electrons is increased. Naturally some states with energy higher than Fermi level are also present but they do not contribute to the system energy. The important ones are only those that are located below Fermi level. Thus the contribution to the energy change of the system stems from the two basically different factors [78 - 80]:

- i) the change of the energy of the states occupied by the electrons,
- ii) the change of the number of the electrons in the system.

Since the number of new added electrons and the number of the newly added states could be different, the second effect may involve the change of the occupation of the surface states by their shift to lower or to the higher energy states. Both directions are possible, depending on the number of electrons and the number of the new states created. These additional electron transitions, between the surface states are different from the bond creation, as the effect involves electrons that are located on the surface states both before and after adsorption, therefore the phenomenon was named intra-surface state electron transition [80].

The intra-surface electron transition contribution thus depends on the position of Fermi level as these states, located close to Fermi energy, donate or accept electrons thus generating additional contribution to the adsorption energy. This effect may exist in adsorption at any surface causing the shift of Fermi level by the coverage increase until the maximum possible value is reached. There exist two different scenarios:

- i) there is no gap in the density of states (DOS) in energy range between the initial and final position of the Fermi level
- ii) there exist DOS gaps, one or more, in the above range.

The initial and final positions of the Fermi level is taken as the Fermi energy at the surface in total absence or close to or at the full coverage of the adsorbate. Thus in some cases the Fermi level may be selected for the coverage not equal but very close to zero or unity.

In the absence of the gap the change of the adsorption energy in function of the coverage is continuous. Thus the adsorption energy change related to the electron transition could be accommodated as the part of the bonding energy. This is the case of metal surfaces and also for

some cases at the surfaces of semiconductors or insulators. The gap case is different, because in the full overage range, there exist critical coverage ($\theta = \theta_{cr}$) at which the part of the surface states is fully occupied and the remaining ones are completely empty (at $T = 0\text{ K}$). At this coverage the adsorption energy may undergo the finite jump to the new value as the electron transition contribution changes in jump-like manner. This phenomenon could be observed for nonmetallic surfaces, i.e. for semiconductors and insulators.

In order to determine this possibility, the application of the procedure denoted as extended electron counting rule (EECR) was proposed in Ref. 67 [67]. First, the possibility of Fermi level jump across any energy gap should be determined. In order to do so the adsorption process has to be considered using smallest periodic surface unit at which the single adsorbate may be attached. The unit has to be defined in such a way that the entire surface is a direct sum of such units. Thus the surface coverage is zero or full. The EECR procedure is used to determine the Fermi level position for jump across the gap at fractional coverage from the analysis of the surface states. In this analysis all available additional information could be used, including the projected density of states (PDOS) and Crystal Orbital Hamilton Population (COHP) data [81, 82].

Technically the EECR calculation is used to determine the average fraction of the units with the adsorbate attached g ($0 \leq g \leq 1$). Assume that the number of the topmost surface atoms (adsorption sites) in the unit is z . Thus the unit may be a single site in the case of the adsorption in the on-top position ($z = 1$), a pair of sites in the case of the bridge configuration ($z = 2$), three sites in the case of H3 or T4 positions ($z = 3$), or even larger. The coverage θ is defined as the ratio of the adsorbates (molecules or atoms) to the number of the topmost sites in the unit i.e. $\theta = g/z$. Assume that the surface electron charge in the unit before adsorption event (i.e. for the coverage θ equal to zero) is $Q_i = \sum_i q$ where the occupation of the broken bond surface states is calculated using ECR prescription described above. The electron charge contributed by the adsorbate is $Q_a = \sum_a q_a$ where q_a are the number of the electrons in the atom a (index a runs over all atoms in the adsorbate). In the fractional occupation g there exist the surface states that were present before and after adsorption. Still they can be occupied due to position of Fermi level after adsorption. The number of such states is N_f . The number of occupied states due to the attached adsorbate is N_a . Then extended electron counting rule (EECR) determines the critical fraction g_{cr} of the units attached at which all states below Fermi level are occupied. The EECR charge balance is obtained from the electron charge (number) conservation equation:

$$Q_i + g_{cr} Q_a = N_a g_{cr} + (1 - g_{cr}) N_f \quad (3a)$$

This is constructed as follows: on the left is the charge in the system before adsorption Q_i . This is charge of the unit including the fraction occupied in accordance to ECR fractions for broken bonds. The second contribution is the charge added by the adsorbate which is proportional to the critical fraction and the charge of the adsorbate, i.e. $g_{cr} Q_a$. On the right hand this charge is distributed into the states of the covered part which is again proportional to critical fraction, i.e. $N_a g_{cr}$. The second term is due to the states that are occupied by the electrons in the fraction of the surface which is not covered, i.e. $(1 - g_{cr}) N_f$. This balance is used to determine the full occupation of the state below and zero above Fermi energy. Thus it is determined for the prescribed Fermi level jump across the gap. In the double spin degenerate case, i.e. $f = 2$ is used for the number of states N_f and N_a . From this relation the critical fraction and the critical coverage may be obtained

$$g_{cr} = z\theta_{cr} = \frac{Q_i - N_f}{(N_a - N_f) - Q_a} \quad (3b)$$

Alternatively, this relation could be understood also calculation of the occupied fraction of the units by consideration of the number of electrons donated and accepted:

- i) in the case of the donation of electrons from the surface state initially occupied ($Q_i > N_f$), i.e. when the Fermi level goes down. The number of the donated electrons from the surface states in the unit is: $Q_i - N_f$ as the initial number of the electrons is Q_i and the number of occupied states after (in ECR all states are occupied or empty) is N_f . The number of accepted electrons at the final state is $[(N_a - N_f) - Q_a]$ because $(N_a - N_f)$ is the number of the electron increase in the final state from which the number of the electrons contributed by the adsorbate, i.e. Q_a , should be subtracted.
- ii) in case of the acceptance of electrons at the initial state, i.e. initially empty ($Q_i < N_f$), i.e. when the Fermi level goes up. The number of accepted electrons is $N_f - Q_i$ as the number of electrons in final state is N_f and this number in initial state is Q_i . The number of donated electrons from the final state is $Q_a - (N_a - N_f)$ as $(N_a - N_o)$ is the number of the electron decrease (due to $N_a >$

N_o) in the final states for which the number of electrons contributed by the adsorbate i.e. Q_a should be added.

As mentioned above, the final state in the calculation correspond to full or close to full coverage $g \cong 1$. In reality a fraction g_{cr} is occupied as determined from the number of available electrons.

Several examples will be discussed here to demonstrate EECR calculation of the charge. First - the case of hydrogen adsorption on-top ($z = 1$) of the topmost Ga atom of GaN (0001) surface (Figs 9 and 10). In this case the initial charge is associated with the number of $3/4$ of gallium electrons associated with Ga broken bond, i.e. $Q_i = 3/4$. These broken bond states are located in the vicinity of CBM (Fig. 9). Hydrogen brings one electron i.e. $Q_a = 1$. In the final state Ga-H state is at VBM, therefore $N_a = 2$ and after adsorption (i.e. occupation close to unity) the broken Ga bond state is above Fermi level thus it is empty, i.e. $N_f = 0$ (Fig. 10). From this data it follows from Eq. 2b that $g_{cr} = \theta_{cr-H} = 3/4$.

The alternative determination based on argument (i) is as follows: broken bond state has $3/4$ electrons initially ($Q_i = 3/4$), and zero in the final state ($N_o = 0$). The adsorption of hydrogen brings one electron ($Q_a = 1$), thus in the final state we have from the adsorption $1 \frac{3}{4}$ electrons, i.e. $1/4$ electron is missing. This has to be borrowed from Ga broken bond states that is higher in energy. In fact single Ga broken bond state provides $3/4$ electrons i.e. sufficient to occupy fully 3 Ga-H states. Therefore the ratio of covered to empty sites is $3 : 1$, for three covered sites we have on site empty, and accordingly the critical coverage is $\theta_{H-cr} = 3/4$.

The second example is the mixed $\text{NH}_2\text{-NH}_3$ coverage where GaN(0001) surface is covered by mixture of NH_2 radicals ($\theta_{\text{NH}_2} = 0.75 \text{ ML}$) and NH_3 admolecules ($\theta_{\text{NH}_3} = 0.25 \text{ ML}$) [55] presented in Fig. 13. The EECR condition can be determined as follows: the coverage is full, i.e. all sites are covered either by NH_2 radicals or by NH_3 molecules. Therefore the change from NH_2 to NH_3 configuration may be treated as an attachment of H atom. The surface unit can be selected including single Ga surface atom site, i.e. $z = 1$. Thus the initial configuration consists of Ga broken bond with attached NH_2 radical. All NH_2 states are degenerated with the valence band: Ga-N states are located deep while N broken bond is at VBM. This confirms the location of the Fermi level at the midgap and the absence of the field inside the slab. Moreover the projected density of states (PDOS) and Crystal Orbital Hamilton Population (COHP) diagrams confirms that nitrogen and hydrogen s and p overlapped states are located in the valence band.

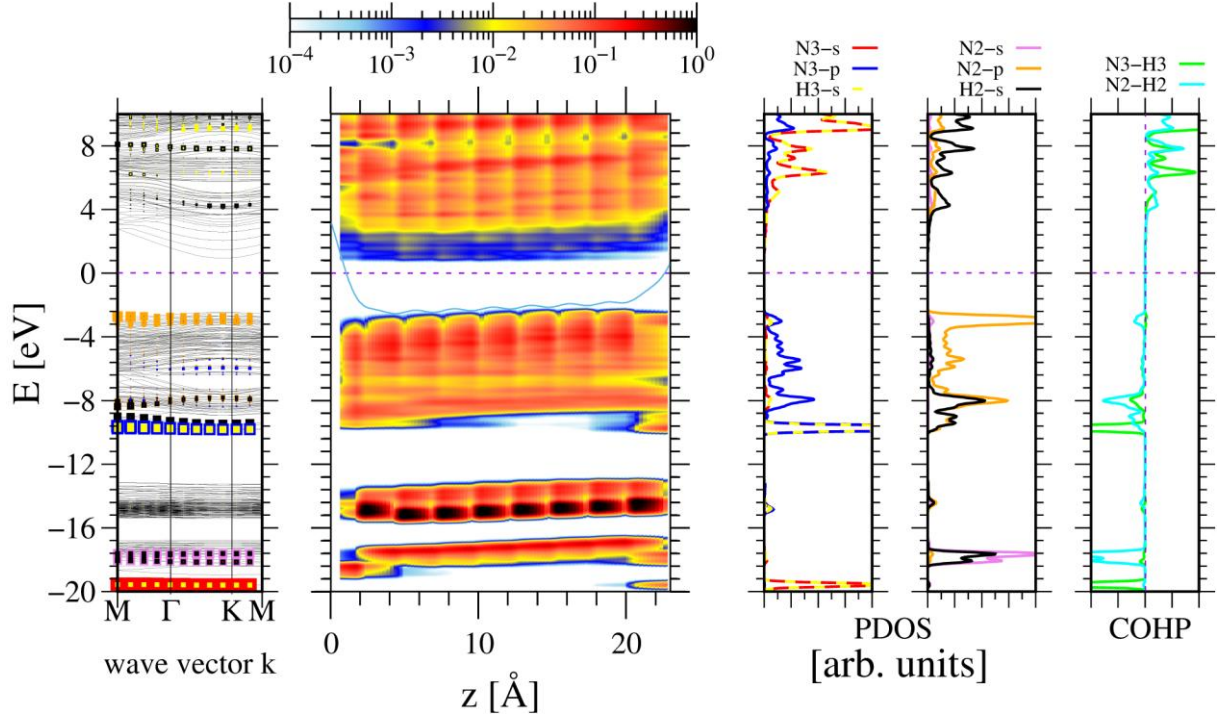


Fig. 13. Electronic properties of the (2×2) 8 GaN DALs slab, covered by single NH_3 admolecule and three NH_2 radicals representing GaN(0001) surface with $\theta_{\text{NH}_3} = 0.25 \text{ ML}$ and $\theta_{\text{NH}_2} = 0.75 \text{ ML}$ coverage. Two left panels - the band diagrams of the slab in momentum and real space respectively. Right panels – the first two present density of states (DOS) projected on the atom quantum s and p states of the nitrogen atom in HN_3 admolecule and NH_2 radical respectively. The rightmost panel present Crystal Orbital Hamilton Population (COHP) of nitrogen and hydrogen atoms in the admolecule and the radicals, respectively [54,55]. The color codes in PDOS and momentum diagrams are identical.

This remains in full agreement with the data presented in Fig. 13. More interesting are the nitrogen p states of NH_2 radicals without overlap. As indicated by COHP diagram these states are located at the top of valence band, thus they are also occupied. Therefore the occupation is full but $3/4$ electrons are borrowed from valence band. Accordingly the initial charge is $Q_i = 3/4 + 7$ in which $3/4$ in Ga-broken bond contribution and 7 stems from 5 electrons in nitrogen and 2 electrons from two hydrogen atoms. After adsorption the number of the states is $N_f = 8$. Thus all NH_3 states are occupied and $1/4$ electrons is shifted to conduction band as there is no states in the gap. The adsorbate, i.e. hydrogen atom charge is $Q_a = 1$. From Eq 3b it follows that $g_{\text{cr-H}} = \theta_{\text{cr-H}} = \theta_{\text{cr-NH}_3} = 1/4$. Thus the critical coverage is the mixture of NH_2 radicals ($\theta_{\text{NH}_2-\text{cr}} = 0.75 \text{ ML}$) and NH_3 admolecules ($\theta_{\text{NH}_3-\text{cr}} = 0.25 \text{ ML}$).

It is worth to note that EECR critical state does not correspond to any energetically preferable state of the surface, it is the coverage at which the Fermi level is liberated, i.e. located in the gap between one pinning state and the other. As such it is mere termination of the coverage range in which the jump of the Fermi level corresponds to the jump in adsorption energy. As argued above, this change usually corresponds to the absence of the internal dipole layer because the Fermi level is governed by its position in the bulk, i.e. no surface-internal charge is present. The example of the absence of the electric field in the slab is presented in Fig. 14.

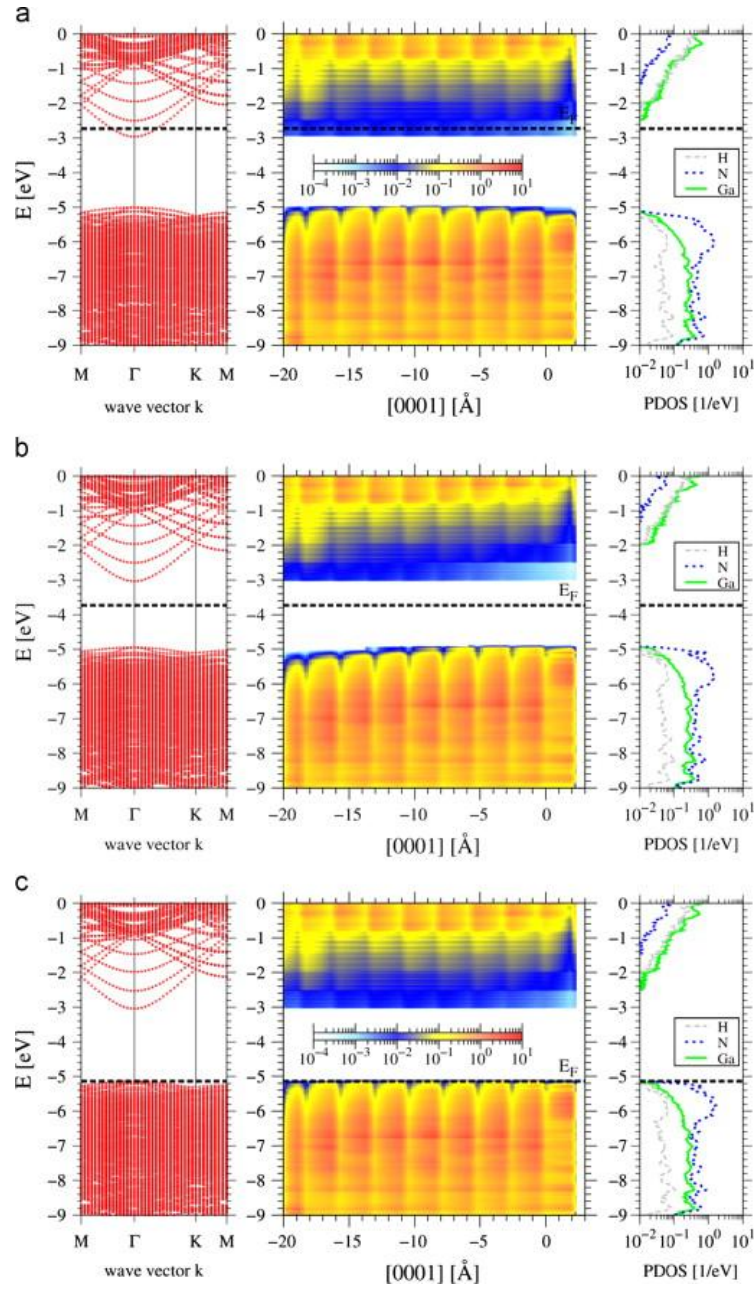


Fig. 14. Electronic properties of the (4x4) 8 GaN DALs slab representing GaN(0001) surface covered with 0.25 NH₃ ad molecules and 0.75 NH₂ radicals. Left – the band diagram

of the slab; middle – DOS projected on the atom quantum states (PDOS), showing the spatial variation of the valence and conduction bands in the slab; right – DOS of the topmost Ga atoms and NH_3/NH_2 admolecules. The states density scale (logarithmic) is included in the diagrams. Top, middle and bottom panels represent n -type, semi-insulating and p -type material respectively, simulated by charge background procedure implemented in SIESTA package. Reproduced Fig. 5 from Ref. 80 [80].

It is therefore expected that in the vicinity of the EECR state the adsorption energy depends on the doping in the bulk. The band profiles presented in Fig. 14 confirm this prediction, the bands are flat and the Fermi level is located in CB, VB and in the midgap for n -type, p -type and semi-insulating bulk GaN, respectively. As it was claimed, the adsorption energy should be approximately constant for wide range of the coverage (it may depend on adsorbate-adsorbate interaction only) and undergo considerable jump at EECR state where the Fermi level is liberated to be shifted to the other pinning state. This was best shown in the case of hydrogen adsorption at GaN(0001) surface. In this case molecular hydrogen is dissociated during adsorption and the resulting hydrogen atoms are located in the on-top positions. Hydrogen is exemplary case because it is small, so the quantum overlap is extremely small so that these atoms are essentially noninteracting [81]. The surface unit consist of single Ga site, to which H atom is attached. The Ga broken bond state is located 0.5 eV below CBM, therefore it is empty, i.e. $n_i = 0$, it is fractionally charged by $3/4$ electron thus $q_i = 3/4$. Ga-H two spin states are located at VBM, therefore it is occupied thus $n_f = 2$. Hydrogen brings single electron therefore $q_a = 1$. From Eq. 2a the EECR critical hydrogen coverage is $\theta_{H-cr} = 3/4$. At this coverage Fermi level is free, for $\theta < \theta_{H-cr}$ Fermi level is pinned by Ga-broken bond state below CBM, for $\theta > \theta_{H-cr}$ it is pinned by G-H state at VBM. Therefore it is expected that the adsorption energy have a jump as presented in Fig. 15. The adsorption energy was obtained from *ab initio* calculations, according to the formula:

$$\Delta E_{DFT}^{ads-GaN}(H) = E_{DFT}^{tot}(slab + H) - E_{DFT}^{tot}(slab) - E_{DFT}^{tot}(H) \quad (4)$$

and plotted in Fig 15 for entire range hydrogen coverage ($0 \leq \theta_H \leq 1$). The adsorption energies were calculated for the atomic hydrogen adsorption [$H(v) \rightarrow H(s)$] and the molecular adsorption [$H_2(v) \rightarrow 2H(s)$] are [81]:

$$\Delta E_{DFT}^{ads-GaN}(H) = \begin{cases} -3.40 \text{ eV} & \theta_H < 0.75 \text{ ML} \\ -1.10 \text{ eV} & \theta_H > 0.75 \text{ ML} \end{cases} \quad (5a)$$

and

$$\Delta E_{DFT}^{ads-GaN}(H_2) = \begin{cases} -2.24 \text{ eV} & \theta_H < 0.75 \text{ ML} \\ 2.36 \text{ eV} & \theta_H > 0.75 \text{ ML} \end{cases} \quad (5b)$$

The jump by about 2.30eV is due to electron transfer from Ga broken bond to H bonding state located below VBM, present and absent for low and high coverage, respectively. The energy difference, obtained for dissociative adsorption of molecular hydrogen and the adsorption of atomic hydrogen is in accordance with the molecular hydrogen dissociation energy. This energy was taken $E_{DFT}^{diss}(H_2) = 4.56 \text{ eV}$. This is slightly different from the experimental value $E_{exp}^{diss}(H_2) = 4.58 \text{ eV}$ [83]. As it is shown in Fig. 15 the adsorption energy is constant with the random variation below 0.1 eV.

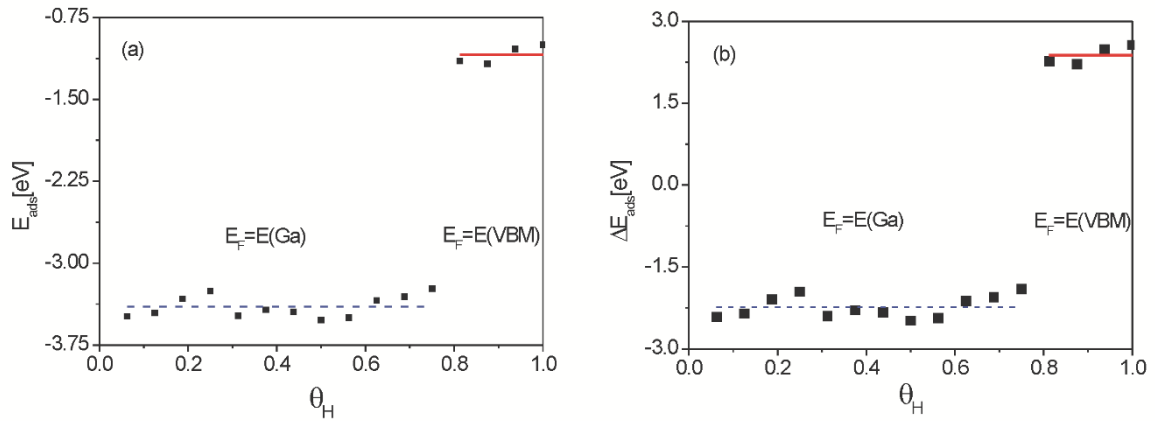


Fig. 15. Atomic (a - Eq. 3a) and molecular (b - Eq. 3b) hydrogen adsorption energy in function of hydrogen coverage of the GaN(0001) surface (black squares), calculated using 4 x 4 slab. The horizontal lines represent coverage independent energy values for low and high coverage regime, denoted by dashed blue and solid red lines respectively. Reproduced Fig. 7 from Ref. 81 [81].

Additional effect is observed for the above presented case of NH_2/NH_3 coverage of GaN(0001) surface [81]. The band structure of the surface covered by $\theta_{\text{NH}_2-cr} = 3/4$ and $\theta_{\text{NH}_3-cr} = 1/4$ is presented in Figs 11 and 11. As it was shown in Fig. 12, n-type, SI and p-type doped crystals has the Fermi level descending from CBM, midgap to VBM. The NH_2 to NH_3 conversion is essentially an attachment of a single hydrogen atom. The adsorption energy presented in Fig 14 shows the energy change during attachment of H_2 molecule at (4×4) i.e.

16 site slab. The adsorption for the case of finite state above critical value, i.e. $\theta > \theta_{cr-NH_3} = 1/4$ leads to the shift of electrons to the other states, i.e. above Fermi energy. As it is shown in Fig. 16, the reduction of the energy gain occurs exactly at $\theta = \theta_{cr-NH_3} = 1/4$ for n-type as these electrons are shifted up very high. Subsequently, this reduction is observed for SI and p-type as in these cases these electrons are located first in the partially empty VB states. Further increase of the coverage leads to the energy gain until energy gain finally becomes negative due to electron transfer over the gallium nitride bandgap. This effect is second confirmation of the electron character of the observed effect of adsorption energy change.

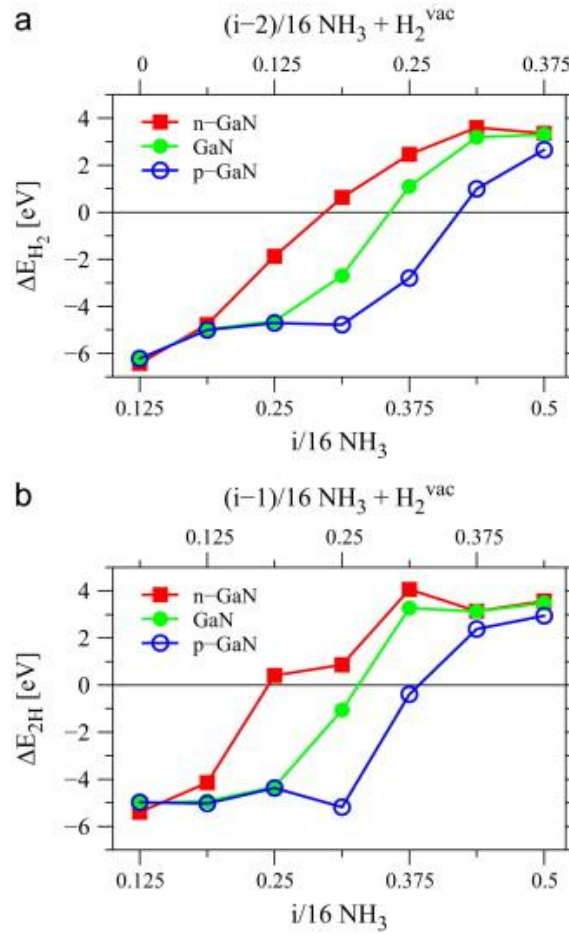


Fig. 16. Energy changes during adsorption/desorption of H_2 molecule on GaN(0001) surface covered with various NH_3/NH_2 mixture. The data are obtained for *n*-, *p*-type and semi-insulating bulk. The negative value of energy means that the surface configuration indicated on the bottom horizontal axis has a lower energy than the configuration marked on the upper axis. Reproduced Fig. 4 from Ref. 80 [80].

It is worth to stress out that the adsorption energy jump related to intra-surface electron transfer exerts profound effect on the thermodynamic properties of the two-phase semiconductor-vapor systems. From Van t'Hoff relation it follows that the equilibrium pressure of the adsorbate p depends exponentially on the evaporation energy ΔH , i.e. $p \approx \exp\left(-\frac{\Delta H}{kT}\right)$. Generally the evaporation energy ΔH can additionally change due to thermal contribution to the enthalpy, i.e. $\Delta H(T) = \Delta H(T_o) + \int_{T_o}^T \Delta C(T)dT$. The thermal contribution to this difference may be calculated assuming that:

- i) for the vapor phase, the thermal contributions stem from the translational, rotational and vibrational degrees of freedom [84-88],
- ii) for the adsorbate the thermal contribution to enthalpy, entropy and free energy arises from the lattice vibrations only [83].

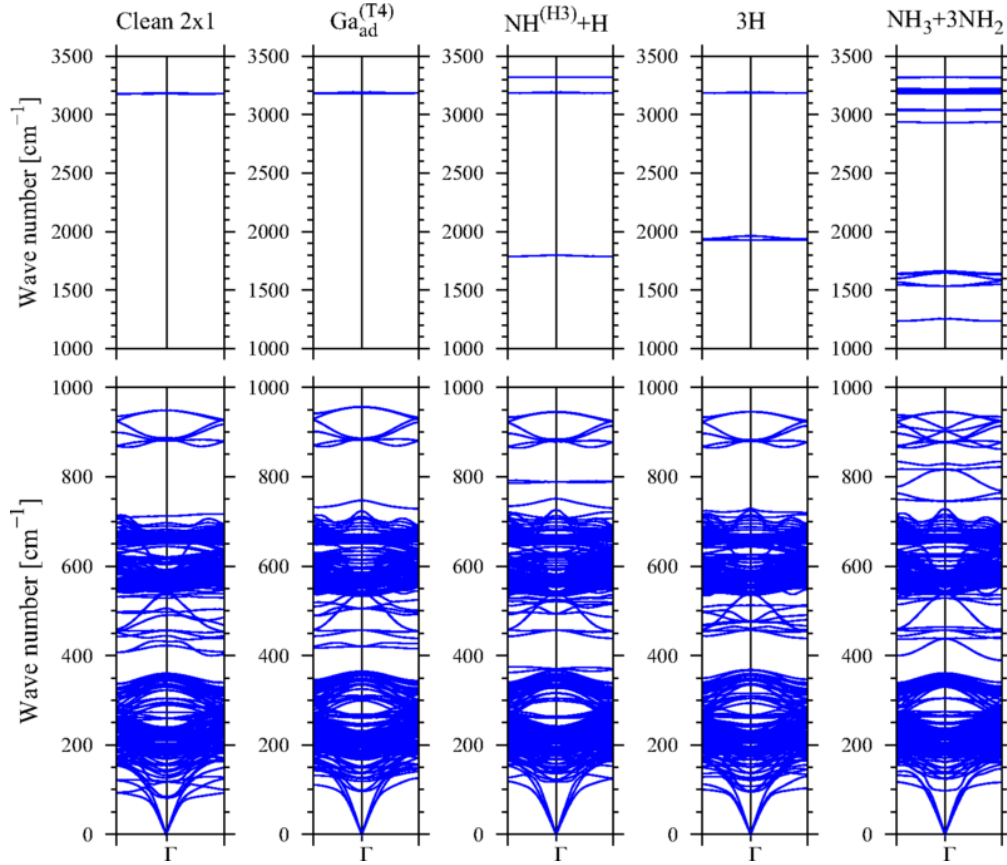


Fig. 16. Phonon dispersion relations of (2 x 2) slab representing GaN(0001) surface: lower row – full slab spectra, upper row – only spectra associated with different adsorbate: from the left: none, Ga adatom, NH-radical in H3 position plus H adatom, 3 H adatoms, NH₃ admolecule and 3 NH₂ radicals. In addition, the modes associated with pseudo-hydrogen termination atoms at the opposite surface are shown (approximately 3200 cm^{-1}). The bands in the range between

850 cm^{-1} and 950 cm^{-1} are related to N atom close to the termination. Reproduced Fig. 3 from Ref. 87 [87].

The adsorbate part was treated in a simplified way employing the vibrational degrees of freedom only (ii). This is in some sense reduction of the more general approach (i) used for the derivation of the data shown in the thermochemical tables for the molecules and atoms. Since the adsorbates are located in the lattice sites, only the vibrational calculations were applied [87]. In this case, the adsorbate contribution is defined as the difference between the vibrational spectrum of the slab with and without adsorbate. The example of such calculation results is presented in Fig. 16 for the case of GaN(0001) surface with several adsorbates. The results show additional modes associated with the several adsorbates. In addition, by direct summation the zero point energy may be calculated as difference of the energies of the ground quantum states of the adsorbed atoms and the molecule in the vapor: $\Delta E_{sv}^{ZPE} = 2E_s^{ZPE}(H) - E_v^{ZPE}(H_2)$

From these spectra the standard thermodynamic formulae may be used to derive thermodynamic quantities by direct summation [87-89]

$$E^{vib}(x) = k_B T \sum_j \frac{x_j}{\exp(x_j) - 1} \quad (6a)$$

$$C^{vib}(x) = k_B \sum_j \frac{x_j^2 \exp(x_j)}{[\exp(x_j) - 1]^2} \quad (6b)$$

$$S^{vib}(x) = k_B \sum_j \frac{x_j}{\exp(x_j) - 1} - \ln[1 - \exp(-x_j)] \quad (6c)$$

$$F^{vib}(x) = k_B T \sum_j \ln[1 - \exp(-x_j)] \quad (6d)$$

where $x_j \equiv \frac{\hbar \omega_j}{k_B T}$ and ω_j is phonon frequency of a j-th phonon mode. From these formulae the temperature dependent free energy vibrational contribution $\Delta F^{vib}(T)$ and zero point energy contribution was ΔE^{ZPE} were calculated for several adsorbates at GaN(0001) surface [89]. The

results are shown in Fig. 17.

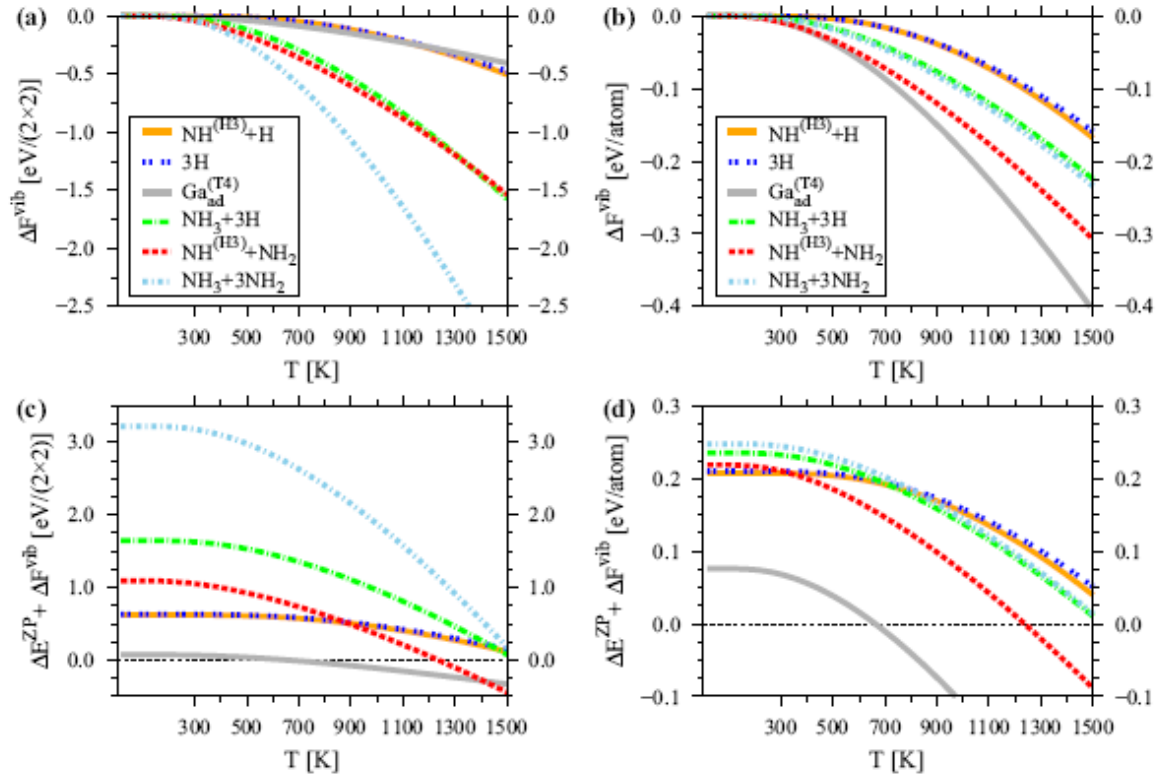


Fig 17. Changes in the vibrational free energy versus temperature for the GaN(0001) surface covered with different adsorbates, determined in relation to clean surface with 2×1 reconstruction; (a), (b) $\Delta F^{vib}(T)$ dependence; (c), (d) $\Delta F^{vib}(T)$ dependence including zero-point ΔE^{ZPE} offset. Graphs (a) and (c) show energies of the entire 2×2 surface cell, while graphs (b) and (d) show the average energy per atom. Fig 4 from Ref 87 [87].

A simplified treatment may be alternatively used, based on Debye theory in which the acoustic phonon frequencies are approximated by linear dependence on the wavevector. Accordingly, the maximum phonon energy, known as the Debye energy, and its equivalents: the Debye frequency and the Debye temperature, are related as follows: $E_D = \hbar\omega_D = k_B\theta_D$. Using this simplified representation, thus the complex summation is replaced by integration [89]:

$$E^{vib}(T) = 9k_B T \left(\frac{T}{\theta_D}\right)^3 \int_0^{\theta_D/T} \frac{x^3 dx}{\exp(x)-1} \quad (7a)$$

$$C^{vib}(T) = 9k_B \left(\frac{T}{\theta_D}\right)^2 \int_0^{\theta_D/T} \frac{x^4 \exp(x) dx}{[\exp(x)-1]^2} \quad (7b)$$

$$S^{vib}(T) = 9k_B \left(\frac{T}{\theta_D}\right)^3 \int_0^{\theta_D/T} \left\{ \frac{x}{\exp(x)-1} - \ln[1 - \exp(-x)] \right\} x^2 dx \quad (7c)$$

$$F^{vib}(T) = 9k_B T \left(\frac{T}{\theta_D}\right)^3 \int_0^{\theta_D/T} x^2 \ln[1 - \exp(-x)] dx \quad (7d)$$

In case of hydrogen adsorbed at GaN(0001) surface, the Debye formulation provided satisfactory approximation to exact summation [89]. This formulation show that the interaction between the adsorbate and the substrate may be complex, quite different from simple increase of the number of the degrees of freedom and emergence of additional frequencies. The interaction may affect the elastic lattice properties so that the specific heat change may be negative at low temperature due to the lower excitement of large number of lattice vibrations that can offset the increase of the number of degrees of freedom during adsorption. Generally, this is reflected in the coverage dependence of the effective Debye temperature, which for complex adsorbate may be substantial. Thus in the case of Al adsorption at AlN(0001) surface [90] it is

$$\theta_D(\theta_{Al}) \cong \begin{cases} 1002.4 - 1254.5\theta_{Al} + 745.1\theta_{Al}^2 & \theta_{Al} \leq 1 \\ 493 & 1 < \theta_{Al} \leq 2 \end{cases} \quad (8)$$

which reflects the dramatic reduction of the stiffness for higher Al coverage, e.g. $T_D(\theta_{Al} = 0.1) = 875 \text{ K}$ which is reduced to $T_D(\theta_{Al} = 0.75) = 550 \text{ K}$ [90]. Naturally, zero point energy is also coverage dependent:

$$E_{Al}^{ZPE}(\theta_{Al}) \cong 0.097 - 0.101\theta_{Al} + 0.06\theta_{Al}^2 \quad (9)$$

That complicates use of simplified formulation. It is worth to note that the presence of the adsorbate may lead to the increase but also to decrease of the heat capacity. This is shown for the case of Al adsorption on AlN(000-1) surface presented in Fig. 18.

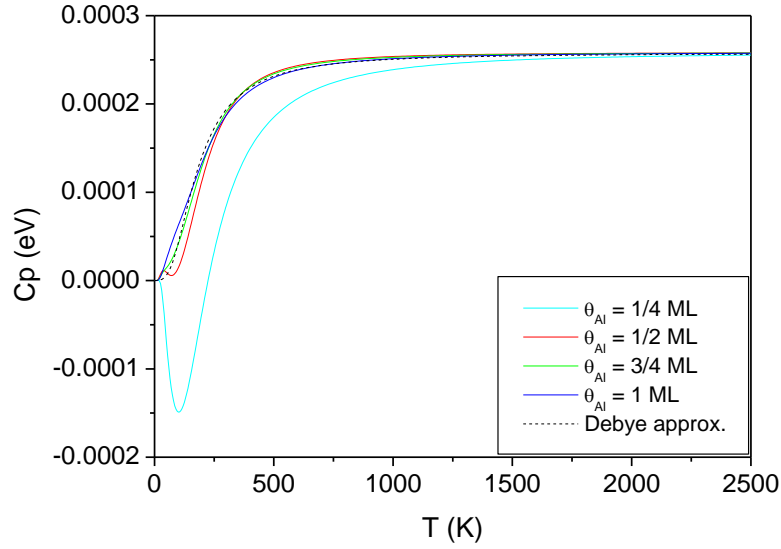


Fig. 18. Temperature dependence of the specific heat related to Al adatoms, attached to 4×4 slab representing AlN(0001) surface, obtained from phonon frequency summation (solid lines). For the comparison, the specific heat obtained for the Debye temperature $\theta_D = 740$ K is plotted using broken line. Reproduced Fig. 13 from Ref 90 [90].

The specific heat becomes negative for low Al coverage at low temperature. Since the obtained increase of the heat difference due to attachment of Al adatoms is compensated by the negative contribution related to the adsorption that stiffen the lattice, so that the overall contribution is negative. This is observed for low temperature only, for higher temperature all degrees are excited so the increase is positive.

The thermodynamic quantities of the vapor phase were calculated according to the formulation (i) and tabulated for large number of substances that may be used for derivation of effective formulae for enthalpy, entropy and free energy. These tables provide thermodynamic data for all elements and compound in two basic states of matter: vapor at normal pressure $p = 1\text{ bar}$ and the condensed phase (solid/liquid) up to 3000 K. Therefore it is sufficient to obtain sufficiently precise data which could be used for the vapor phase contributions.

Accordingly the exact calculation of the equilibrium is possible. This was formulated first for 3-d transitions by Jackson and Walsh [91] and independently for surface adsorption (2-d) by Kempisty et al. [84]. Remarkably, the results formulated as solid/surface-vapor chemical potential difference $\Delta\mu_{sv}$, were identical. Here we present chemical potential difference (which is zero at equilibrium) formulae for dissociative adsorption of molecular hydrogen (H_2) at GaN(0001) gallium terminated gallium nitride surface [88]:

$$\begin{aligned}
\Delta\mu_{sv}(p, T) &= \mu_{H(s)}(T, x) - \frac{1}{2}\mu_{H_2(v)} = \Delta H_{dis}^{DFT}(0) + \Delta G_{ads} + \Delta H_{therm} + \Delta G_{S-therm} + \\
&\Delta G_{pres} + \Delta G_{conc}(T, \theta_N) = \Delta H_{ads}^{DFT} - T_o \Delta s_{sv} + \int_0^{T_o} (C_s - C_v) dT - \int_{T_o}^T (s_s - s_v) dT + \\
&\int_{p_o}^p (v_s - v_v) dp + k_B T \ln \left(\frac{\theta_N}{1 - \theta_N} \right) = 0
\end{aligned} \tag{10}$$

where the surface-vapor chemical potential difference $\Delta\mu_{sv}$ is expressed as sum of:

- i) enthalpy change at adsorption $\Delta H_{ads}^{DFT} = \Delta E_{DFT}^{ads-GaN}(H_2) + \Delta E_{sv}^{ZPE}$, taken as the sum of adsorption energy and zero point energy difference. The former is obtained from *ab initio* calculations, and given by Eq. 4. Note that this quantity undergoes jump at $\theta_H = \theta_{H-cr} = 0.75 ML$. The latter is given as $\Delta E_{sv}^{ZPE} = 2E_s^{ZPE}(H) - E_v^{ZPE}(H_2)$. This value was obtained from *ab initio* phonon calculations $\Delta E_{sv}^{ZPE} = -0.21 eV$ [87] and is much smaller than the enthalpy change.
- ii) the free energy $\Delta G_{ads} = -T_o \Delta s_{sv}$ related to the entropy change at adsorption that could be obtained as the difference of entropies of nitrogen at the surface and in the vapor $\Delta s_{sv} = 2s_s - s_v$, where solid phase entropy is due to phonon contribution only as solid phase entropy is zero thus free energy contribution is therefore $\Delta G_{ads} = 0.633 eV$ [88].
- iii) the thermal enthalpy change $\Delta H_{therm} = 2h_s(T_o) - h_v(T_o) = \int_0^{T_o} (2C_s - C_v) dT$ in which the enthalpy of the adsorbate is $h_s(T_o) = 1.71 \times 10^{-4} eV$ and $h_v(T_o) = 8.99 \times 10^{-2} eV$ that gives $\Delta H_{therm} = -0.051 eV$ [88]. This component is relatively small.
- iv) the thermal entropy change $\Delta G_{S-therm} = \int_{T_o}^T (2s_s - s_v) dT = [2[\mu_{H-s}(T) - \mu_{N-s}(T_o)] - \mu_{H_2}(T) - \mu_{H_2}(T_o)]$ which could be obtained from free energy dependence of ideal H_2 vapor at 1 bar, given as [92]:

$$\mu_{H_2}(T) = -1.22 \times 10^{-3} T - 0.26 \times 10^{-6} T^2 + 2.4 \times 10^{-11} T^3 \tag{10}$$

while the chemical nitrogen chemical potential of nitrogen at the surface could be approximated to Debye thermal dependence as

$$\mu_{H-s}(T) = 7.56 \times 10^{-6} T - 2.38 \times 10^{-7} T^2 + 3.26 \times 10^{-11} T^3 \tag{11}$$

which combined $\Delta G_{S-therm}(T) = 2\mu_{H-s}(T) - \mu_{H_2}(T)$ give the

$$\mu_{H_2}(T) - 2\mu_{H-s}(T) = -1.23 \times 10^{-3}T - 2.82 \times 10^{-7}T^2 + 1.54 \times 10^{-11}T^3 \quad (12)$$

that determines this value at any T. At $T = 1300 \text{ K}$ this contribution is

$$G_{S-therm}(1300 \text{ K}) = -1.497 \text{ eV}.$$

- v) pressure dependent term can be used in ideal gas approximations, as the typical growth nitride vapor growth conditions correspond to high temperature and limited pressure : $\Delta G_{pres} = k_B T \ln(p_{N_2}/p_o)$ where $p_o = 1 \text{ bar}$.
- vi) the configuration term $\Delta G_{conc}(T, \theta_N) = k_B T \ln(\theta_N/(1 - \theta_N))$. The term is responsible for Langmuir singularity at $\theta_N = 1$, therefore in the vicinity of the full coverage can attain very high values.

In total, several terms contribute similar values. The pressure dependent term can be used for the determination of the equilibrium pressure of hydrogen at GaN surface at any temperature according to the formula [88]:

$$\frac{p}{p_o} = \left(\frac{\theta_H}{1-\theta_H}\right)^2 \exp\left\{\frac{-[\Delta H_{vap} + \Delta H_{therm} + \Delta G_{S-vap} + \Delta G_{S-therm}]}{k_B T}\right\} \quad (14)$$

The results of these calculations are given at Fig. 19.

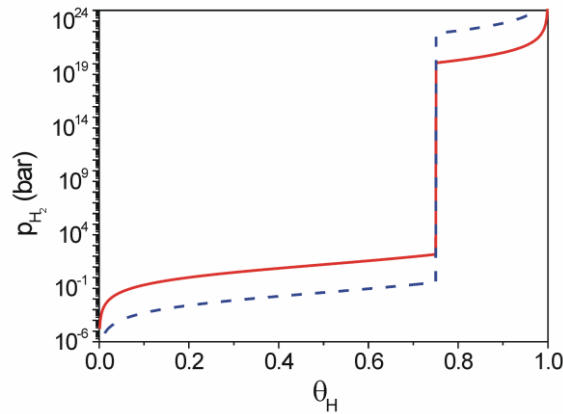


Fig. 19. Equilibrium pressure of molecular hydrogen at GaN(0001) in function of hydrogen coverage. The two lines: dashed blue and solid red correspond to 1000K and 1300K, respectively. Reproduced Fig. 2 from Ref 88 [88].

From these data it follows that the equilibrium pressure of the vapor strongly depends on the temperature which is related to the thermal contribution to the chemical potential difference (ii-v). Nevertheless the most important is jump-like change at the critical coverage $\theta_H = \theta_{H-cr} = 0.75 ML$ where the pressure change is by far the greatest. Additionally, at both ends, i.e. $\theta_H = 0$ and $\theta_H = 1 ML$, the entropy contribution diverges asymptotically. In summary, the charge related term is most important contribution affecting equilibrium between molecular hydrogen and GaN(0001) surface. Below we discuss the vapor-solid equilibria historically showing that this phenomenon was identified in many systems thus changing the physics of these systems.

2. Historical resume and material review

Historically, the contribution of intra-surface electron transfer was obtained first in the paper devoted to determination of the adsorption energy of hydrogen at GaN(0001) surface, published in 2012 [82]. Specifically, the adsorption energy of single hydrogen atom at the surface was about 3.4 eV for hydrogen coverage below 0.75 monolayer ($\theta_H < 0.75 ML$), and was reduced to 1.4 eV for higher coverage ($\theta_H = 0.75 ML$) [82]. The first diagram showing this adsorption energy change is reproduced in Fig. 20. In the following years far more precise and extensive calculations of hydrogen adsorption was published proving that the energy gain follows Eq. 4a and Eq. 4b for atomic and molecular hydrogen, respectively [82]. It was shown that far away from the critical coverage, i.e. $\theta_H = 0.75 ML$, adsorption energy is essentially constant, independent on the doping, i.e. H adatom effectively do not interact with the neighbors. In the close vicinity of critical coverage, i.e. for Fermi level not pinned at the surface, the adsorption energy depends on the doping in the bulk, finally confirming electron transfer contribution.

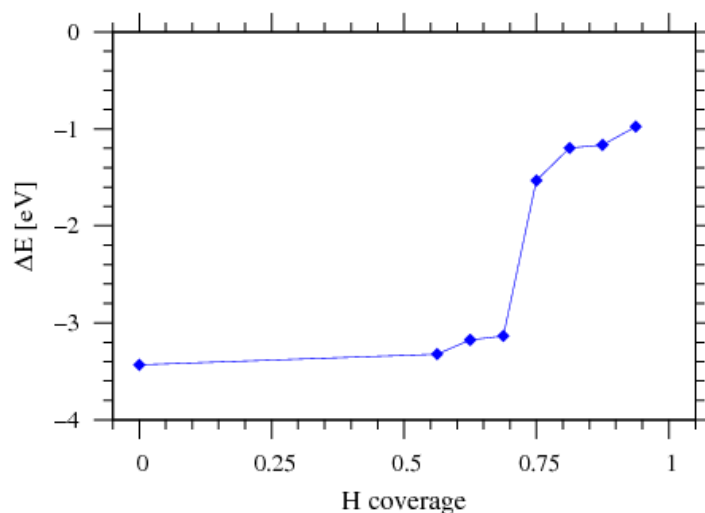


Fig. 20. Adsorption energy of single hydrogen atom, at differently covered GaN(0001) surface, obtained using 4 x 4 supercells. Reproduced Fig. 5 from Ref. 82 [82].

Somewhat later, phonon related contribution was introduced, so that free energy of the hydrogen adsorbate was temperature dependent [87]. Afterwards, the full contribution to chemical potential of both adsorbate and the vapor was determined allowing to obtain complete equilibrium [88]. Therefore hydrogen vapor adsorption on the Ga terminated GaN(0001) surface is fully determined in terms of the surface coverage, temperature and the pressure of the vapor.

Several month after the first publication of adsorption energy dependence on the coverage [82], Chen and Kuo published investigation of wetting of GaN(0001) surface [76]. Actually, they calculated the energy change during adsorption of water molecule at the surface in the three different forms:

- i) molecular,
- ii) fully dissociated water,
- iii) molecular hydrogen plus O adatom.

They observed some changes of the adsorption energy during adsorption of four water molecules. These changes were relatively small and of different nature: generally smaller for the set of four molecules. No clear identification of the profound difference was identified. The authors speculated that this was due to reconstruction contribution, which they discussed earlier. This identification as related to reconstruction contribution and the magnitude of the effect is different from later confirmed contribution from the charge transfer. Thus the clear identification of the effect was not obtained.

Molecular hydrogen adsorption on the opposite, N-terminated GaN (000-1) surface was also investigated showing that as on the opposite face, hydrogen adsorption process is dissociative and barrierless [93]. Hydrogen atom is adsorbed in the on-top position, therefore the EECR unit have single N topmost atom ($z = 1$). Their fractional charge is $q_i = 5/4$ thus $Q_i = q_i = 5/4$. As it was shown N-terminated surface is different from Ga-terminated because N-broken bond states energies are located close to VBM [38]. Thus the Fermi level is pinned there at clean GaN(000-1) surface. The number of the states before and after the adsorption is identical $N_a = N_f = 2$. Thus from Eq. 2b we obtain $g_{cr} = \theta_{cr} = \frac{3}{4}$. In other words, addition of hydrogen charge $Q_a = 1$ creates a surplus of $1/4$ electron which is donated to the other N-broken bond state that are not saturated. As the N-broken bond state can accept $3/4$ electron, the three H-adsorbed sites are needed for full saturation of single N-broken bond so that the critical condition for filling all broken states is at $\theta_H = \theta_{H-cr} = 0.75 ML$ [93]. Thus the energy change in adsorption of hydrogen molecule at fractionally H-covered GaN(000-1) surface is:

$$\Delta E_{DFT}^{ads-GaN}(H_2) = \begin{cases} -7.04 \text{ eV} & \theta_H < 0.75 ML \\ -1.60 \text{ eV} & \theta_H > 0.75 ML \end{cases} \quad (15)$$

The jump is considerable as for high coverage the $1/2$ electron is shifted to conduction band across the bandgap. These data were used to estimate hydrogen equilibrium pressure at the benchmark temperature $T = 1300 K$ via simple van t'Hoff approach to be $p \cong 10^{-21} bar$ and $p \cong 1 bar$ for $\theta_H < 0.75 ML$ and $\theta_H > 0.75 ML$, respectively. Thus GaN(000-1) surface adsorbs molecular hydrogen rapidly which can lead to the decomposition via desorption of ammonia. The high coverage of hydrogen are therefore not accessible for experimental investigation of hydrogen at GaN(000-1) surface, unless ammonia ambient is used. Until present no further theoretical investigations of this process has been made. Nevertheless, these scarce data confirm decisive role charge transfer contribution in this process.

Epitaxial processes widely used for creation of nitride devices use either plasma activated nitrogen [94,95] or ammonia [96-98]. The growth is conducted almost exclusively on GaN(0001) surface by metal organic vapor phase epitaxy (MOVPE) as these layers have superior optical properties, useful for optoelectronic devices. Therefore adsorption of ammonia is of considerable interest and was investigated by many researchers. The early stage of these investigations was summarized by Van de Walle and Neugebauer in their Letter [99]. They

presented phase diagram for GaN(0001) surface in which the nitrogen-hydrogen rich region of the surface can be divided into:

- i) hydrogen covered at $\theta_H = 0.75 \text{ ML}$
- ii) mixed $\text{HN}_3 - \text{NH}_2$ covered at $\theta_{\text{NH}_3} = 0.25 \text{ ML}$ and at $\theta_{\text{NH}_2} = 0.75 \text{ ML}$
- iii) mixed $\text{HN}_3 - \text{H}$ covered at $\theta_{\text{NH}_3} = 0.25 \text{ ML}$ and at $\theta_H = 0.75 \text{ ML}$.

The remaining part of the diagram correspond to Ga-rich diagram which is not relevant to ammonia adsorption. This diagram was obtained using (2×2) slab, therefore these data indicate basic features only. In fact these values correspond to critical coverages at which the Fermi level becomes free as it was proved above for the case of hydrogen ($\theta_{H-cr} = 0.75 \text{ ML}$) and mixture of NH_2 radicals ($\theta_{\text{NH}_2-cr} = 0.75 \text{ ML}$) and NH_3 admolecules ($\theta_{\text{NH}_3-cr} = 0.25 \text{ ML}$). As it will be shown below, from the point of the charge NH_2 radicals and equivalent to H adatoms, therefore the mixture ($\theta_{H-cr} = 0.75 \text{ ML}$) and NH_3 admolecules ($\theta_{\text{NH}_3-cr} = 0.25 \text{ ML}$) is also critical. In accordance to the above described arguments, the coverages indicated in the phase diagram are therefore the points in which the change of the electron transfer occurs corresponding to jump-like change of the adsorption energies.

The investigations in the following prove that the data presented in Ref. 96 are basically correct but simplified the issue overly. In fact they correspond to relatively high pressure of ammonia and hydrogen in the vapor. Several years later the detailed investigations started from ammonia adsorption at clean GaN(0001) surface. Since ammonia decomposition leads to hydrogen release, the incorporation of hydrogen coverage into NH_3 investigations was indispensable. It was shown that two different adsorption scenarios are possible: ammonia can be adsorbed molecularly with the energy $\Delta E_{DFT}^{ads-mol}(\text{NH}_3) = 2.0 \text{ eV}$ or dissociatively with $\Delta E_{DFT}^{ads-mol}(\text{NH}_3) = 2.6 \text{ eV}$ for hydrogen coverage $\theta_H < 0.75 \text{ ML}$ [100]. For higher coverage, the molecular adsorption energy remain unchanged while the dissociative adsorption energy becomes negative [100]. As shown in Fig. 13, all states of NH_3 admolecule are degenerate with valence band so they are occupied. Ammonia molecular adsorption is neutral as it brings 8 electrons to occupy all states. Therefore 3/4 electron is shifted into conduction band. Thus no EERC condition is possible and the adsorption energy is reduced by the electron transfer for any hydrogen coverage. The dissociative adsorption is creates NH_2 admolecule and H adatom. Both cases are equivalent, 1/4 electron is missing. Therefore the number of electrons transferred from Ga broken bonds state is doubled, and accordingly this creates substantial contribution to the adsorption energy. The energy difference at the critical coverage $\theta_{cr-H} = 3/4$ is close to 5 eV [100].

More detailed investigations revealed complex pattern of ammonia dissociative adsorption, especially to low surface coverage [66, 76]. Several configurations are possible:

- i) NH radical in H3 position
- ii) NH radical on-top
- iii) NH₂ radical – bridge
- iv) NH₂ radical – on top

According to the data [100], all states of these radicals are degenerate with valence band. In case of the on-top the unit is single site ($z = 1$). Thus the charge is $Q_i = 3/4$. In the case of the NH radical, the adsorbate charge is $Q_a = 6$. Number of initial occupied states after adsorption is $N_f = 0$, configuration number of states after adsorption $N_a = 8$. This leads to the NH critical coverage at coverage $\theta_{cr-NH-top} = 3/8$. And accordingly, the adsorption energy gain of dissociative adsorption of ammonia at $\theta_{NH-top} < 0.375 ML$ is $\Delta E_{NH-top}^{DFT} \cong 1.42 eV$. For higher coverage this gain is negative.

In the case of NH radical in the H3 position the unit contains 3 Ga sites, i.e. ($z = 3$), so that the initial charge $Q_i = 9/4$. The adsorbate charge is $Q_a = 6$. The number of occupied initial states after adsorption is $N_i = 0$, configuration number of occupied states after adsorption $N_a = 8$. This leads to critical fraction $g_{cr-NH-H3} = 9/8$. Accordingly the critical coverage is $\theta_{cr-NH-H3} = 3/8$. Therefore this energy jump should be observed $\theta_{NH-top} \cong 0.375 ML$. This is in accordance of general result, the adsorption energy gain of dissociative adsorption of ammonia at $\theta_{NH-top} < 0.375 ML$ is $\Delta E_{NH-top}^{DFT} \cong 1.42 eV$. For higher coverage this gain is negative.

In the case of NH₂ radical in the bridge position the unit contains 2 Ga sites, i.e. ($z = 2$), so that the initial charge $Q_i = 3/2$. The adsorbate charge is $Q_a = 7$. The number of occupied initial states after adsorption is $N_f = 0$, configuration number of occupied states after adsorption is $N_a = 8$. This leads to critical fraction $g_{cr-NH2-bridge} = 3/2$. Accordingly the critical coverage is $\theta_{cr-NH2-bridge} = 3/4$. This is not possible as the top coverage is $\theta_{cr-NH2-bridge} = 1/2$.

Finally, the case of NH₂ radical in the on-top position ($z = 1$), thus the initial charge is $Q_i = 3/4$, the adsorbate charge is $Q_a = 7$. The number of occupied initial states after adsorption is $N_f = 0$, configuration number of occupied states after adsorption is $N_a = 8$. This leads to critical fraction $g_{cr-NH2-on-top} = 3/4$. Accordingly the critical coverage is

$\theta_{cr-NH_2-on-top} = 3/4$. Therefore this energy jump should be observed $\theta_{NH_2-on-top} \cong 0.75 ML$. No such investigation has been done because this configuration is unstable.

These investigations were finished before full thermodynamic procedure for determination of vapor-surface equilibria was formulated [84,87]. Therefore the thermal contribution was limited to the configurational entropy. Using this the estimate of the mixed hydrogen-ammonia pressure in equilibrium with the specified coverage of GaN(0001) was obtained [81]. The coverage by both type ammonia derived radicals: NH (on-top) and NH₂ (on-top and bridge) is limited to hydrogen pressure below $p_{H_2}(min) = 10^{-5} bar$ and ammonia pressure below $p_{NH_3}(min) = 10^{-2} bar$. These conditions cannot be achieved separately in ammonia growth of GaN due to thermal decomposition of ammonia, therefore this suggest that the standard coverage of GaN(0001) surface is full NH₂ – NH₃ mixed coverage. The relative ratio of the radicals and the molecule depends on the ammonia to hydrogen pressure ratio. It has to be stressed out that this is rough estimate, precise determination of the coverage at given temperature-pressures conditions requires a number of simulations in the future. These investigations should include phonon simulations which are extremely demanding numerically. On the other hand, the complex atomic structure of the adsorbate indicate on much larger phono contribution to free energy which will affect the equilibrium much more than in the case of hydrogen. Thus one can expect that the phonon contribution is comparable to the adsorption energy. Therefore the obtained equilibria may be modified considerably. Since MOCVE and HVPE methods are very important technologically, these calculations are needed in the nearest possible future.

An important example of the influence of the electronic charge on the results of the MOVPE growth of nitrides is well known problem of the growth of GaInN necessary for visible range active LED's and LDs [101-103]. The growth is conducted at high V-III ratio, of about 4000 for GaN and 10000 for InGaIn. In addition, incorporation of indium into the nitride layers is totally blocked by minuscule presence of hydrogen in the vapor. Thus in InGaIn epitaxy molecular nitrogen is used as group III metals carrier gas and the ammonia is the second main component. The typical pressure ratio of the ammonia and the carrier gas is 1 : 1. Nitrogen is essentially inert and therefore the vapor consists of the two active components: ammonia and molecular hydrogen, which is generated due to ammonia thermal decomposition. The total vapor pressures used in the MOVPE processes is in the (0.1 bar ÷ 1 bar) range. Thus the ammonia partial pressure are in the same range. Hydrogen pressures are fraction of this value.

In the *ab initio* calculations it was assumed that the mixed $NH_2 - NH_3$ coverage of GaN(0001) surface is full, i.e. all topmost Ga atoms have their broken bonds saturated either by NH_2 radicals or NH_3 ad molecules located in the on-top positions. The electronic properties of such system were presented above in Fig 13 and 13 [80]. All states of the adsorbates, including unsaturated N state in NH_2 radical are degenerate with valence band. In these simulations (4×4) slab was used in which the $NH_2 - NH_3$ ratio was changed by addition of single hydrogen so that the ammonia ad molecules coverage was $(\theta_{NH_3} = 0, 1/16, \text{ up to } 5/16)$, thus for the coverage range $(\theta_{NH_3} \leq 0.25 \text{ ML})$ an accordingly $(\theta_{NH_2} \geq 0.75 \text{ ML})$. In all cases $(\theta_{NH_3} < 1/4)$, the Fermi level is located at VBM. For higher NH_3 coverage $(\theta_{NH_3} = 1/4)$ Fermi level is free in the gap and for higher coverage, e.g. for coverage $(\theta_{NH_3} = 5/16)$, is in the conduction band.

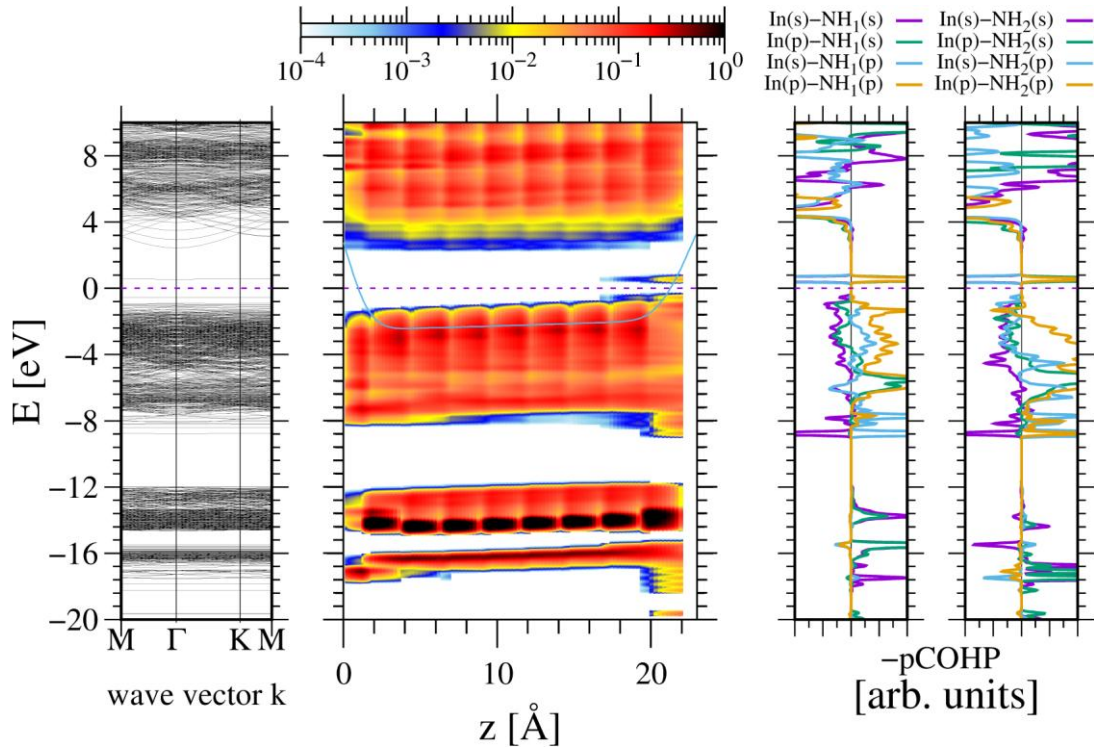


Fig. 21. Electronic properties of 4×4 slab representing single In adatom at fully NH_2 covered GaN(0001) surface. The panels from the left present: electron energy in momentum space (band diagram); electron energy in real space, plotted in the direction perpendicular to the surface; Crystal Orbital Hamilton Population (COHP) [54,55] of In and N atoms with NH, NH_2 radicals. The surface is located at the right hand edge of real space diagram. Reproduced from Fig. 3 Ref. 101 [101].

Indium carrier trimethylindium (TMI) is highly unstable at temperature $T > 600\text{ }^{\circ}\text{C}$. Therefore in the typical GaInN growth conditions at the temperature $T \cong 800\text{ }^{\circ}\text{C}$ it is decomposed and single In atom is adsorbed. The stable configuration of In adatom and the NH_3/NH_2 coverage depends on the coverage ratio. In case of the low NH_3 coverage ($\theta_{\text{NH}_3} \leq 1/16$) In adatom is located in the vicinity of the symmetrical H3 site, bonded to two NH and one NH_2 radicals. Thus one NH_2 neighbor remains intact while the two others loose one H atom each, i.e. they are converted into NH radicals. In the consequence the two more distant NH_2 radicals are converted into NH_3 ad molecules. Thus the In adatoms is shifted away from NH_3 ad molecules that indicates on a strong repulsion.

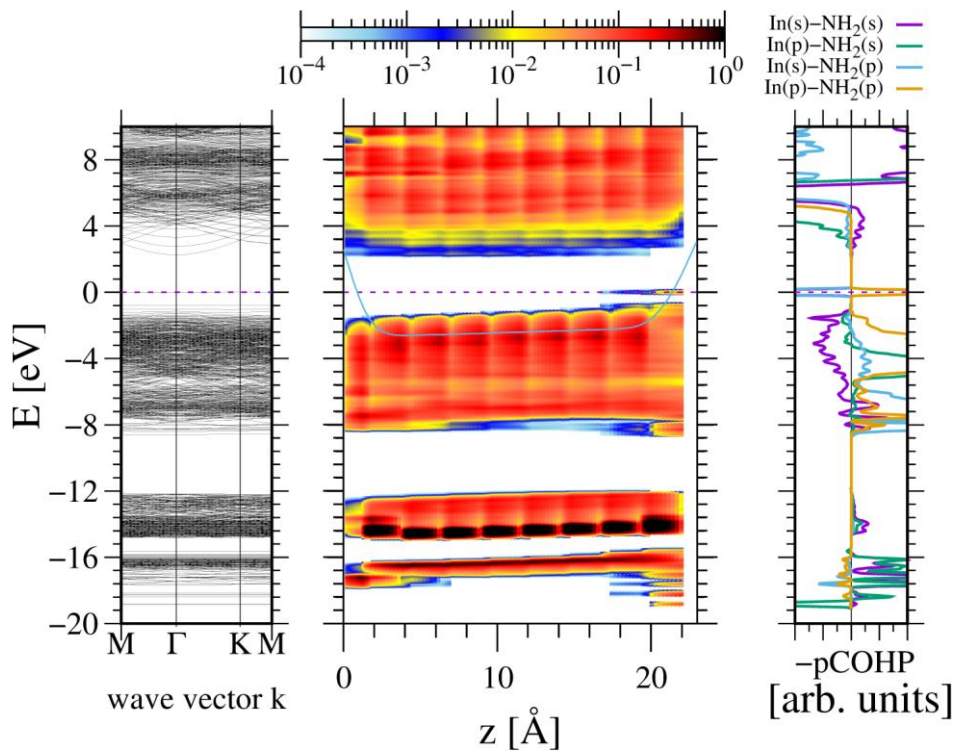


Fig. 22. Electronic properties of 4×4 slab representing In adatom at GaN(0001) surface covered by 14 NH_2 radicals and 2 NH_3 molecules ($x = 1/8$). The panels from the left present: electron energy in momentum space (band diagram); electron energy in real space, plotted in the direction perpendicular to the surface; COHP In and N atoms from NH_2 radicals. No NH are present so this overlap is missing. The surface is located at the right hand edge of real space diagram. Reproduced from Fig. 4 Ref. 101 [101].

Since the system considered is changes by fraction of NH_3/NH_2 occupation, it is necessary to use entire slab as EECR unit, i.e. 16 surface sites. The initial charge of the unit

depends on the number ammonia admolecules. In the case of full NH_2 coverage, the initial charge is of 16 radicals ($q_{NH_2} = 7$) and broken Ga bonds ($q_{Ga-br} = 3/4$) that gives in total $Q_i = 124$. We have to account presence of single In atom that adds the adsorbate charge by $q_{In} = 3$ to $Q_i = 124$. Replacement of single NH_2 radical by NH_3 admolecule, i.e. coverage change by $\theta_{NH_3} = 1/16$, is equivalent of adsorption of single hydrogen atom with the charge $Q_a = 1$. All states of radicals and admolecules are occupied that adds 8 states for each. In summary the number of original states that are occupied by adsorption is $N_f = 16 \times 8 = 128$. The EECR rule gives the following $g = 1$. Thus the fully NH_2 covered slab with attached single In admolecule will have Fermi level at VBM. Accordingly, attachment of single NH_3 admolecule leads to EECR condition with all states filled. This is in accordance with the band diagram plotted in Fig 21 where the Fermi level is located in the gap between VBM and In antibonding states. Additional hydrogen, i.e. $\theta_{NH_3} = 1/8$ leads to Fermi level pinned at the latter state as shown in Fig. 22.

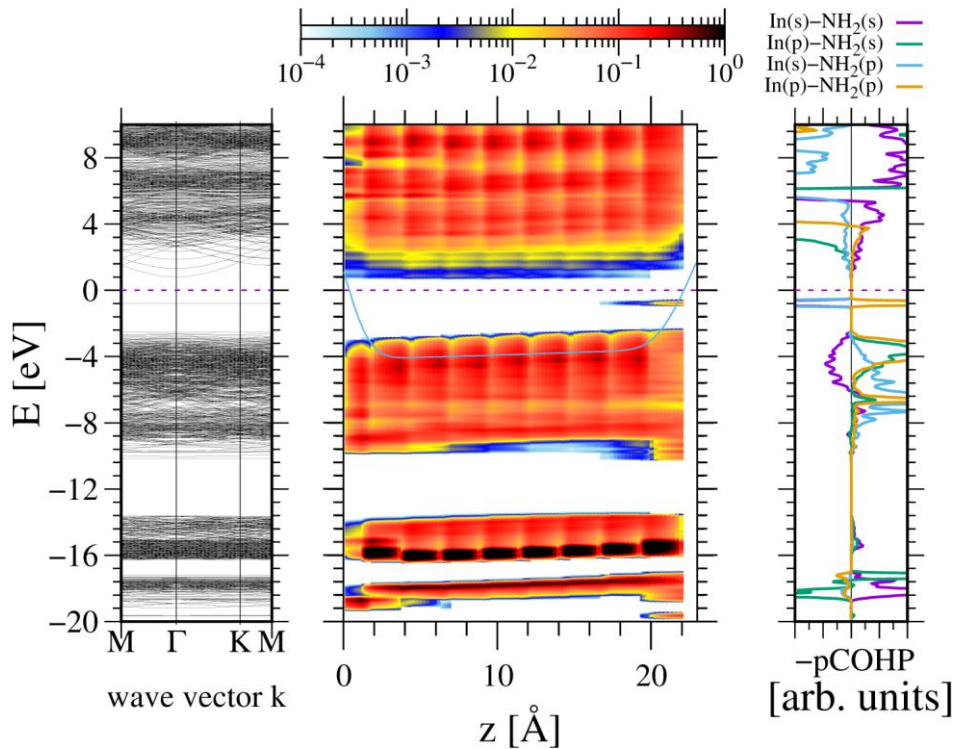


Fig 23. Electronic properties of 4×4 slab representing In adatom at GaN(0001) surface covered by 13 NH_2 radicals and 3 NH_3 molecules ($x = 3/16$). The panels are identical to those in Fig 20. Reproduced from Fig. 4 Ref. 101 [101].

In the higher NH_3 coverage ($\theta_{\text{NH}_3} = 1/8$) up to ($\theta_{\text{NH}_3} = 1/4$) In adatom is located in T4 site, surrounded by NH_2 radicals only. No NH_3 admolecules are present within the neighbors. For the case $\theta_{\text{NH}_3} = 3/16$ the second EECR condition is fulfilled, the Fermi level is located between In- NH_2 antibonding states and conduction band minimum (CBM). After consecutive hydrogen addition, i.e. for $\theta_{\text{NH}_3} = 1/4$ Fermi level is shifted up to CBM. Drastically different case is observed for the highest simulated coverage i.e. ($\theta_{\text{NH}_3} = 5/16$). The atom is located close to the NH_3 admolecule and connected to two or NH_2 radicals. Fermi level is located again in CBM.

Adsorption energy of indium is therefore dependent on GaN(0001) surface coverage. The contribution is important as the number of electrons shifted may reach three. The adsorption energy in function of the coverage is presented in Fig 24.

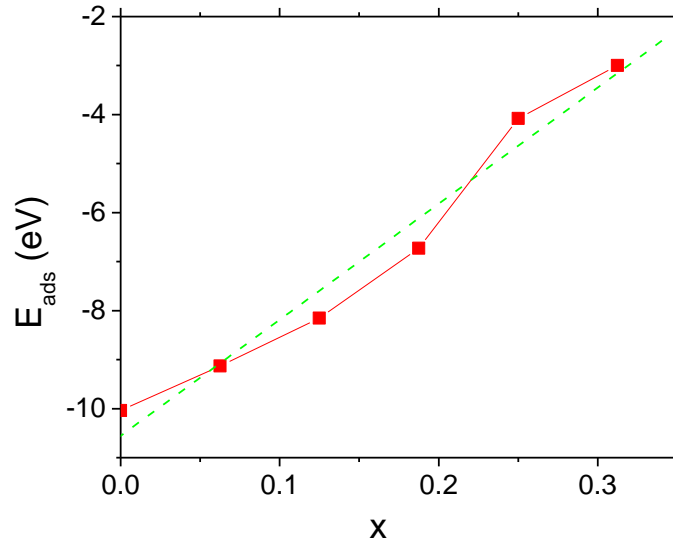


Fig. 24. Indium adsorption energy in function of the NH_3 molecules (n_{NH_3}) to NH_2 radicals (n_{NH_2}) ratio (x), simulated using 4×4 slab. All sites of GaN(0001) surface are occupied by NH_3 molecules or by NH_2 radicals. Green dashed line represent the linear approximation in Eq. 15. Reproduced from Fig 8 Ref 101 [101].

These data were approximated by the following expression

$$E_{ads}^{DFT}(x) = -10.55 + 23.68 x \quad (16)$$

where the energy is expressed in eV. The difference between n- and p-type bulk is negligible. As it is shown, the dependence is steep, thus the energy is small for higher ammonia coverage. The thermodynamics of In adsorption was also investigated, showing drastic reduction of the probability of In adsorption for increased hydrogen pressure. This is confirmed by MOVPE growth experiments where slight presence of hydrogen blocks incorporation of In in the growth layers [102 - 105]. Moreover, this effect was used in the technology as the growth of In-free GaN does not require termination of In flow. Much faster is addition of hydrogen in the flow which leads to growth of GaN layers [106 - 109].

In the recent years an important part of the nitride investigations were redirected towards the shorter wavelength devices, active in UV range [113-115]. That entails growth of Al-rich structures and AlN substrates. AlGaIn layers crack under tensile strain when grown on GaN substrates, therefore growth of high quality AlN single crystals is indispensable [113-115]. The most promising method is physical vapor transport growth from Al and N₂ [115]. These crystals are grown on polar AlN surfaces: Al-terminated AlN(0001) and N-terminated AlN(000-1). Therefore adsorption of both Al and N₂ was investigated by *at initio* methods [116-119]. It is important that these processes are hydrogen-free.

Adsorption of nitrogen at AlN(0001) surface was investigated first [116]. It was shown that bare AlN surface has no reconstruction with partially filled Al-broken bond state located below CBM. Molecular nitrogen is adsorbed dissociatively without any energy barrier at clean AlN(0001) surface in H3 position. The adsorbed nitrogen *Ns* state is located deep in the valence band while *Np* states are located in the bandgap, below Al-broken bond state. Thus at low coverage these states are occupied by electrons drawn from Al-broken bond state. The EECR unit may encompass three Al sites, i.e. ($z = 3$). The Al broken bond charge is $q_{Al-br} = 3/4$ thus initial electron charge of the unit is $Q_i = 9/4$. Adsorbed N atoms brings 5 electrons, i.e. $Q_a = 5$. The number of the initial states that are occupied after adsorption is $N_f = 0$. The number of occupied states after adsorption is $N_a = 0$. Therefore the EECR condition is $g_N = 3/4$ from which the critical N coverage is $\theta_{N-cr} = 1/4$. The *ab initio* data confirm this prediction, at $\theta_{N-cr} = 1/4$ Fermi level is at the top of the highest energy N state [116]. Accordingly, the adsorption energy of molecular nitrogen has a jump at this coverage as shown in Fig. 25.

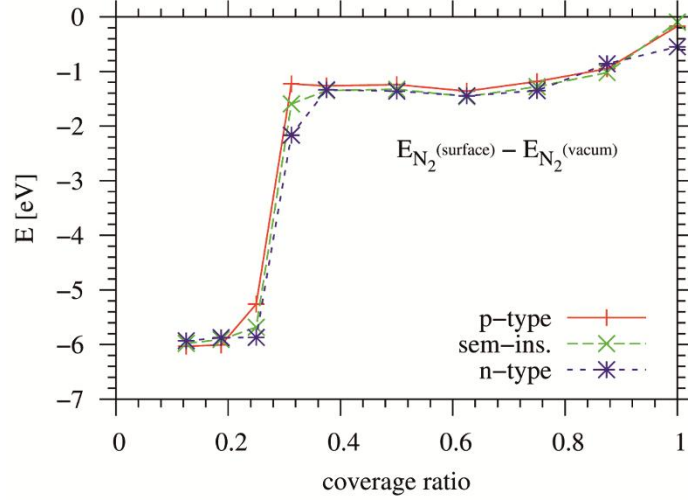


Fig. 25. Adsorption energy of N_2 molecule calculated using an energetically stable configuration: for $\theta_N < 0.25 \text{ ML}$ - dissociative process leading to concentration of separate N atoms in H3 position, for $\theta_N > 0.25 \text{ ML}$ - the excess nitrogen is in the form of N_2 admolecule in a skewed-vertical position located on top of an Al surface atom. The colors present data for a slab representing the following dominant doping in the bulk: *p*-type, *semi-insulating*, and *n*-type. Carrier concentration was set to $2.4 \times 10^{20} \text{ e/cm}^3$. Reproduced from Fig. 9 Ref 116 [116].

The obtained adsorption energy change for N_2 molecule could be summarized as follows:

$$\Delta E_{DFT}^{ads-AlN}(N_2) = \begin{cases} -6.0 \text{ eV} & \theta_N < 0.25 \text{ ML} \\ -1.0 \text{ eV} & \theta_N > 0.25 \text{ ML} \end{cases} \quad (17)$$

For $\theta_N < 0.25 \text{ ML}$ the adsorption is dissociative, for the remaining part the adsorption has no electron transfer contribution which lowers the energy gain is 5.6 eV which is much below the nitrogen molecule dissociation energy. Therefore for $\theta_N > 0.25 \text{ ML}$ adsorption is molecular with the energy gain equal to 1.0 eV. Thus the drastic difference in the adsorption type and the energy is related to electron transfer. From that the equilibrium pressure of nitrogen was estimated, without full thermodynamic analysis. The result the saturation nitrogen pressure below 0.01 bar for the nitrogen coverage below critical ($\theta_N < 0.25 \text{ ML}$) at PVT AlN growth temperature $T = 2300 \text{ K}$. For molecular adsorption ($\theta_N > 0.25 \text{ ML}$) the required nitrogen pressure is prohibitively high, of order of 10^5 bar .

Molecular nitrogen adsorption at the opposite N-terminated AlN(000-1) surface is drastically different [117]. Clean N-terminated AlN(000-1) surface has no reconstruction. Molecular nitrogen interact with the surface by weak Van der Waals forced typical for closed

shell systems. Therefore it is adsorbed molecularly without localization with the energy gain of about $\Delta E_{DFT}^{ads-AlN}(N_2) = 1.0 \text{ eV}$. In case of Al covered surface molecular nitrogen is dissociated with the energy gain given by the relation (in eV):

$$\Delta E_{DFT}^{ads-AlN}(N_2, \theta_N) = 2\Delta E_{DFT}^{ads-AlN}(N, \theta_N) - \Delta E_{DFT}^{diss}(N_2) = -8.32 + 4.88 \theta_N \quad (18)$$

which reflects transformation of the metallic surface into semiconducting, gradual downward motion of the Fermi level and reduction of the electron transfer contribution to adsorbed N adatom. Single N adatom has 8 atomic states while the number of the electron is $N_e = 7\frac{1}{4}$ thus $\frac{3}{4}$ electron is transferred from top energy states of Al coverage. Therefore the change of the adsorption energy is considerable. The thermodynamics of nitrogen adsorption was formulated based on vibrational energy contribution to the chemical potential of adsorbed nitrogen at high temperatures. The results show considerable variation of the pressure for limited coverage which remains in agreement for propensity of creation of metallic Al inclusions during growth.

The complementary process of Al adsorption at principal AlN surfaces was also investigated [90, 118]. Al is adsorbed at Al-terminated AlN(0001) surface without any energy barrier. The adsorption energy depends on the Al coverage in the following way:

$$\Delta E_{DFT}^{ads-AlN}(Al) = \begin{cases} -5.06 + 0.02 \theta_{Al} & \theta_{Al} < 1 \\ -6.02 - 8.35 (\theta_{Al} - 1) + 47.45 (\theta_{Al} - 1)^2 & 1 \leq \theta_{Al} \leq 1.2 \\ -3.43 - 1.64(\theta_{Al} - 1) & \theta_{Al} > 1.25 \end{cases} \quad (19)$$

The energy gain has maximum of about 6.1 eV for $\theta_{Al} = 1.1$. Thus the contracted layer model formulated for Ga coverage of GaN(0001) surface is applicable for AlN(0001) surface also [90]. No direct confirmation of the role of electron transfer was found. Thus this process is similar to the typical adsorption processes at metal surfaces.

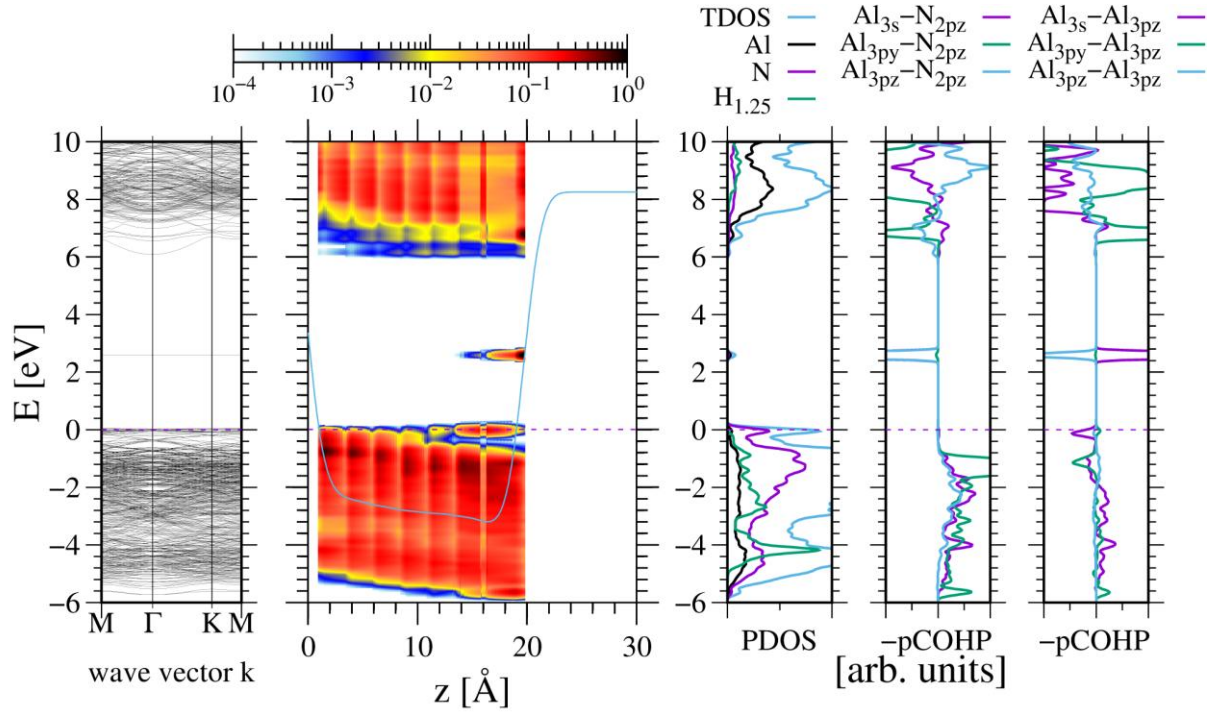


Fig. 26. Electronic properties of 4 x 4 AlN slab with single Al adatom, representing AlN(000-1) surface with $\theta_{Al} = 0.0625$ ML coverage. The panels from the left present: electron energy in momentum space (band diagram); electron energy in real space (obtained by projection of the density of states of each atom on the atomic eigentstates and associated with position of the atom), plotted in the direction perpendicular to the surface; total density of states (DOS), projection of the minus crystal orbital Hamilton population (-pCOHP) [54,55] of Al adatom and neighboring N and Al surface atoms, respectively. The surface is located at the right hand edge of real space diagram, close to 20Å. Reproduced from Ref. 118 [118].

Different, complex picture was obtained in investigations of adsorption of Al at the opposite, N-terminated AlN(000-1) surface [118]. The electron contribution plays important role in the adsorption. As it is shown in Fig. 26, Al atoms creates bonding states with three topmost N atoms thus the unit has three sites ($z = 3$). The $Al3s$, $Al3p_x$ (and equivalently $Al3p_y$) and $Al3p_z$ overlaps with nitrogen atom $N2p_z$ state create bonding states. The first three are degenerate with VB thus they are occupied but $Al3p_z-N2p_z$ state is located in the bandgap, thus it is empty. Therefore 6 Al states are occupied ($N_a = 6$). Al atom contributes three electrons, hence $Q_a = 3$. The number of electrons in each N surface atoms is $q_N = 5/4$ which gives $Q_i = 15/4$. Nitrogen states and full after adsorption $N_f = 6$. Therefore EECR critical fraction for occupation of 6 states is $g_{Al-cr} = 3/4$ and accordingly, the critical Al coverage is $\theta_{Al-cr} = 1/4$. Naturally Al adsorption creates surplus of $3/4$ electrons which is shifted to other N-

broken bond states which are located close to VBM. At the critical coverage this charge is sufficient to fill single N atom broken bond state to 2 electrons. Thus both Al states and N broken bond states are occupied and the further increase of Al coverage leads to electron transfer to higher energy states. This is considerable energy cost therefore for the coverage above critical $\theta > \theta_{Al-cr} = 1/4$ the Al adsorption energy should be lower. The Al adsorption energy in function of Al coverage is presented in Fig. 27.

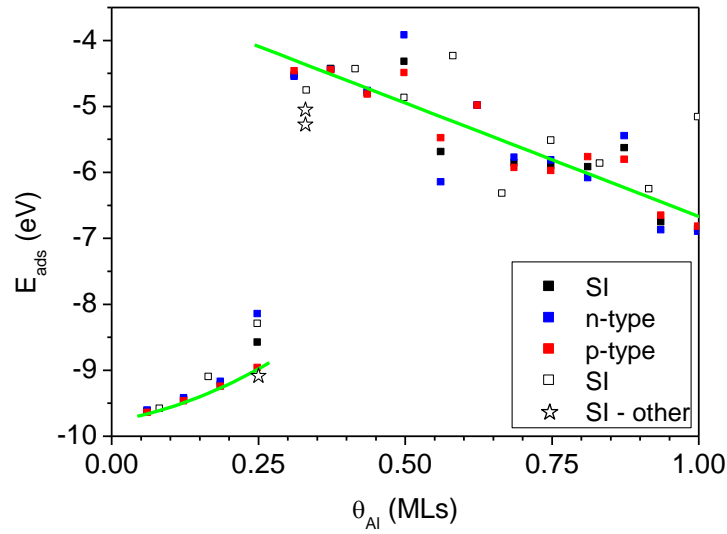


Fig 27. Adsorption energy of Al atom at AlN(0001) surface, in function of Al coverage. Full squares represent data obtained using 4×4 slab, empty squares - $2\sqrt{3} \times 2\sqrt{3}$ slab, empty stars – additional configurations in $2\sqrt{3} \times 2\sqrt{3}$ slab. The coverage on the horizontal axis refers to the value after the process. Green dashed line presents polynomial approximation to ab initio data. Reproduced from Fig. 3 Ref 118 [118].

The obtained energy may be approximated by the formula:

$$E_{ads}(Al) = \begin{cases} -9.776 + 1.470 \theta_{Al} + 6.856 \theta_{Al}^2 & \theta_{Al} < \frac{1}{4} \\ -4.089 - 3.438 \times \left(\theta_{Al} - \frac{1}{4} \right) & \theta_{Al} \geq \frac{1}{4} \end{cases} \quad (20)$$

As predicted at the critical coverage adsorption energy has the jump by about 3.5 eV. The high coverage dependence is due to transition of the surface to metallic state and closing the gap. The full thermodynamic analysis was made to obtain extremely low pressure values for coverage below critical. The second stability region corresponds to coverage close to full, which is stable at somewhat higher but still also relatively low Al pressure. Thus N-terminated surface has strong tendency to attain metallic state.

These investigations were concentrated predominantly into investigations of nitride semiconductor surfaces. This was related to rapid development of nitride based optoelectronic devices mostly light emitting diodes (LEDs) and laser diodes. This was fortunate because GaN and AlN have wide bandgaps. This is essential because the gas is required to recognize electron transfer contribution during adsorption as a result of the jump-like change of Fermi energy. The other widegap semiconductor, outside nitride family, suitable for these investigations, is silicon carbide SiC [119]. Clean Si-terminated SiC(0001) surface has Fermi level pinned by broken bond state located 0.8 eV below CBM. Si atom is adsorbed in H3 site, saturating three broken bonds of Si topmost atoms ($z = 3$). The four bonds are created, thus 8 states are occupied ($N_a = 8$). Si topmost atom contributes one electron, thus for three atoms $Q_i = 3$. Si adsorbed atom has four electrons therefore $Q_a = 4$. Si broken bond states are empty after adsorption thus $N_f = 0$. Therefore EECR critical fraction for occupation of 6 states is $g_{Si-cr} = 3/4$ and accordingly, the critical Si coverage is $\theta_{Si-cr} = 1/4$. The Si adsorption energy is plotted in Fig. 26. As it is shown at the coverage in the neighborhood of the critical value, Si adsorption energy is reduced.

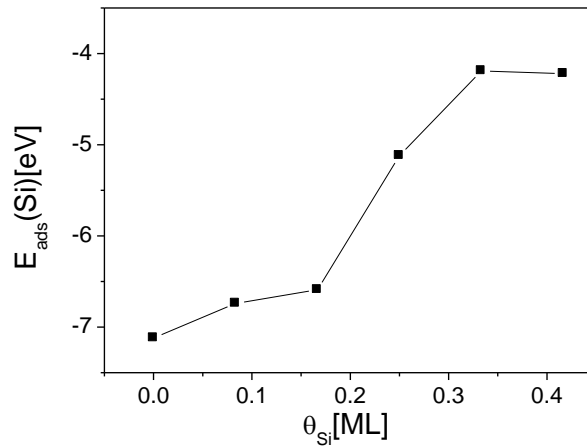


Fig. 28. Adsorption energy of Si adatoms located in H3 sites at the SiC(0001) surface simulated using $(2\sqrt{3} \times 2\sqrt{3})$ slab. The coverage is defined as the ratio of the Si adatoms before adsorption to the number of the Si topmost atoms in the SiC lattice. Thus in case of finite coverage this points should be shifted to the right to the neighboring value. Reproduced from Fig. 10 Ref 119 [119].

As it is shown again, Si adsorption is reduced by the fact that for the coverage above critical $\theta_{Si} > \theta_{Si-cr} = 1/4$ one electron should be shifted to higher energy state. This causes adsorption energy in the neighborhood of the critical value. This behavior indicates that the process is more complex and that needs further investigations.

Fairly recently, more extensive simulations of the interactions between polar GaN surfaces and mixed NH_3/H_2 vapor [120]. They confirmed dependence on the adsorption energy on the Fermi level pinning at the surface. They identified three different adsorption regimes for adsorption of gallium on both Ga- and N-terminated surfaces. As shown in Fig 29, the adsorption energies varies considerably.

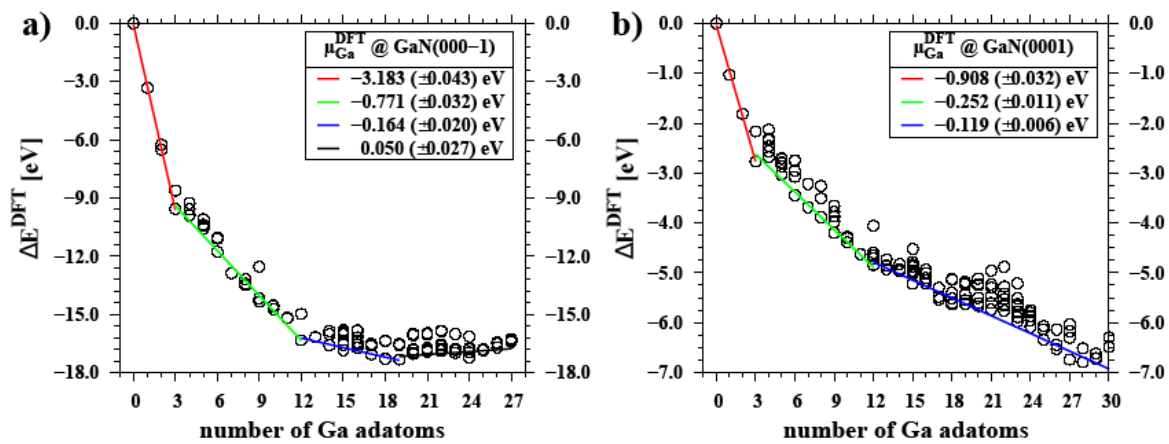


Fig. 29. Change of DFT total energy as a function of the number of Ga adatoms on polar GaN surfaces, (a) GaN(000-1), (b) GaN(0001). The reference level is the sum of energies of the clean Surface and the corresponding number of Ga atoms bound in the crystal. All data points (circles) represent energies obtained from DFT calculations for different adatom distributions on the surface. Linear relationships were fitted to the points with the lowest energies. In summary, these reviews of adsorption processes show that the above listed cases show jump-like change of the adsorption energy at the critical coverage for many systems. In some cases this process is gradual and in these cases the other factors may be invoked. In case of jump-like changes such additional factor were not found thus we could conclude that the effect has been proven. Reproduced from Fig. 3 of Ref 120 [120].

The data on these diagrams corresponds to the surface free energy change calculated as the difference between the surface with Ga adatom attached and the surface and G atom separate in function of the attached atom. It is shown that the dependence is linear in three separate parts. The slope of this lines defines the adsorption energy at these coverage.

Using these data the authors were able to determine the chemical potential surface of Ga adatom at both surfaces. These data were projected on the MOVPE and HVPE growth conditions allowing to determine basic thermodynamic state of the surfaces during growth of GaN layers by these methods.

VIII. Charge role in diffusion

Surface diffusion is related to the surface mobility of localized species, i.e. effectively jumps between the minimal energy positions at the surface. In consequence this is simulated using NEB procedure typically [121,122]. This assumption leads to single value of diffusion barrier, obtained as the energy difference between the activated complex and the initial value [123]. It is widely used in many cases including surface diffusion [124].

Recently it was recognized that the phenomenon has to be investigated with explicit incorporation of the quantum effects in bonding and statistics [12]. The several possible scenario was formulated, depending on the bonding type and statistics, in function of the Fermi level position. These cases are presented in Fig. 30. As it is shown the diffusion barrier may be affected by the initial energy by: (i) bonding via standard (Fig 30(a)) (ii) bonding and statistics of resonant states (Fig 30(b)), (iii) statistics via change of the activated complex quantum states close to Fermi energy level, (iv) electron transfer to other state pinning the Fermi level in case for the activated complex quantum states attaining the energy above Fermi energy and in consequence empty.

As an exemplary case for the investigation of the diffusion mechanism was selected the case of diffusion of nitrogen adatoms at Ga-terminated GaN(0001) surface. This case is important also from technological point of view as one of the growth method of nitride structures used in the devices in plasma activated molecular beam epitaxy (PA-MBE) [94,95]. The layers are grown in metal-rich conditions thus it is assumed that metal layer covers the surface. Accordingly the diffusion model was proposed in which the nitrogen atom diffuses underneath, known as “new diffusion channel”[125]. Initially, the energy barrier for diffusion of N adatom at clean GaN(0001) surface was found to be $\Delta E_{bar} = 1.3 \text{ eV}$ [126]. This was corrected later to higher value $\Delta E_{bar} \geq 1.5 \text{ eV}$ [125]. In case of GaN(0001) surface fully covered by indium adlayer, this barrier was dramatically lower $\Delta E_{bar} = 0.5 \text{ eV}$. High barrier for clean GaN(0001) surface was attributed to breaking of two Ga-N bonds which was supposed to cost about 3.0 eV while in case of indium coverage creation of strong In-N bond compensates this effect. It was concluded that in case of gallium coverage this effect is similar which leads to emergence of fast

diffusion channel. Afterwards this effect was used in interpretation of PA-MBE growth experiments [95, 128].

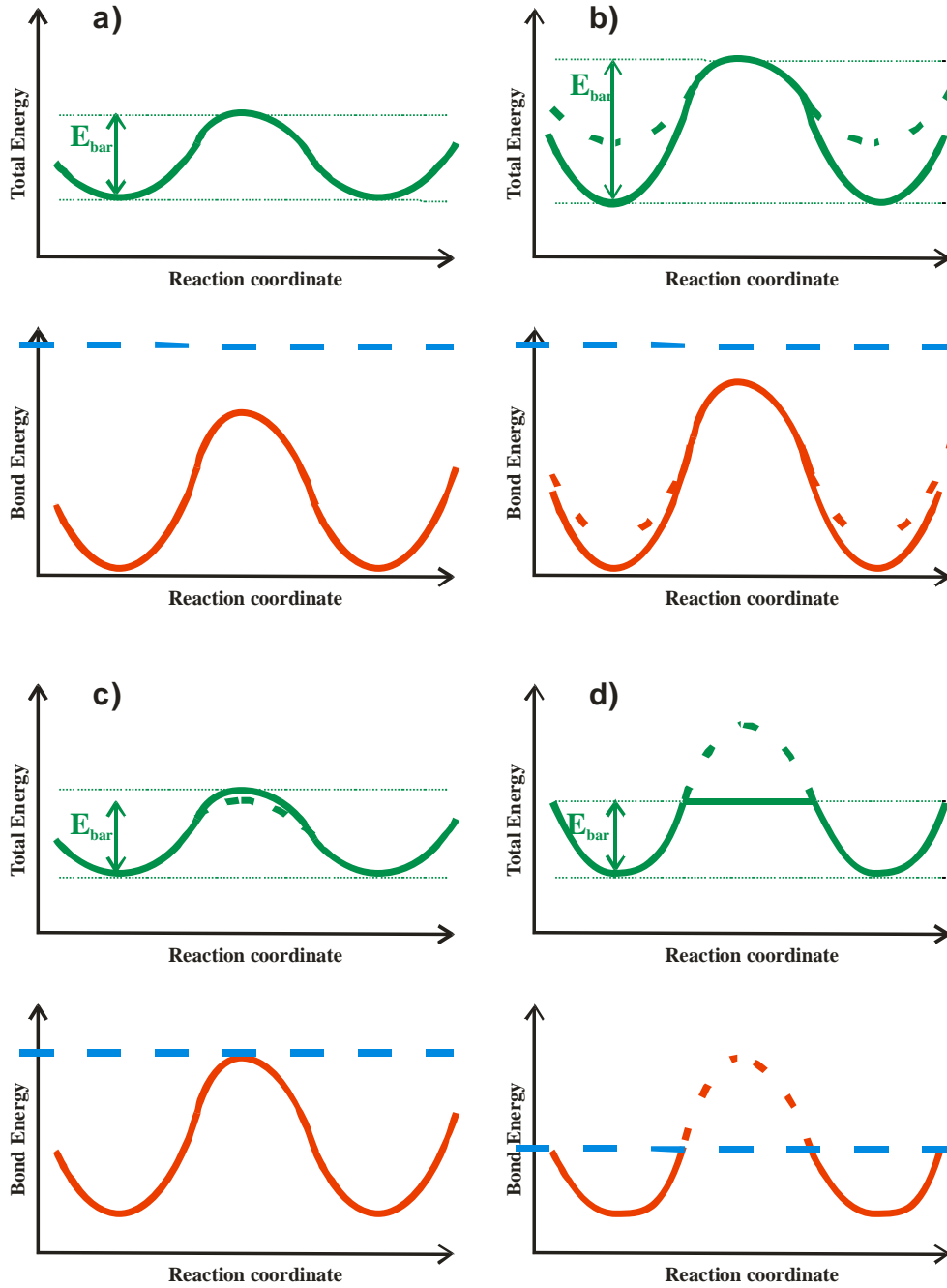


Fig. 30. The factors affecting the effective barrier for diffusion via modification of the energy of the quantum states (red line) and the resulting total energy change (green line) in the course of the jump between two sites: a) standard case: the energy of quantum state remains far below Fermi energy, b) the energy and the occupation of quantum states, standard and resonant in initial state is changed affecting the barrier c) the energy of quantum states approaches the Fermi energy – the barrier affected via occupation of the states, d) the energy of quantum states extends over the Fermi energy – the energy of the barrier is determined by

the Fermi level. The energy of quantum state pinning the Fermi energy (and the Fermi energy itself) is denoted by blue line. Reproduced from Fig. 1 Ref 12 [12].

Therefore the case of N adatom diffusion at GaN(0001) surface under various Ga coverage was investigated. It was shown that for low Ga coverage diffusion path is from lowest energy point at H3 site via saddle point in bridge configuration to T4 site and across the symmetric part. Therefore we investigated the N adatom energy change along the NEB surface diffusion path. The results of these investigations for the fractional coverage of GaN(0001) surface by Ga adatoms are plotted in Fig. 31.

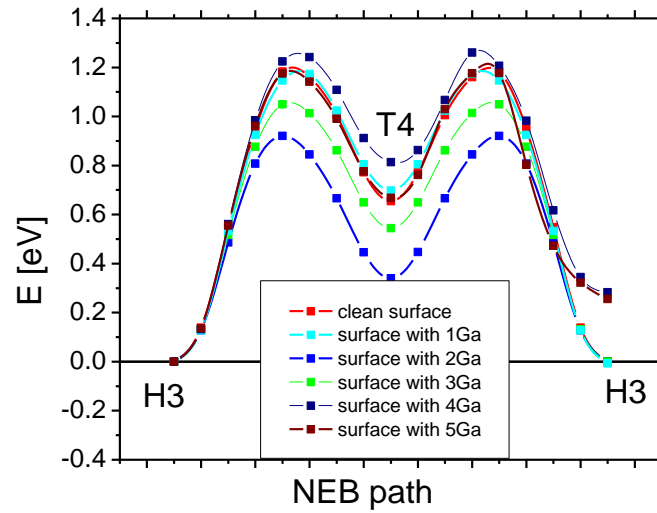


Fig 31. System energy change during motion of the nitrogen adatom along the jump path over GaN(0001) surface partially covered with Ga adatoms. The number of Ga atoms refer to $(2\sqrt{3} \times 2\sqrt{3})$ slab representing GaN(0001) surface, thus a single Ga adatom refer to $1/12$ ML Ga coverage. The “clean” surface corresponds to the absence of Ga adatoms, i.e. with N adatom present. Reproduced from Fig. 5 Ref 12 [12].

As it is shown the diffusion energy barrier for clean GaN(0001) surface is $\Delta E_{bar} = 1.18$ eV which is good agreement with the results in Ref. 125 and basically also with Ref 126. The barrier was determined using refer to $(2\sqrt{3} \times 2\sqrt{3})$ slab representing GaN(0001) surface, thus the coverage change was $(1/12)$ ML [52]. The lowest barrier obtained was $\Delta E_{bar} = 0.92$ eV for $(1/6)$ ML Ga coverage. For higher coverage the barrier was increased again.

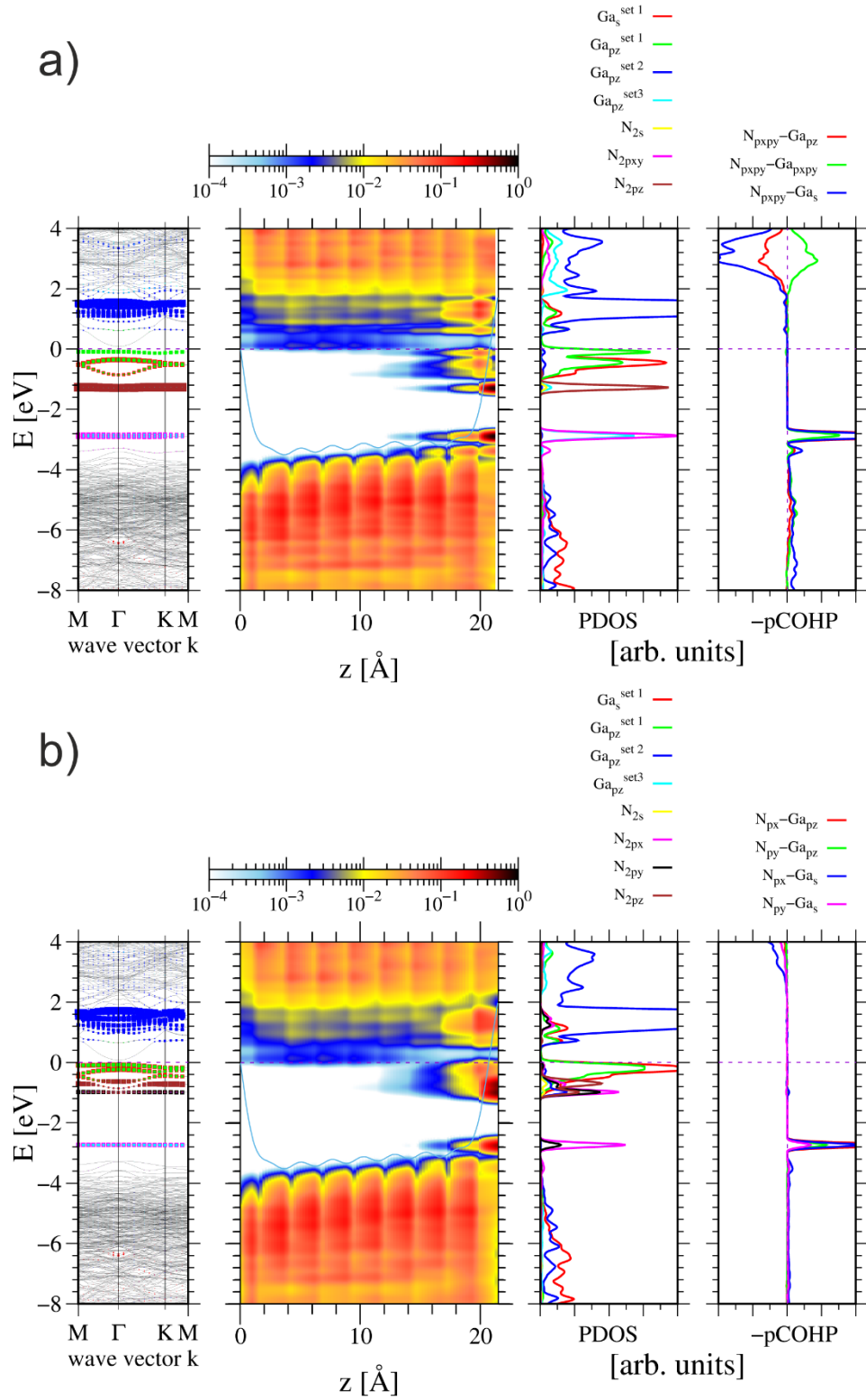


Fig 32. Energies of the quantum states of the $(2\sqrt{3} \times 2\sqrt{3})$ slab representing clean GaN(0001) surface with single N adatom located in: (a) – H3 site, (b) MAX - max energy position. The panels represents, from the left: energy of the quantum states in the momentum and the position space, projected density of states (PDOS) of the top Ga atoms and N adatom, and the rightmost

panel - Crystal Orbital Hamilton Population (COHP) of the atoms distinguished in Fig. 6 [54, 55]. Thus the COHP data correspond to N adatom and the closest topmost Ga atoms. The Fermi energy is set to zero. COHP positive values correspond to the bonding overlap. Reproduced from Fig. 7 Ref 12 [12].

Therefore the detailed studies of the bonding properties for the path were undertaken. As it is shown in Fig. 32 the bonding of N adatom in H3 site is related to the existence of the three resonating bonds discussed earlier. They are located 2.4 eV below Fermi level which is pinned by broken bond sp^3 hybridized state of top layer Ga atoms. Thus they are fully occupied, due to their resonating character with the probability $P = 2/3$. In addition the fourth N bond is broken having its energy about 0.5 eV below Fermi energy and is also occupied. In the bridge configuration one of these bond is broken with the energy located 0.68 eV below the Fermi levels. Therefore it is still occupied. The barrier energy difference between H3 and bridge configuration is related to the change of the energy of fully occupied state. No N state is empty which is related to generally low energy of the nitrogen atom quantum states.

The increase of Ga coverage to $(1/6) ML$ leads to the change of the Fermi level pinning as these top layer Ga atoms have Ga adatom attached. Some other still preserve $sp^2 - p_z$ configuration in which p_z state is empty. The Fermi level is pinned to bonding $|Ga_{4p_z}\rangle - |Ga_{sp^3}\rangle$ states and therefore lower. Therefore the broken bond nitrogen state has changed its occupation which leads to the energy barrier decrease to $\Delta E_{bar} = 0.92 \text{ eV}$ for $(1/6) ML$.

The energy barrier for full Ga coverage (13 adatoms for $(2\sqrt{3} \times 2\sqrt{3})$ slab) was also investigated. As it was shown, minimal energy N adatom position is changed to the on-top. This has important consequences to general understanding of atomic GaN growth mechanism in MBE. In fact the on-top position is required to build a new crystalline layer of GaN. The N adatom is bonded to the three Ga atoms: one from top layer of GaN lattice and the two from adlayer. The other two Ga neighbors belong to the Ga adlayer. The quantum states created by overlap between $|N_{2p}\rangle$ and $|Ga_{sp^3}\rangle$ hybridized states are identified at $E_1 = -7.97 \text{ eV}$ and $E_2 = -7.68 \text{ eV}$. These states and their overlaps are clearly identified in Fig. 33 (a) and Fig. 33 (b).

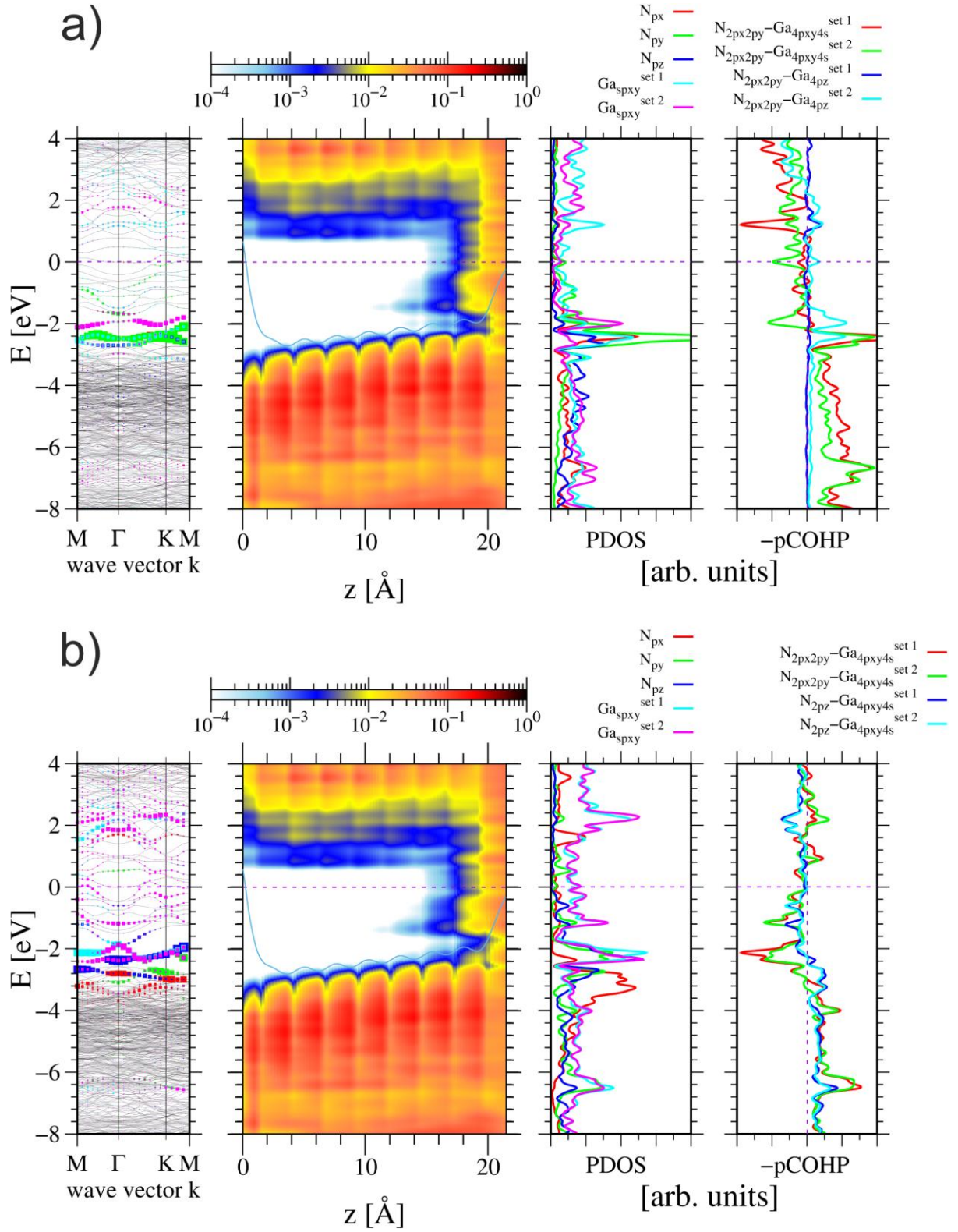


Fig 33. Energies of the quantum states of the $(2\sqrt{3} \times 2\sqrt{3})$ slab representing GaN(0001) surface fully covered by Ga adatoms, a single N adatom located in: (a) – on-top, (b) max energy position (H3). The symbols are analogous to Fig. 29. Reproduced from Fig. 14 Ref 52 [52].

The motion along the diffusional path leads to the energy maximum which is located at H3 site. In this case the path avoids the bridge location so the overlap is different from the earlier results. Due to the coverage by excess of Ga adatoms, no nitrogen broken bond states are created. In fact the N adatom creates full bonding with the Ga neighbors. Nevertheless, the energies of these states changes considerably to $E_1 = -7.54 \text{ eV}$ and $E_2 = -7.33 \text{ eV}$. Thus the energy change is substantial at $\Delta E_1 = 0.43 \text{ eV}$ and $E_2 = 0.35 \text{ eV}$. The change of the energy of the extended state cannot be assessed. Nevertheless, since these changes involve 4 electrons, they fully explain the existence of the barrier $\Delta E_{bar} = 1.23 \text{ eV}$. Thus such barrier is associated with the change of the energy of the quantum states. The energy profile is presented in Fig 34.

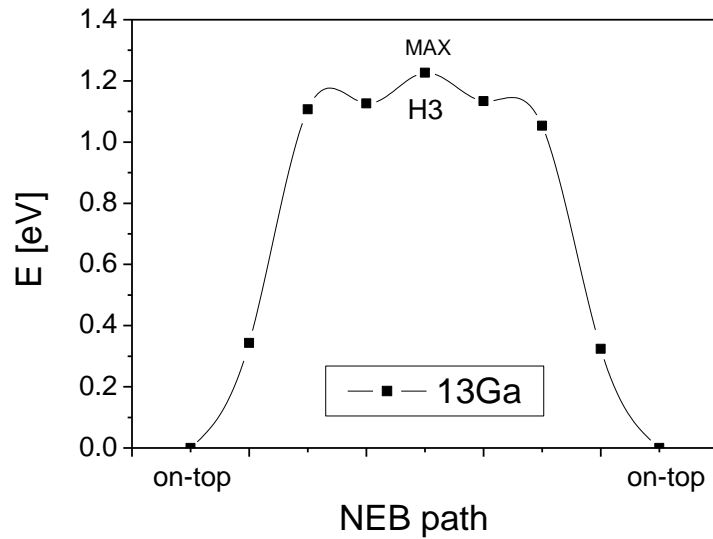


Fig 34. System energy change during motion of the nitrogen adatom along the jump path over GaN(0001) surface fully covered by Ga adatoms. The number of Ga atoms refer (13) to $(2\sqrt{3} \times 2\sqrt{3})$ slab representing GaN(0001) surface, thus it is excess of Ga single layer coverage $\theta_{Ga} = (13/12) \text{ ML}$. Reproduced from Fig. 12 Ref. 12 [12].

From these data it follows that the energy barrier for full Ga coverage is $\Delta E_{bar} = 1.23 \text{ eV}$. Thus it is higher than to $\Delta E_{bar} = 0.92 \text{ eV}$ for $(1/6) \text{ ML}$ Ga fractional coverage. Therefore the existence of the diffusion channel for gallium coverage was not confirmed. It has to be added that the low energy barrier is related to relatively low energy of the broken bond state of N adatoms. The entire picture is therefore related to quantum statistics and quantum bonding affecting the properties of N adatom

IX. Summary

This review summarizes the *ab initio* investigations of the charge properties of semiconductor surfaces in the recent period. These results are summarized by representing the state of art before these investigations, the results obtained and the state of art after. These results include the methodology and the physical picture.

Therefore the state of the art before this research was made may be summarized as follows:

1. The surface dipole charge leads to emergence of the potential coupling of the slab copies via PBC which can be counterbalanced by introduction of the compensating opposite dipole in the vacuum between the slab copies.
2. Adsorption energy is obtained by direct calculation of the energy difference between the far distance and at the surface total energy values
3. Separation of the real and termination surface by several atomic layers leads to the asymptotic behavior in which the surfaces are independent so that the system properties are independent of the number of the layers in the slab.
4. Surface states band diagram is obtained by direct projection of all states in the slab.
5. Gallium nitride and other wurtzite nitride semiconductors are bonded by the overlap of sp^3 hybridized orbitals that leads to emergence of single valence band and the bandgap.
6. Thermalization of the adsorbate is relatively minor issue in adsorption, dissipation of the excess kinetic energy proceeds via motion of “hot” atoms along the surface
7. Reconstruction is related to the minimization energy of the broken bonds. The period is intrinsic property of the surface
8. ECR analysis is related to the charge at the surface.
9. Adsorption energy is the inherent value of the adsorbate and the surface bonding only, that could be affected by adsorbate interactions only. In case of absence of the interaction adsorption energy is described properly by single value energy gain.
10. Temperature is not accounted explicitly in the thermodynamic properties of the adsorption at the surfaces.
11. Diffusion energy barrier is single value, independent on Fermi level and the quantum statical properties of the bonding.

The results in this field obtained in the reported period may be summarized as follows:

1. The existence of the surface slab dipole and the introduction of the opposite compensating dipole is physically sound approach. The problem may arise with the precision of the calculated dipole. The other method, known as Laplace correction, of zeroing the electric field by additional solution of Laplace equation may possibly lead to better precision.
2. The system consisting of the two isolated subsystems: the slab and the species at far distance may possibly have two different Fermi energy levels. The *ab initio* procedures uses single Fermi energy and accordingly distributes the electrons to the energy level of both subsystems. This may lead to charging both the slab and the adsorbate. In that the energy of the system composed of two parts is different from the energy calculated separately for both parts.
3. Asymptotic far distance behavior of the wavefunction of any finite system is exponential with no cutoff value. Thus separation of the real and termination surface leads to decrease of the overlap magnitude of their wavefunctions. Therefore asymptotically it is possible to reduce that magnitude only.
4. The electric potential of the slab and the following band diagram is controlled by the charge distribution in the slab. In case of Fermi level pinning and the charge of surface states, the profile has the slope, in case of bulk charge the profile has additional parabolic component. Thus the best way of the analysis is to use real space potential and band distribution. The nonzero electric field slab solution reflects real semiconductor surface in which the internal surface charge layer exists.
5. Gallium nitride bonding occurs via creation of two separate subbands: the upper due to overlap of the sp^3 hybridized gallium states and nitrogen p states, the lower due to overlap of gallium d states and nitrogen s states. Wurtzite tetrahedral symmetry of the lattice is stable due to resonant states of nitrogen bonding where four nitrogen states are bonding to the gallium neighbors according to resonant states created from three nitrogen p orbitals and occupied with fractional probability.
6. Thermalization of the adsorbate occurs via tunneling of electrons from adsorbate to the solid in external dipole charge electric field. In the following positively charged adsorbate is decelerated by this field losing the excess kinetic energy.
7. Reconstruction is correctly recognized as minimization energy process. In addition however, the reconstructed surface patters from the charge balance between the surface states as it could be determined from ECR.
8. ECR analysis may be extended to the charge of the adsorbate and the occupation of the new and old states. Thus ECR may be extended to EECR.

9. Adsorption leads to emergence and disappearance of the new quantum states which are occupied by the electron of the slab and the adsorbate. This may lead to total occupation of some states and the drastic change of the adsorption energy value at some coverage. At this point Fermi level is not pinned by surface states and changes freely. This is followed by drastic changes of the equilibrium pressures at some specific conditions. That drives crystal growth condition to these points at which the Fermi level is not pinned.
10. Entropic contribution may play important role in the thermodynamic properties of the adsorption.
11. Diffusion energy barrier may be affected by the change of the energy of the bonding states that may be close or even crossed Fermi level. This may affect the energy barrier drastically.
12. Diffusion energy barrier may be affected by the quantum statistics influence on the initial states either via resonant state or due to Fermi energy change.

The state of art after the reported research, as different from the previous. The mains changes are therefore:

1. Interaction of the subsystems, both the slab copies and the far distant adsorbate are analyzed using electric potential distribution.
2. Asymptotic behavior of the wavefunction is elucidated.
3. Resonant bonding of nitrogen both in the bulk and at some configuration as the adsorbate.
4. The role of external charge dipole layer in thermalization of the adsorbate.
5. The existence of internal charge dipole layer and its role in the ab initio representation of the wavefunctions, the potential profile and the charge distribution.
6. The charge role in the clean and adsorbate covered surfaces – EECR role in the selection of the structure and periodicity of the reconstructed surfaces.
7. Charge role in adsorption – energy gain and thermodynamics in temperature dependent equilibria
8. The role of quantum effects in bonding and statistics in determination of surface diffusion barrier, both in the initial state and the activated energy complex.

In summary, the reported development have changed the scientific picture of the semiconductor surfaces drastically. It has to be added that the development is not completed in any sense. This state require horizontal directed research towards extension of the scope of the

semiconductor systems and the surfaces. The finished cases are tiny fraction of the cases that should be investigated. Fortunately, the basic formulation is advanced which provides good opportunity of application of massive approach based on algorithm of artificial intelligence (AI).

The second direction is to proceed in the vertical direction, i.e. toward investigation of completely new systems. This include a number of the surfaces with different structure and composition. This may include, the step structures, and the kink structures. Here a number of the assumption used in the presently used model has to be considerably modified. These approach require creative approach which cannot be solved by AI based methods. These investigation such as steps were already started. At this moment they used the old approach which has limited chance of success. Therefore considerable extension of these models are necessary in the future.

References

- [1] C.P. Correia V. Bernardo, R. A. Marques Lameirinhas, J. P. de Melo Cunha, J. P. N. Torres, A revision of the semiconductor theory from history to applications. Disc. Appl. Sci. 6, 316 (2024). <https://doi.org/10.1007/s42452-024-06001-1>
- [2] L. Lukasiak, A. Jakubowski, History of Semiconductors. J. Telecommun. Inf. Technol. 1, 3 (2010).
- [3] W. Monch, *Semiconductor Surfaces and Interfaces*. Springer Berlin 1993.
- [4] L. Kronik, Y. Shapira, Surface photovoltage phenomena: theory, experiment and applications. Surf. Sci. Rep. 37, 1 (1999). [https://doi.org/10.1016/S0167-5729\(99\)00002-3](https://doi.org/10.1016/S0167-5729(99)00002-3)
- [5] L. Kronik, Y. Shapira, Surface photovoltage spectroscopy of semiconductor structures: at the crossroads of physics, chemistry and electrical engineering. Surf. Interface Anal. 31, 954 (2001). <https://doi.org/10.1002/sia.1132>
- [6] V. Bermudez, The fundamental surface science of gallium nitride. Surf. Sci. Rep. 72, 147 (2017). <http://dx.doi.org/10.1016/j.surfrep.2017.05.001>
- [7] N.D. Lang and W. Kohn, Theory of Metal Surfaces: Charge Density and Surface Energy. Phys. Rev. B 1, 4555 (1970). <https://doi.org/10.1103/PhysRevB.1.4555>
- [8] N.D. Lang and W. Kohn, Theory of Metal Surfaces: Work Function. Phys. Rev. B 3, 1215 (1973). <https://doi.org/10.1103/PhysRevB.3.1215>

- [9] M. Magnuson, F. Mattesini, C. Hoglund, J. Birch, L. Hultman, Electronic structure and bonding anisotropy investigation of wurtzite AlN, Phys. Rev. B 80, 155105 (2009). <https://doi.org/10.1103/PhysRevB.80.155105>
- [10] M. Magnuson, F. Mattesini, C. Hoglund, J. Birch, L. Hultman, Electronic structure of GaN and Ga investigated by soft x-ray spectroscopy and first-principles methods. Phys. Rev. B 82, 085125 (2010). <https://doi.org/10.1103/PhysRevB.81.085125>
- [11] Maria Ptasinska, Jakub Sołtys, Jacek Piechota, Stanisław Krukowski, Electronic properties on GaN(0001) surface – ab initio investigation. Vacuum 99, 166 (2013). <http://dx.doi.org/10.1016/j.vacuum.2013.05.006>
- [12] P. Strak, C. Sobczak, S. Krukowski. Quantum effects in surface diffusion: application to diffusion of nitrogen adatoms over GaN(0001) surface. [arXiv:2501.19079](https://arxiv.org/abs/2501.19079)
<https://arxiv.org/abs/2501.19079>
- [13] J. Neugebauer and M. Scheffler, Adsorbate-substrate and adsorbate-adsorbate interactions of Na and K adlayers on Al(111). Phys. Rev. B 46, 16067 (1992). <https://doi.org/10.1103/PhysRevB.46.16067>
- [14] L. Bengtsson, Dipole correction for surface supercell calculations, Phys. Rev. B 59 12301 – 12304 (1999). <https://doi.org/10.1103/PhysRevB.59.12301>
- [15] S. Krukowski, P. Kempisty, P. Strak, Electrostatic condition for the termination of the opposite face of the slab in DFT simulations of semiconductor surfaces. J. Appl. Phys. 105, 113701 (2009). <http://dx.doi.org/10.1063/1.3130156>
- [16] P. Strak, P. Kempisty, K. Sakowski, J. Piechota, I. Grzegory, E. Monroy, A. Kaminska, S. Krukowski, Polarization spontaneous and piezo: fundamentals and their implementation in *ab initio* calculations. Arxiv 2407.01134.
<https://arxiv.org/abs/2407.01134>
- [17] L.D. Landau, E. M. Lifshitz, *Electrodynamics of continuous media*, Pergamon Press, Londyn, 1960.
- [18] C. Wood, D. Jena, *Polarization Effects in Semiconductors*, Springer Berlin 2008
- [19] F. Bernardini, V. Fiorentini, and D. Vanderbilt, Spontaneous polarization and piezoelectric constants of III-V nitrides, Phys. Rev. B 56 (2001) R10024.
<https://doi.org/10.1103/PhysRevB.56.R10024>
- [20] V. Fiorentini, F. Bernardini, F. Della Sala, A. Di Carlo, and P. Lugli, Phys. Rev. B 60, 8849 (1999). <https://doi.org/10.1103/PhysRevB.60.8849>

- [21] P. Strak, P. Kempisty, K. Sakowski, A. Kaminska, D. Jankowski, K. P. Korona, K. Sobczak, J. Borysiuk, M. Beeler, E. Grzanka, E. Monroy, S. Krukowski, *Ab initio* and experimental studies of polarization and polarization related fields in nitrides and nitride structures, AIP Adv. 7, 015027 (2017). <https://dx.doi.org/10.1063/1.4974249>
- [22] C. E. Dreyer, A. Janotti, C. G. Van de Walle, D. Vanderbilt, Correct Implementation of Polarization Constant in Wurtzite Materials and Impact on III-Nitrides, Phys. Rev. X 6, 021038 (2016). <https://doi.org/10.1103/PhysRevX.6.021038>
- [23] A. Yoshiasa, Y. Murai, O. Ohtaka, T. Katsura, Detailed Structures of Hexagonal Diamond (lonsdaleite) and Wurtzite-type BN, Jpn. J. Appl. Phys. 42, 1694 (2003). <https://doi.org/10.1143/JJAP.42.1694>
- [24] H. Angerer, D. Brunner, F. Freudenberger, O. Ambacher, M. Stutzmann, R. Höppler, T. Metzger, E. Born, G. Dollinger, A. Bergmaier, S. Karsch, H. -J. Korner. Determination of the Al Mole Fraction and the Band Gap Bowing of Epitaxial $\text{Al}_x\text{Ga}_{1-x}\text{N}$ Films. Appl. Phys. Lett. 71, 1504 (1997). <https://doi.org/10.1063/1.119949>
- [25] M. Leszczynski, H. Teisseyre, T. Suski, I. Grzegory, M. Bockowski, J. Jun, S. Porowski, K. Pakula, J.M. Baranowski, C.T. Foxon, T.S. Cheng, Lattice parameters of gallium nitride, Appl. Phys. Lett. 69, 73 (1996). <https://doi.org/10.1063/1.118123>
- [26] W. Paszkowicz, J. Adamczyk, S. Krukowski, M. Leszczynski, S. Porowski, J. A. Sokołowski, M. Michalec, W. Lasocha, Lattice parameters, density and thermal expansion of InN microcrystals grown by the reaction of nitrogen plasma with liquid indium. Phil. Mag. A 79 1145 (1999). <https://doi.org/10.1080/01418619908210352>
- [27] P. Kempisty, S. Krukowski, On the nature of Surface States Stark Effect at clean GaN(0001) surface. J. Appl. Phys. 112, 113704 (2012). <https://doi.org/10.1063/1.4768256>
- [28] M. Revesz, I. Bertoti, G. Mink, I. Mayer, On the use of pseudo-atoms in cluster calculations for modeling of molecular fragments, solids and surfaces, J. Mol. Struct.-Theochem. 50, 335 (1988). [https://doi.org/10.1016/0166-1280\(88\)80500-1](https://doi.org/10.1016/0166-1280(88)80500-1)
- [29] N. N. Ilchenko, L. G. Gorb, V. V. Goncharuk, The application of “pseudoatoms” to quantum chemistry simulation of solid-surfaces with hypervalence coordination environment - $\alpha\text{-Al}_2\text{O}_3$. J. Mol. Struct.-Theochem. 95, 17 (1992). [https://doi.org/10.1016/0166-1280\(92\)80020-M](https://doi.org/10.1016/0166-1280(92)80020-M)
- [30] S. Krukowski, P. Kempisty, P. Strak, Foundations of ab initio simulations of electric charges and fields at semiconductor surfaces within slab models. J. Appl. Phys. 114, 143705 (2013). <http://dx.doi.org/10.1063/1.4824800>

- [31] S.H. Yoo, M. Todorova, D. Wickramaratne, L. Weston, C. G. Van de Walle, J. Neugebauer, Finite-size correction for slab supercell calculations of materials with spontaneous polarization, *NPJ Comp. Mater.* 7, 58 (2021).
<https://doi.org/10.1038/s41524-021-00529-1>
- [32] J. E. Northrup, J. Neugebauer, Theory of GaN (10 $\bar{1}$ 0) and (11 $\bar{2}$ 0) surfaces. *Phys. Rev. B* 53, R10 477 (1995). <https://doi.org/10.1103/PhysRevB.53.R10477>
- [33] K. Rapcewicz, M. Buongiorno Nardelli, J. Bernholc, Theory of morphology of wurtzite GaN (0001) surfaces. *Phys. Rev. B* 56, R12 725 (1997).
<https://doi.org/10.1103/PhysRevB.56.R12725>
- [34] F.-H. Wang, P. Kruger, J. Pollmann, Electronic structure of (1 \times 1) GaN(0001) and GaN(000 $\bar{1}$) surfaces. *Phys. Rev. B* 64, 035305 (2001).
<https://doi.org/10.1103/PhysRevB.64.035305>
- [35] A. L. Rosa, J. Neugebauer, First-principles calculations of the structural and electronic properties of clean GaN(0001) surfaces. *Phys. Rev. B* 73, 205346 (2006).
<https://doi.org/10.1103/PhysRevB.73.205346>
- [36] C. G. Van de Walle, D. Segev, Microscopic origin of surface states on nitride surfaces. *J. Appl. Phys.* 101, 081704 (2007). <https://doi.org/10.1063/1.2722731>
- [37] D. Segev, C. G. Van de Walle, Electronic structure of nitride surfaces. *J. Cryst. Growth* 300, 199 (2007). <https://doi.org/10.1016/j.jcrysgro.2006.11.039>
- [38] P. Strak, P. Kempisty, K. Sakowski, S. Krukowski, Ab initio determination of electron affinity of polar nitride surfaces, clean and under Cs coverage. *J. Vac. Sci. Technol. A* 35, 021406 (2017). <http://dx.doi.org/10.1116/1.4975332>
- [39] P. Kempisty, S. Krukowski, P. Strak, K. Sakowski, Ab initio studies of electronic properties of bare GaN(0001) surface. *J. Appl. Phys.* 106, 054901 (2009).
<http://dx.doi.org/10.1063/1.3204965>
- [40] J. Soltys, J. Piechota, M. Lopuszynski, S. Krukowski, A comparative DFT Study of electronic properties of 2H-, 4H- and 6H-SiC(0001) and SiC(000 $\bar{1}$) clean surfaces. *N. J. Phys.* 12, 043204 (2010). <http://dx.doi.org/10.1088/1367-2630/12/4/043024>
- [41] P. Strak, P. Kempisty, M. Ptasinska, S. Krukowski, Principal physical properties of GaN/AlN multiquantum well (MQW) systems determined by density functional theory (DFT) calculations. *J. Appl. Phys.* 113, 193706 (2013).
<http://dx.doi.org/10.1063/1.4805057>

- [42] P. Witczak, P. Kempisty, P. Strak, S. Krukowski, Ab initio study of Ga-GaN system: transition from adsorbed metal atoms to a metal-semiconductor junction. J. Vac. Sci. Technol. A 33, 061101 (2015). <http://dx.doi.org/10.1116/1.4927166>
- [43] J. Heyd, G. E. Scuseria, M. Ernzerhof, Hybrid functionals based on a screened Coulomb potential, J. Chem. Phys. 118, 8207 (2003).
- [44] L. S. Pedroza, A. J. R. da Silva, and K. Capelle, Gradient-dependent density functionals of the Perdew-Burke-Ernzerhof type for atoms, molecules, and solids, Phys. Rev. B 79, 201106(R) (2009). <https://doi.org/10.1103/PhysRevB.79.201106>
- [45] M. M. Odashima, K. Capelle, and S. B. Trickey, Tightened Lieb-Oxford Bound for Systems of Fixed Particle Number, J. Chem. Theory Comput. 5, 798 (2009) . <https://doi.org/10.1021/ct8005634>
- [46] L.G. Ferreira, M. Marques, and L.K. Teles, Approximation to density functional theory for the calculation of band gaps of semiconductors. Phys. Rev. B 78, 125116 (2008). <https://doi.org/10.1103/PhysRevB.78.125116>
- [47] M. Ribeiro, L.R.C. Fonseca, and L.G. Ferreira, Accurate prediction of the Si/SiO₂ interface band offset using the self-consistent *ab initio* DFT/LDA-1/2 method. Phys. Rev. B, 79, 241312 (2009). <https://doi.org/10.1103/PhysRevB.79.241312>
- [48] W. Harrison, *Electronic Structure and the Properties of Solids* . Freeman San Francisco 1980
- [49] P. Y. Yu, M. Cardona, *Fundamentals of Semiconductors* Springer Heidelberg 2010
- [50] F. A. Kekule, Untersuchungen über aromatische Verbindungen. Liebigs Annalen der Chemie und Pharmacie 137, 129 (1866). <https://doi.org/10.1002%2Fjlac.18661370202> (in German)
- [51] P. A. Schultz, R. P. Messmer, Are There π Bonds in Benzene? Phys. Rev. Lett. 58, 2416 (1987). <https://doi.org/10.1103/PhysRevLett.58.2416>
- [52] P. W. Anderson, The Resonating Bond State in La₂CuO₄ and Superconductivity. Science 235, 1196 (1987). <https://doi.org/10.1126/science.235.4793.1196>
- [53] C. Weber, Variational Study of Strongly Correlated Electronic Models. PhD thesis. EPFL Lausanne 2007.
- [54] R. Dronskowski, P. E. Blochl, Crystal orbital Hamilton populations (COHP): energy-resolved visualization of chemical bonding in solids based on density-functional calculations. J. Phys. Chem. 97, 8617 (1993). <https://doi.org/10.1021/j100135a014>

- [55] V. L. Deringer, A. L. Tchougreeff, R. Dronskowski, Crystal Orbital Hamilton Population (COHP) Analysis as Projected from Plane-Wave Basis Sets. *J. Phys. Chem.* 115, 5461 (2011). <https://doi.org/10.1021/jp202489s>
- [56] V. M. Bermudez, C. -I. Wu, A. Kahn, AlN films on GaN: sources of error in the photoemission measurements of electron affinity. *J. Appl. Phys.* 89, 1991 (2001). <https://doi.org/10.1063/1.1333716>
- [57] C. -I. Wu, A. Kahn, N. Taskar, D. Dorman, D. Gallagher, *GaN(0001) – (1 × 1)* surfaces: Composition and electronic properties. *J. Appl. Phys.* 83, 4249 (1998). <https://doi.org/10.1063/1.367182>
- [58] P. Strak, K. Sakowski, P. Kempisty, S. Krukowski, Dissipation of the excess energy of the adsorbate – thermalization via electron transfer. *Phys. Chem. Chem. Phys.* 19, 9149 (2019). <https://doi.org/10.1039/c7cp00235a>
- [59] H. Brune, J. Wintterlin, R. J. Gehm, and G. Ertl, Surface migration of “hot” adatoms in the course of dissociative chemisorption of oxygen on Al(111). *Phys. Rev. Lett.* 68, 624 (1992). <https://doi.org/10.1103/PhysRevLett.68.624>
- [60] S. Schindke, S. Messerli, K. Morgenstern, J. Nieminen, and W.-D. Schneider, *J. Chem. Phys.* 114, 4206 (2001). <https://doi.org/10.1063/1.1346687>
- [61] A. Gross, Ab Initio Molecular Dynamics Study of Hot Atom Dynamics after Dissociative Adsorption of H_2 on Pd(100). *Phys. Rev. Lett.* 103, 246101 (2009). <https://doi.org/10.1103/PhysRevLett.103.246101>
- [62] W. W. Hayes and J. R. Manson, Argon scattering from Ru(0001): Calculations and comparison with experiment. *Phys. Rev. B*, 75, 113408 (2007). <https://doi.org/10.1103/PhysRevB.75.113408>
- [63] L. C. Ciacchi and M. C. Payne, “Hot-Atom” O_2 Dissociation and Oxide Nucleation on Al(111). *Phys. Rev. Lett.* 92, 176104 (2004). <https://doi.org/10.1103/PhysRevLett.92.176104>
- [64] H. Siegle, G. Kaczmarczyk, L. Fillipidis, A. P. Litwinchuk, A. Hoffmann, C. Thomsen, Zone-boundary phonons in hexagonal and cubic GaN, *Phys. Rev. B* 55, 7000 (1997). <https://doi.org/10.1103/PhysRevB.55.7000>
- [65] A. K. Tiwari, S. Nave, and B. Jackson, Methane Dissociation on Ni(111): A New Understanding of the Lattice Effect. *Phys. Rev. Lett.* 103, 253201 (2009). <https://doi.org/10.1103/PhysRevLett.103.253201>
- [66] J. Lindhard, On the properties of gas of charged particles. *K. Dan. Vidensk. Selsk. Mat. Fys. Medd.* 28, 57 (1954).

- [67] P. Kempisty, S. Krukowski, Adsorption of ammonia at GaN(0001) surface in the mixed ammonia/hydrogen ambient - a summary of ab initio data. AIP Adv. 4, 117109 (2014). <http://dx.doi.org/10.1063/1.4901922>
- [68] G. P. Srivastava, Theory of semiconductor surface reconstruction, Rep. Prog., Phys. 60, 561 (1997). <https://doi.org/10.1088/0034-4885/60/5/002>
- [69] H. Neddemeyer, Scanning tunneling microscopy of semiconductor surfaces. Rep. Prog. Phys. 59, 701 (1996). <https://doi.org/10.1088/0034-4885/59/6/001>
- [70] D. J. Chadi, Atomic structure of GaAs(100)-(2x1) and (2x4) reconstructed surfaces. J. Vac. Sci. Technol. A 5, 834 (1987). <https://doi.org/10.1116/1.574366>
- [71] M. D. Pashley. Electron counting model and its application to island structures on molecular-beam epitaxy grown GaAs(001) and ZnSe(001). Phys. Rev. B 40, 10481 - 10487 (1989). <https://doi.org/10.1103/PhysRevB.40.10481>
- [72] S.-H. Yoo, L. Lymperakis, J. Neugebauer, Efficient electronic passivation scheme for computing low-symmetry compound semiconductor surfaces in density-functional theory slab calculation. Phys. Rev. Mater. 5, 044605 (2021). <https://doi.org/10.1103/PhysRevMaterials.5.044605>
- [73] J. S. Griffith, L. E. Orgel, Ligand-field theory. Q. Rev. Chem. Soc. 11, 381 (1957). <https://doi.org/10.1039/QR9571100381>
- [74] N. A. Modine, E. Kaxiras. Theory of the (3 x 2) reconstruction of the GaAs(0001) surface. Mater. Sci. Eng. B 67, 1 (1999). [https://doi.org/10.1016/S0921-5107\(99\)00202-0](https://doi.org/10.1016/S0921-5107(99)00202-0)
- [75] P. Kempisty, P. Strak and S. Krukowski, Ab initio determination of atomic structure and energy of surface states of bare and hydrogen covered GaN (0001) surface - existence of the Surface States Stark Effect (SSSE). Surf. Sci. **605**, 695 - 703 (2011). <http://dx.doi.org/10.1016/j.susc.2011.01.005>
- [76] Y.-W. Chen, J.-L. Kuo, Density functional study of the First Wetting Layer on the GaN (0001) surface. J. Phys. Chem. C 117, 8774 (2013). <https://doi.org/10.1021/jp312377t>
- [77] P. Strak, W. Miller, S. Krukowski Charge-Controlled Energy Optimization of the Reconstruction of Semiconductor Surfaces: $sp^3 - sp^2$ Transformation of Stoichiometric surface to (4 × 4) Pattern, Materials 17, 2614 (2024). <https://doi.org/10.3390/ma17112614>

- [78] S. Krukowski, P. Kempisty, P. Strak, K. Sakowski, Fermi level pinning and the charge transfer contribution to the energy of adsorption at semiconducting surfaces. *J. Appl. Phys.* 115, 043529 (2014). <http://dx.doi.org/10.1063/1.4863338>
- [79] P. Kempisty, S. Krukowski, P. Strak, Fermi level influence on the adsorption at semiconductor surfaces - ab initio simulations. *J. Appl. Phys.* 114, 0637507 (2013). <http://dx.doi.org/10.1063/1.4817903>
- [80] P. Kempisty, P. Strak, K. Sakowski, S. Krukowski, General aspects of the vapor growth of semiconductor crystals - a study based on DFT simulations of the NH_3/NH_2 covered GaN(0001) surface in hydrogen ambient, *J. Cryst. Growth* 390, 71 (2014). <http://dx.doi.org/10.1016/j.jcrysgro.2013.12.039>
- [81] P. Kempisty, P. Strak, K. Sakowski, S. Krukowski, Thermodynamics of GaN(s)- $\text{NH}_3(\text{v})+\text{N}_2(\text{v})+\text{H}_2(\text{v})$ system - electronic aspects of the processes at GaN(0001) Surface, *Surf. Sci.* 662, 12 (2017). <https://doi.org/10.1016/j.susc.2017.03.007>
- [82] P. Kempisty, S. Krukowski, Ab initio investigation of adsorption of atomic and molecular hydrogen at GaN(0001) surface. *J. Cryst. Growth* 358, 64 (2012). <http://dx.doi.org/10.1016/j.jcrysgro.2012.08.004>
- [83] M. Chase, C. Davies, J. Downey, D. Frurip, R. McDonald, A.N. Sverud, JANAF Thermochemical Tables. *J. Phys. Chem. Ref. Data Suppl.* 14 (1985) 1002.
- [84] W. P. Glushko (ed.) *Termodinamiczeskije swoistwa indywidualnych wescestw*. Nauka, Moscow, 1978
- [85] I. Barin, *Thermochemical Data of Pure Substances*, VCH, Weinheim 1994.
- [86] NIST-JANAF Thermochemical Tables. NIST Standard Reference Database 13, <https://doi.org/10.18434/T42S31>
- [87] P. Kempisty, Y. Kangawa, Evolution of the free energy of the GaN(0001) surface based on first-principles phonon calculations. *Phys. Rev. B* 100, 085304 (2019). <https://doi.org/10.1103/PhysRevB.100.085304>
- [88] P. Kempisty, P. Strak, K. Sakowski, Y. Kangawa, S. Krukowski, Thermodynamic foundations of applications of ab initio methods for determination of the adsorbate equilibria: hydrogen at GaN(0001) surface. *Phys. Chem. Chem. Phys.* 19 (2017) 29676 – 29684. <http://dx.doi.org/10.1039/c7cp05214f>
- [89] J. Piechota, S. Krukowski, P. Sadovyi, B. Sadovyi, S. Porowski, I. Grzegory, Nitrogen Dissolution in liquid Ga and Fe: Comprehensive Ab initio Analysis. Relevance for Crystal Growth, *Materials* 14 (2021) 1306. <https://dx.doi.org/10.3390/ma14051306>

- [90] P. Strak, A. Ahmad, P. Kempisty, J. Piechota, K. Sakowski, G. Nowak, Y. Kangawa, J. Łażewski, and Stanislaw Krukowski, Al coverage of AlN(0001) surface and Al vapor pressure – thermodynamic assessment based on *ab initio* calculations. Comp. Mater. Sci. 203 (2022) 111159. <https://doi.org/10.1016/j.commatsci.2021.111159>
- [91] A. J. Jackson, A. Walsh, 2013. Oxidation of GaN: An *ab initio* thermodynamic approach. Phys. Rev. B 88, 165201. <https://doi.org/10.1103/PhysRevB.88.165201>
- [92] S. Krukowski, P. Kempisty, A. Jalbout, 2008. Thermodynamic and kinetic approach in DFT studies of microscopic structure of GaN(0001) surface in ammonia-rich conditions. J. Chem. Phys. 129, 234705 . <http://dx.doi.org/10.1063/1.3037218>
- [93] M. Ptasińska, J. Piechota, S. Krukowski, Adsorption of Hydrogen at GaN(0001) surface – *Ab Initio* Study. J. Phys. Chem. C. 119, 11563 (2015). <http://dx.doi.org/10.1021/acs.jpcc.5b00836>
- [94] T. D. Moustakas, B. Paiella, Optoelectronic device physics and technology of nitride semiconductors from the UV to terahertz. Rep. Prog. Phys. 80, 106501 (2017). <https://doi.org/10.1088/1361-6633/aa7bb2>
- [95] C. Skierbiszewski, Z. R. Wasilewski, I. Grzegory, S. Porowski, Nitride-based laser diodes by plasma-assisted MBE- from violet to green emission. J. Cryst. Growth 311, 1632- 1639 (2008). <https://doi.org/10.1016/j.jcrysgro.2008.12.040>
- [96] T. Taki, M. Strassburg, Visible LEDs: More than Efficient Light. ECS J. Solid State Sci. Technol. 9, 015017 (2020). <https://www.doi.org/10.1149/2.0402001JSS>
- [97] M. Kneissl, T. Y. Seong, J. Han, H. Amano, The emergence and prospects of deep-ultraviolet light-emitting diode technologies. Nature Photonics 13, 233-244 (2019). <https://www.doi.org/10.1038/s41566-019-0359-9>
- [98] I. M. Watson, Metal organic vapour phase epitaxy of AlN, GaN, InN and their alloys: A key chemical technology for advanced device applications, Coord. Chem. Rev. 257 2120 – 2141 (2013). <https://doi.org/10.1016/j.ccr.2012.10.020>
- [99] C. Van de Walle, J. Neugebauer, First-Principles Surface Phase Diagram for Hydrogen on GaN Surfaces. Phys. Rev. Lett. 88, 066103 (2002). <https://doi.org/10.1103/PhysRevLett.88.066103>
- [100] P. Kempisty, P. Strak, K. Sakowski, S. Krukowski, Adsorption of ammonia on hydrogen covered GaN(0001) surface – a Density Functional Theory study. J. Cryst. Growth 401, 514 (2014). <https://doi.org/10.1016/j.jcrysgro.2013.10.061>
- [101] P. Kempisty, A. Ahmad, P. Strak, K. Sakowski, A. Kafar, J. Piechota, and Stanislaw Krukowski, Incorporation of indium into GaN layers in the context of MOVPE

- thermodynamics and growth - *ab initio* studies, *Comp. Mater. Sci.* 230, 112489 (2023). <https://doi.org/10.1016/j.commatsci.2023.112489>
- [102] E. L. Piner, M. K. Behbehani, N. A. El-Masry, F. G. McIntosh, J. C. Roberts, K. S. Boutros, S. M. Bedair, Effect of hydrogen on the indium incorporation in InGaN epitaxial films, *Appl. Phys. Lett.* 70 (1997) 461-463.
 - [103] F. Scholz, Metalorganic vapour phase epitaxy of GaN and GaInN/GaN heterostructures and quantum wells, *Prog. Cryst. Growth Charact. Mater.* 35 (1997) 243-262.
 - [104] R. Czernecki, S. Kret, P. Kempisty, E. Grzanka, J. Plesiewicz, G. Targowski, S. Grzanka, M. Bilska, J. Smalc-Koziorowska, S. Krukowski, T. Suski, P. Perlin, M. Leszczynski, Influence of hydrogen and TMIn on indium incorporation in MOVPE growth of InGaN layers, *J. Cryst. Growth* 402 (2014) 330-336.
 - [105] R. Czernecki, E. Grzanka, P. Strak, G. Targowski, S. Krukowski, P. Perlin, T. Suski, M. Leszczynski, Influence of hydrogen pre-growth flow on indium incorporation into InGaN layers, *J. Cryst. Growth* 464 (2017) 123-126.
 - [106] R. Czernecki, E. Grzanka, J. Smalc-Koziorowska, S. Grzanka, D. Schiavon, G. Targowski, J. Plesiewicz, P. Prystawko, T. Suski, P. Perlin, M. Leszczynski, Effect of hydrogen during growth of quantum barriers on the properties of InGaN quantum wells, *J. Cryst. Growth* 414 (2015) 38-41.
 - [107] Y. Zhu, T. Lu, X. Zhou, G. Zhao, H. Dong, Z. Jia, X. Liu, B. Xu, Effect of small flow hydrogen treatment at the upper well/barrier interface on the properties of InGaN/GaN multiple quantum wells, *Superlattices Microstruct.* 107 (2017) 293-298.
 - [108] H.-L. Wang, X.-H. Zhang, H.-X. Wang, B. Li, C. Chen, Y.-X. Li, H. Yan, Z.-S. Wu, H. Jiang, Suppression of indium-composition fluctuations in InGaN epitaxial layers by periodically-pulsed mixture of N₂ and H₂ carrier gas, *Chin. Phys. B* 27 (2018) 127805.
 - [109] H. Wang, Z. Lv, C. Chen, S. Zhang, Y. Guo, B. Li, Z. Wu, H. Jiang, Reduction of nonradiative recombination in InGaN epilayers grown with periodical dilute hydrogen carrier gas, *Appl. Surf. Sci.* 494 (2019) 285-292.
 - [110] H. Hirayama, in “Nitride Semiconductor Technology” ed. F. Roccaforte, M. Leszczynski, Wiley, 2020
 - [111] F. Roccaforte, M. Leszczynski, Introduction to Gallium Nitride Properties and Applications, in: F. Roccaforte, M. Leszczynski (Eds.), *Nitride Semiconductor Technology. Power Electronics and Optoelectronic Devices*, Wiley-VCH, Weinheim, Germany, 2020, pp. 1 – 39.

- [112] D.B. Li, K. Jiang, X.J. Sun, C. L. Guo, AlGa_N photonics: recent advances in materials and ultraviolet devices, *Adv Opt. Photon.* 10 (2018) 43-110.
<https://doi.org/10.1364/AOP.10.000043>.
- [113] C. K Tan, W. Sun, D. Borovac, N. Tansu, 2016. Large Optical Gain AlInN-Delta-GaN Quantum Well for Deep Ultraviolet Emitters. *Sci. Rep.* 6, 22983 .
<https://doi.org/10.1038/srep22983>
- [114] H. Taketomi, Y. Aoki, Y. Takagi, A. Sugiyama, M. Kuwabara, H. Yoshida, 2016. Over 1 W record-peak-power operation of a 338 nm AlGa_N multiple-quantum-well laser diode on a Ga_N substrate. *Jpn. J. Appl. Phys.* 55, 05FJ05.
<https://doi.org/10.7567/JJAP.55.05FJ05>
- [115] A. Yadav, H. Hirayama, E.U. Rafailov, Light Emitting Diodes, in F. Roccaforte, M. Leszczynski (Eds) *Nitride Semiconductor Technology. Power Electronics and Optoelectronic Devices*, Wiley-VCH, Weinheim, Germany, 2020, pp. 253–299.
- [116] G. Selvaduray, L. Sheet, Aluminium nitride: review of synthesis methods. *Mater. Sci. Technol.* 9 (1993) 463-473. <https://doi.org/10.1179/mst.1993.9.6.463>
- [116] P. Strak, K. Sakowski, P. Kempisty, S. Krukowski, Structural and electronic properties of AlN(0001) surface under partial N coverage as determined by ab initio approach, *J. Appl. Phys.* 118, 095705 (2015). <http://dx.doi.org/10.1063/1.4929823>
- [117] P. Strak, K. Sakowski, J. Piechota, A. Ahmad, I. Grzegory, Y. Kangawa, S. Krukowski, Adsorption of nitrogen at AlN(000-1) surface – decisive role of structural and electronic factors. *Surf. Sci.* 713, 096503 (2021).
<https://doi.org/10.1016/j.susc.2021.121891>
- [118] P. Kempisty, P. Strak, K. Sakowski, Y. Kangawa, and Stanislaw Krukowski, *Ab initio* and thermodynamic picture of Al adsorption of AlN(0001) surface - role of bond creation and electron transition contributions. *Appl. Surf. Sci.* 532, 147719 (2020).
<https://doi.org/10.1016/j.apsusc.2020.147419>
- [119] J. Soltys, J. Piechota, P. Strak, S. Krukowski, Electronic Charge Transfer Contribution in Adsorption of Silicon at the SiC(0001) Surface – A Density Functional Theory (DFT) Study. *Appl. Surf. Sci.* 393, 168 (2017).
<http://dx.doi.org/10.1016/j.apsusc.2016.10.007>
- [120] P. Kempisty, K. Kawka, A. Kusaba, Y. Kangawa, Polar ga_N surfaces under Gallium Rich Conditions: Revised Thermodynamic Insights from Ab Initio Calculations. *Materials* 16, 5982 (2023). <https://doi.org/10.390/ma16175982>

- [121] G. Henkelman, B.P. Uberuaga and H. Jonsson, A climbing image nudged elastic band method for finding saddle points and minimum energy paths. *J. Chem. Phys.* **113**, 9901 – 9904 (2000). <https://doi.org/10.1063/1.1329672>
- [122] G. Henkelman, H. Jonsson, Improved tangent estimate in the nudged elastic band method for finding minimum energy paths and saddle points. *J. Chem. Phys.* **111**, 9978 - 9985 (2000). <https://doi.org/10.1063/1.1323224>
- [123] H. Eyring, The activated complex in chemical reactions. *J. Chem. Phys.* **3**, 107 (1935). <https://doi.org/10.1063/1.1749604>
- [124] R. Gomer, Diffusion of adsorbates on metal surfaces. *Rep. Prog. Phys.* **53**, 917 (1990). <https://doi.org/10.1088/0034-4885/53/7/002>
- [125] J. Neugebauer, T. K. Zywietz, M. Scheffler, J. E. Northrup, H. Chen, R.M. Feenstra, Adatom Kinetics On and Below the Surface: The Existence of a New Diffusion Channel. *Phys. Rev. Lett.* **90**, 056101 (2003). <https://doi.org/10.1103/PhysRevLett.90.056101>
- [126] T. Zywietz, J. Neugebauer, M. Scheffler, Adatom diffusion at GaN(0001) and (000 $\bar{1}$) surface. *Appl. Phys. Lett.* **73**, 487 (1998). <https://doi.org/10.1063/1.121909>
- [127] A. R. Smith, R. M. Feenstra, D. W. Greve, M.-S. Shin, M. Skowronski, J. Neugebauer, J. E. Northrup, GaN(0001) surface structures studied using scanning tunneling microscopy and first-principles total energy calculations. *Surf. Sci.* **423**, 70 (1990). [https://doi.org/10.1016/S0039-6028\(98\)00903-0](https://doi.org/10.1016/S0039-6028(98)00903-0)
- [128] S. Porowski, C. Skierbiszewski, Potential of MME for gallium nitride based lasers. *Proc. SPIE* **5968**, 59580Z (2005). <https://doi.org/10.1117/12.622908>
- [126] T. Akiyama, T. Kawamura, Ab initio study for adsorption behavior on AlN(0001) surface with steps and kinks during metal-organic vapor-phase epitaxy, *Jpn. J. Appl. Phys.* **63**, 02SP71 (2024). <https://doi.org/10.35848/1347-4065/ad1896>
- [127] T. Akiyama, T. Kawamura, Structural Stability of Vicinal AlN(0001) and GaN(0001) Surface with Steps and Kinks under Metal-Organic Vapor-Phase Epitaxy Condition: A First-Principles Study, *Cryst. Growth Des.* **24**, 5906 (2024). <https://doi.org/10.1021/acs.cgd.4c00121>